References

References

Adachi M., Yamamoto K. and Sugisaki R., 1986. Hydrothermal chert and associated siliceous rocks from the northern Pacific: their geological significance. Sedimentary Geology, 47: 125-148.

Allen R.L., 1988. False pyroclastic textures in altered silicic lavas, with implications for volcanic-associated mineralization. Econ. Geol., 83: 1424-1446.

Allen R.L., 1992. Reconstruction of the tectonic, volcanic and sedimentary setting of strongly deformed Zn-Cu massive sulfide deposits at Benambra, Victoria. Econ. Geol., 87: 825-854.

Allen R.L., 1994. Syn-volcanic, subseafloor replacement model for Rosebery and other massive sulfide ores. In: Cooke D.R. and Kitto P.A., Contentious issues in Tasmania Geology, Geol. Soc. Aust. Abstracts, 39: 107-108.

Allen R.L. and Cas R.A.F., 1990. The Rosebery controversy: distinguishing prospective submarine ignimbrite-like units from true subaerial ignimbrites in the Rosebery-Hercules ZnCuPb massive sulphide district, Tasmania. Geological Society of Australia, Abstracts, 25: 31-32.

Allen R.L. and Hunns S.R., 1990. Excursion Guide E1. The Mount Read Volcanics and related ore deposits. 10th Aust. Geol. Conv., Hobart, 15-27.

Allen R.L., Weihed P. and Svenson S.Å., 1996b. Setting of Zn-Cu-Au-Ag massive sulfide deposits in the evolution and facies architecture of a 1.9 Ga Marine Volcanic Arc, Skellefte District, Sweden. Econ. Geol., 91: 1022-1053.

Alt J.C., 1988. The chemistry and sulfur isotope composition of massive sulfide and associated deposits on Green Seamount, eastern Pacific. Econ. Geol., 83: 1026-1033.

Alt J.C., Lonsdale P., Haymon R. and Muehlenbachs K., 1987. Hydrothermal sulfide and oxide deposits on seamounts near 21° N, East Pacific Rise. Geol. Soc. Am. Bull., 98: 157-168.

Ashley P.M., Dudley R.J., Lesh R.J., Marr R.H. and Ryall A.W., 1988. The Scuddles Cu-Zn prospect, and Archean volcanogenic massive sulfide deposit, Golden Grove district, Western Australia. Econ. Geol., 83: 918-951.

Barley M.E., 1992. A review of Archean volcanic-hosted massive sulfide and sulfate mineralisation in Western Australia. Econ. Geol., 87: 855-872.

Barrett T.J., Jarvis I., Longstaffe F.J. and Farquhar R., 1988. Geochemical aspects of hydrothermal sediments in the Eastern Pacific Ocean. Canadian Mineralogist, 26: 841-858.

Barrett T.J., Jarvis I. and Jarvis K.E., 1990. Rare earth element geochemistry of massive sulfide-sulfates and gossans on the Southern Explorer Ridge. Geology, 18: 583-586.

Bates R.L. and Jackson J.A., 1987. Glossary of Geology. American Geological Institute, Alexandria, 3rd edition: 805 pp.

Batiza R., Fornari D.J., Vanko D.A. and Lonsdale P., 1984. Craters, calderas, and hyaloclastites on young Pacific seamounts. J. Geophys. Res., 89: 8371-8390.

Batiza R., Smith T.I. and Niu Y., 1989. Geological and petrologic evolution of seamounts near the EPR based on a submersible and camera study. Marine Geophysical Research, 11: 169-236.

Bauld J., D'Amelio E. and Farmer J.D., 1992. Modern microbial mats. In: Schopf, J. W. and Klein, C. (eds.) The Proterozoic biosphere - a multidisciplinary study. Cambridge University Press, 261-269.

Beams S.D. and Dronseika E.V., 1995. The exploration history, geology and geochemistry of the polymetallic Reward and Highway deposits, Mt Windsor Subprovince. 17th International Geochemical Exploration Symposium. Mineral deposits of northeast Queensland: Geology and geophysics, Townsville, Queensland, Abstracts, 137-153.

Beams S.D. and Jenkins D.R., 1995. Regional exploration geochemistry and the regolith of northeast Queensland. 17th International Geochemical Exploration Symposium. Mineral deposits of northeast Queensland: Geology and geophysics, Townsville, Queensland, Abstracts, 33-53.

Beams S., Laing W. and O'Neill D., 1989. The exploration history and geology of the polymetallic Reward deposit, Mt Windsor Volcanic Belt, north Queensland. North Queensland Gold '89 Conference, Townsville, Queensland, 95-102.

Beams S.D., Laurie J.P. and O'Neill D.M., 1990. Reward polymetallic sulfide deposit. In: Hughes, F. E. (ed.) Geology of the mineral deposits of Australia and Papua New Guinea. Australasian Inst. Mining Metall. Mono., 14: 1339-1543.

Beams S., Laing W. and O'Neill D., 1993. The exploration history and geology of the polymetallic Reward deposit, Mt Windsor Volcanic Belt, north Queensland. In: Henderson, R. (eds.) Guide to the economic geology of the Charters Towers region, northeastern Queensland, 81-91.

Bell T.H., 1980. The deformation history of northeastern Queensland - a new framework. In: Henserson, R. A. and Stephenson, P. J. (eds.) The geology and geophysics of northeastern Australia. Geol. Soc. Aust., Queensland division, 307-313.

Bergh S.G. and Sigvaldason G.E., 1991. Pleistocene mass-flow deposits of basaltic hyaloclastite on a shallow submarine shelf, South Iceland. Bull. Volc., 53: 597-611.

Berry R.F., 1989. Structure of the Mount Windsor Sub-province. CODES, University of Tasmania, [unpub.] Report 1: 51-73.

Berry R.F., 1991 Structure of the Mount Windsor Sub-Province. In: Pongratz, J. and Large, R. (eds.) Geological controls on VMS mineralisation in the Mt Windsor Volcanic Belt. [unpub.] CODES, University of Tasmania, Australia: 1-22.

Berry R.F., Huston D.L., Stolz A.J., Hill A.P., Beams S.D., Kuronen U. and Taube A., 1992. Stratigraphy, structure, and volcanic-hosted mineralisation of the Mount Windsor Subprovince, north Queensland, Australia. Econ. Geol., 87: 739-763.

Binns R.A. and Scott S.D., 1993. Actively forming polymetallic sulfide deposits associated with felsic volcanic rocks in the eastern Manus Basin, Papua New Guinea. Econ. Geol., 88: 2226-2236.

Binns R.A., Scott S.D. and PACMANUS participants, 1992. Discovery of active hydrothermal sulfide deposition associated with submarine felsic volcanism, Pual Ridge, Eastern Manus Basin, Papua New Guinea. Geol. Soc. Aust. Abstracts, 32: 41-42.

Binns R.A., Scott S.D., Bogdanov Y.A., Lisitzin A.P., Gordeev V.V., Gurvich E.G., Finlayson E.F., Boyd T., Dotter L.E., Wheller G.E. and Muravyev K., 1993. Hydrothermal oxide and gold-rich deposits of Franklin Seamount, Western Woodlark Basin, Papua New Guinea. Econ. Geol., 88: 2122-2153.

Bodon S.B. and Valenta R.K., 1995. Primary and tectonic features of the Currawong Zn-Cu-Pb(-Au) massive sulfide deposit, Benambra, Victoria: Implications for ore genesis. Econ. Geol., 90: 1694-1721.

Böhlke J.K. and Shanks III W.C., 1994. Stable isotope study of hydrothermal vents at Escanaba Trough: observed and calculated effects of sediment-seawater interaction. In: Morton, J., Zierenberg, R. and Reiss, C. A. (eds.) Geologic, hydrothermal and biological studies at Escanaba Trough, Gorda Ridge, offshore California. US Geol. Surv. Bull., 2022: 223-239.

Boulter C.A., 1993a. High-level peperitic sills at Rio Tinto, Spain: implications for stratigraphy and mineralization. Trans. Instn. Min. Metall., 102: B30-B38.

Boulter C.A., 1993b. Comparison of Rio Tinto, Spain, and Guaymus Basin, Gulf of California: An explanation of a supergiant massive sulfide deposit in an ancient sill-sediment complex. Geology, 21: 801-804.

Boyd T., Scott S.D. and Hekinian R., 1993. Trace element patterns in Fe-Si-Mn Oxyhydroxides at three hydrothermally active seafloor regions. Resource Geology Special Issue, 17: 83-95.

Boynton W.V., 1984 Geochemistry of the rare earth elements: meteorite studies. In: Henderson, P. (ed.) Rare earth element geochemistry. Elsevier, 63-114.

Branney M.J. and Suthren R.J., 1988. High-level peperitic sills in the English Lake District: distinction from block lavas, and implications for Borrowdale Volcanic Group stratigraphy. Geol. J., 23: 171-187.

Branney M.J. and Sparks R.S.J., 1990. Fiamme formed by diagenesis and burial-compaction in soils and subaqueous sediments. J. Geol. Soc. London, 147: 919-922.

Brooks E.R., 1995. Palaeozoic fluidisation, folding, and peperite formation, northern Sierra Nevada, California. Can. J. Earth Sci., 32: 314-324.

Brooks E.R., Wood M.M. and Garbutt P.L., 1982. Origin and metamorphism of peperite and associated rocks in the Devonian Elwell Formation, northern Sierra Nevada, California. Geol. Soc. Am. Bull., 93: 1208-1231.

Burne R.V., 1994. The stromatolite controversies. 12th Australian Geological Convention, Perth, Abstracts, 494-495.

Burne R.V. and Moore L.S., 1987. Microbialites: Organosedimentary deposits of benthic microbial communities. PALAIOS, 2: 241-254.

Busby-Spera C.J., 1986. Depositional features of rhyolitic and andesitic volcaniclastic rocks of the Mineral King submarine complex, Sierra Nevada, California. J. Geophys. Res., 27: 43-76.

Busby-Spera C.J. and White J.D.L., 1987. Variation in peperite textures associated with differing host-sediment properties. Bull. Volc., 49: 765-775.

Campbell I.N.H., Lesher C.M., Coad P., Franklin J.M., Gorton M.P. and Thurston P.C., 1984. Rare-earth element mobility in alteration pipes below massive Cu-Zn sulfide deposits. Chem. Geol., 45: 181-202.

Carey S.N. and Sigurdsson H., 1980. The Roseau Ash: deep-sea tephra deposits from a major eruption on Dominica, Lesser Antilles Arc. J. Volcanol. Geotherm. Res., 7: 67-86.

Carey S., Sigurdsson H., Mandeville C. and Bronto S., 1996. Pyroclastic flows and surges over water: an example from the 1883 Krakatau eruption. Bull. Volc., 57: 493-511.

Carlisle D., 1963. Pillow breccias and their aquagene tuffs, Quadra Island, British Columbia. J. Geol., 71: 48-71.

Cas R.A.F., 1978. Silicic lavas in Paleozoic flysch-like deposits in New South Wales, Australia: behaviour of deep subaqueous silicic flows. Geol. Soc. Am. Bull., 89: 1708-1714.

Cas R.A.F., 1983. Submarine 'crystal tuffs': their origin using a lower Devonian example from southeastern Australia. Geol. Mag., 120: 471-486.

Cas R.A.F., 1992. Submarine volcanism: eruption styles, products, and relevance to understanding the host-rock successions to volcanic-hosted massive sulfide deposits. Econ. Geol., 87: 511-541.

Cas R.A.F. and Wright J.V., 1987. Volcanic Successions: modern and ancient. Unwin Hyman, London, 528 pp.

Cas R.A.F. and Wright J.V., 1991. Subaqueous pyroclastic flows and ignimbrites: an assessment. Bull. Volc., 53: 357-380.

Cas R. and Bull S., 1993. Influence of environment on contrasting styles of volcanism, volcaniclastics, and sedimentation: The Devonian Boyd Volcanic Complex, southeastern Australia. Aust. Geol. Surv. Organisation. 1993/57: 68 pp.

Cas R.A.F., Allen S.W., Bull S.W., Clifford B.A. and Wright J.V., 1990. Subaqueous, rhyolitic dome-top cones: a model based on the Devonian Bunga Beds, southeastern Australia and a modern analogue. Bull. Volc., 52: 159-174.

Cas R.A.F., Landis C.A. and Fordyce R.E., 1989. A monogenetic, Surtla-type, Surtseyan volcano from the Eocene-Oligocene Waiareka-Deborah volcanics, Otago, New Zealand: a model. Bull. Volc., 51: 281-298.

Cas R., Moore L. and Scutter C., 1994. Preliminary observations: submarine dome volcanism, Ponza, Italy. Research Group of Subaqueous Volcanic Successions, Niiigata University, 3.

Cashman K.V. and Fiske R.S., 1991. Fallout of pyroclastic debris from submarine volcanic eruptions. Science, 253: 275-279.

Clarke D.E. and Paine A.G.L., 1970. Charters Towers, Queensland 1:250,000 geological series-explanatory notes. Bureau of Mineral Resources, Geology and Geophysics, Australia.

Cloud P.E.J. and Semikhatov M.A., 1969. Proterozoic stromatolite zonation. Am. J. Sci., 267: 1017-1061.

Clough B.J., Walker J.V. and Walker G.P.L., 1982. Morphology and dimensions of young comendite lavas of La Primavera volcano, Mexico. Geol. Mag., 5: 477-485.

Cole J.W., 1990. Structural control and origin of volcanism in the Taupo volcanic zone, New Zealand. Bull. Volc., 52: 445-459.

Cortesse M., Frazzetta G. and La Volpe C., 1986. Volcanic history of Lipari (Aeolian Islands, Italy) during the last 10,000 years. J. Volcanol. Geotherm. Res., 27: 117-133.

Davey F.J., Henrys S.A. and Lodolo E., 1995. Asymmetric rifting in a continental back-arc environment, North Island, New Zealand. J. Volcanol. Geotherm. Res., 68: 209-238.

Davidson G., Stolz A.J. and Eggins S.M., 1996. Exhalite geochemistry: A preliminary geochemical documentation of two barren ferruginous chert bodies in the Mount Windsor Volcanics. CODES, University of Tasmania.

Davis B.K. and McPhie J., 1996. Spherulites, quench fractures and relict perlite in a Late Devonian rhyolite dyke, Queensland, Australia. J. Volcanol. Geotherm. Res., 71: 1-11.

Davis E.E. and Villinger H., 1992. Tectonic and thermal structure of the Middle Valley sedimented rift, Northern Juan De Fuca Ridge. Proc ODP, Initial Reports, 139: 9-41.

Davis E.E. and Becker K., 1994. Thermal and tectonic structure of the Escanaba Trough: new heat-flow measurements and seismic reflection profiles. In: Morton, J., Zierenberg, R. and Reiss, C. A. (eds.) Geologic, hydrothermal and biological studies at Escanaba Trough, Gorda Ridge, offshore California. US Geol. Surv. Bull., 2022: 45-64.

Davis L.W., 1975. Captains Flat lead-zinc orebody. Aust. Inst. Mining Metall. Mon., 5: 694-700.

De Rosen-Spence A.F., Provost G., Dimroth E., Gochnauer K. and Owen V., 1980. Archean subaqueous felsic flows, Rouyn-Noranda, Quebec, Canada and their Quaternary equivalents. Precambrian Res., 12: 43-77.

Dean J.A. and Carr G.R., 1992. Final report to Aberfoyle Resources Limited on the Pb isotopic compositions of mineralisation from Highway/Reward, Mt Windsor Joint Venture Project, NE Queensland. CSIRO Australia. Sirotope report SR22.

Delany P.T., 1982. Rapid intrusion of magma into wet rock: groundwater flow due to pore pressure increases. J. Geophys. Res., 87: 7739-7756.

Demicco R.V. and Hardie L.A., 1994. Sedimentary structures and early diagenetic features of shallow marine carbonate deposits. SEPM Atlas Series, 365 pp.

Denlinger R.P. and Holmes M.L., 1994. A thermal and mechanical model for sediment hills and associated sulfide deposits along the Escanaba Trough. In: Morton, J. L., Zierenberg, R. and Reiss, C. A. (eds.) Geologic hydrothermal and biological studies at Escanaba Trough, Gorda Ridge, offshore California. US Geol. Surv. Bull., 2022: 65-75.

Dimroth E. and Yamagishi H., 1987. Criteria for the recognition of ancient subaqueous pyroclastic rocks. Geol. Surv. Hokkaido Rep., 58: 55-88.

Dimroth E., Cousineau P., Leduc M. and Sanschagrin Y., 1978. Structure and organisation of Archean basalt flows, Rouyn-Noranda area, Quebec, Canada. Can. J. Earth Sci., 15: 902-918.

Dolozi M.B. and Ayres L.D., 1991. Early Proterozoic, basaltic andesite tuff breccia: downslope, subaqueous mass transport of phreatomagmatically-generated tephra. Bull. Volc., 53: 477-495.

Doyle M.G., 1994. Facies architecture of a submarine volcanic centre: Highway-Reward, Mount Windsor Volcanics, Cambro-Ordovician, Northern Queensland. In: Henderson, R. A. and Davis, B. K. (eds.) New developments in geology and matallogeny: Northern Tasman Orogenic Zone. EGRU Contribution, 50: 149-150.

Doyle M.G., 1995. Preliminary investigation of alteration at the Highway and Reward deposits, Mount Windsor Volcanics, Queensland. [unpub.] Report 1, AMIRA - P439, 149-160.

Doyle M.G., 1996. Volcanic influences in the formation of iron oxide-silica deposits in a volcanogenic-massive sulfide terrain, Mount Windsor Volcanic belt, Queensland. Australian Mineral Industries Research Association Limited - P439. 87-142.

Doyle M.G. and McPhie J., 1994. A silicic submarine syn-sedimentary intrusive-dome-hyaloclastite host sequence to massive sulfide mineralisation: Mount Windsor Volcanics, Cambro-Ordovician, Australia. IAVCEI International Volcanological Congress, Ankara, Turkey, Theme 10, Abstracts.

Doyle M.G., Allen R.L. and McPhie J., 1993. Textural effects of devitrification and hydrothermal alteration in silicic lavas and shallow intrusions, Mount Read Volcanics (MRV), Cambrian, Tasmania. IAVCEI General Assembly, Ancient Volcanism and Modern Analogues, Abstracts, Canberra, 51.

Duffield W.A., Bacon C.R. and Delaney P.T., 1986. Deformation of poorly consolidated sediment during shallow emplacement of a basalt sill, Coso Range, California. Bull. Volc., 48: 97-107.

Duhig N.C., Davidson G.J. and Stolz J., 1992a. Microbial involvement in the formation of Cambrian sea-floor silica-iron oxide deposits, Australia. Geology, 20: 511-514.

Duhig N.C., Stolz J.S., Davidson G.J. and Large R.R., 1992b. Cambrian microbial and silica gel textures in silica iron exhalites from the Mount Windsor Volcanic Belt, Australia: Their petrography, chemistry, and origin. Econ. Geol., 87: 764-784.

Einsele G., 1986. Interaction between sediments and basalt injections in young Gulf of California-type spreading centres. Geol. Rund., 75: 197-208.

Einsele G., Gieskes J.M., Curray J.R., Moore D.M., Aguayo E., Aubry M.P., Fornari D., Guerrero J., Kastner M., Kelts K., Lyle M., Matoba Y., Molina-Cruz A., Niemitz J., Rueda J., Saunders A., Schrader H., Simoneit B. and Vacquier V., 1980. Intrusion of basaltic sills into highly porous sediments and resulting hydrothermal activity. Nature, 283: 441-445.

Fergusson C.L., Henderson R.A. and Wright J.V., 1994. Facies in a Devonian-Carboniferous volcanic fore-arc succession, Campwyn Volcanics, Mackay district, central Queensland. Aust. J. Earth Sci., 41: 287-300.

Fisher R.V., 1960. Classification of volcanic breccias. Geol. Soc. Am. Bull., 71: 973-982.

Fisher R.V. and Schmincke H.U., 1984. Pyroclastic rocks. Springer-Verlag, Berlin, 472 pp.

Fiske R.S., 1963. Subaqueous pyroclastic flows in the Ohanapecosh Formation, Washington. Geol. Soc. Am. Bull., 74: 391-406.

Fiske R.S. and Matsuda T., 1964. Submarine equivalents of ash flows in the Tokiwa Formation, Japan. Am. J. Sci., 262: 76-106.

Fouquet Y., Von Stackelberg U., Charlou J.L., Erzinger J., Herzig P.M., Muhe R. and Wiedicke M., 1993. Metallogenesis in back-arc environments: The Lau Basin example. Econ. Geol., 88: 2154-2181.

Fournier R.O., 1985. The behaviour of silica in hydrothermal solutions. Reviews in Economic Geology, 2: 45-61.

Francis E.H. and Howells M.F., 1973. Transgressive welded ash-flow tuffs among the Ordovician sediments of NE Snowdonia, N Wales. J. Geol. Soc. London, 129: 621-641.

Franklin J.M., Sangster D.F. and Lydon J.W., 1981. Volcanic-associated massive sulfide deposits. Econ. Geol., 75th Aniv. Vol., 485-627.

Frey R.W. and Pemberton S.G., 1984. Trace fossil models. In: Walker, R. G. (ed.) Facies models. Geoscience Canada, Toronro, 189-207 pp.

Fridleifsson I.B., Furnes H. and Atkins F.B., 1982. Subglacial volcanics - on the control of magma chemistry on pillow dimensions. J. Volcanol. Geotherm. Res., 13: 84-117.

Friedman I. and Smith R.L., 1958. The deuterium content of water in some volcanic glasses. Geochim Cosmochim Acta, 15: 218-228.

Friedman I., Smith R.G. and Long W.D., 1966. Hydration of natural glass and formation of perlite. Geol. Soc. Am. Bull., 77: 323-328.

Furnes H., Fridleifsson I.B. and Atkins F.B., 1980. Subglacial volcanics - on the formation of acid hyaloclastites. J. Volcanol. Geotherm. Res., 8: 95-110.

Galley A.G., Bailes A.H. and Kitzler G., 1993. Geological setting and hydrothermal evolution of the Chisel Lake and North Chisel Zn-Pb-Cu-Ag-Au- massive sulfide deposits, Snow Lake, Manitoba. Explor. Mining. Geol., 2: 271-295.

Galley A.G., Watkinson D.H., Jonasson I.R. and Riverin G., 1995. The subsea-floor formation of volcanic-hosted massive sulfide: Evidence from the Ansil deposit, Rouyn-Noranda, Canada. Econ. Geol., 90: 2006-2017.

Gamble J.A., Wright I.C. and Baker J.A., 1993. Seafloor geology and petrology in the oceanic to continental transition zone of the Kermadec-Havre-Taupo Volcanic Zone. NZ J. Geol. Geophys., 36: 417-435.

German C.R., Klinkhammer G.P., Edmond J.M., Mitra A. and Elderfield H., 1990. Hydrothermal scavenging of rare-earth elements in the ocean. Nature, 345: 516-518.

Goldfarb M.S., Converse D.R., Holland H.D. and Edmond J.M., 1983. The genesis of hot spring deposits on the East Pacific Rise, 21°N. Econ. Geol. Mon., 5: 184-197.

Goodfellow W.D. and Blaise B., 1988. Sulfide formation and hydrothermal alteration of hemipelagic sediment in Middle Valley, Northern Juan de Fuca Ridge. Canadian Mineralogist, 26: 675-696.

Goodfellow W.D. and Franklin J.M., 1993. Geology, mineralogy, and chemistry of sediment-hosted clastic massive sulfides in shallow cores, Middle Valley, Northern Juan de Fuca Ridge. Econ. Geol., 88: 2037-2068.

Goodwin A.M., 1962. Structure, stratigraphy, and origin of iron formations, Michipicoten area, Algoma district, Ontatio, Canada. Geol. Soc. Am. Bull., 73: 561-586.

Goto Y. and McPhie J., 1996. A Miocene basanite peperitic dyke at Stanley, northwestern Tasmania, Australia. J. Volcanol. Geotherm. Res., 74: 111-120.

Graf J.L., 1977. Rare earth elements as hydrothermal tracers during the formation of massive sulfide deposits in volcanic rocks. Econ. Geol., 72: 527-548.

Grant J.A., 1986. The isocon diagram-A simple solution to Gresens' equation for metasomatic alteration. Econ. Geol., 81: 1976-1982.

Green G.R., Solomon M. and Walshe J.L., 1981. The formation of the volcanic-hosted massive sulfide ore deposit at Rosebery, Tasmania. Econ. Geol., 76: 304-338.

Gregory P.W. and Hartley J.S., 1982. The Thalanga Zinc-Lead-Copper-Silver deposit. In: Withnall, I. W. (ed.) Handbook for the 1982 Field Conference-Charters Towers-Greenvale area: Brisbane. Geol. Soc. Aust., Queensland division, 12-21.

Gregory P.W., Hartley J.S. and Wills K.J.A., 1987. The Thalanga massive sulfide deposit. Pacific Rim Congress 87, Proceedings, Gold Coast, Australia, 573-577.

Gregory P.W., Hartley J.S. and Wills K.J.A., 1990. Thalanga zinc-lead-copper-silver deposit. In: Hughes, F. E. (ed.) Geology of the mineral deposits of Australia and Papua New Guinea. Aust. Inst. Mining and Metall. Mono., 14: 1527-1537.

Grey K., 1984. Biostratigraphic studies of stromatolites from the Proterozoic Earaheedy Group, Nabberu Basin, Western Australia. Geol. Surv. Western Australia Bull., 103: 123 pp.

Grey K. and Thorne A.M., 1985. Biostratigraphic significance of stromatolites in upwardly shallowing sequences of the early Proterozoic Duck Creek Dolomite, Western Australia. Precambrian Res., 29: 183-206.

Grimes K.G., 1980. The Tertiary geology of north Queensland. In: Henderson, R. A. and Stephenson, P. J. (eds.) The geology and geophysics of northeastern Australia. Geol. Soc. Aust., Queensland division, 329-347.

Guilbert J.M. and Park C.P., 1986. The geology of ore deposits. Freedman, New York, 985 pp.

Hannington M.D. and Scott S.D., 1988. Mineralogy and geochemistry of a hydrothermal silica-sulfide-sulfate spire in the caldera of axial seamount, Juan De Fuca Ridge. Canadian Mineralogist, 26: 603-625.

Hannington M.D., Jonasson I.R., Herzig P.M. and Peterson S., 1995 Physical and chemical processes of seafloor mineralisation at Mid-Ocean Ridges. In: Humphries, S., Zierenberg, R., Mullineaux, L. and Thomson, R. (eds.) Seafloor hydrothermal systems: physical, chemical, biological, and geological interactions. Geophysical Monograph 91, 115-157.

Hanson R.E., 1991. Quenching and hydroclastic disruption of andesitic to rhyolitic intrusions in an submarine island-arc sequence, northern Sierra Nevada, California. Geol. Soc. Am. Bull., 103: 804-816.

Hanson R.E. and Schweickert R.A., 1982. Chilling and brecciation of a Devonian rhyolitic sill intruded into wet sediments, northern Sierra Nevada, California. J. Geol., 90: 717-724.

Hanson R.E. and Wilson T.J., 1991. Submarine rhyolitic volcanism in a Jurassic proto-marginal basin; southern Andes, Chile and Argintina. In: Harmon, R. S. and Rapela, C. W. (eds.) Andean magmatism and its tectonic setting. Geol. Soc. Am. Spec. Pub., 265: 13-27.

Hanson R.E. and Wilson T.J., 1993. Large-scale rhyolite peperites (Jurassic, southern Chile). J. Volcanol. Geotherm. Res., 54: 247-264.

Hartley J.S., Peters S.G. and Beams S.D., 1989. Current developments in Charters Towers geology and gold mineralisation. North Queensland Gold '89 Proceedings, Townsville, Queensland, 7-14.

Hartley J.S., Peters S.G. and Beams S.D., 1993. Geological context and concepts of mineralisation in the Charters Towers region. In: Henderson, R. A. (ed.) Guide to the economic geology of the Charters Towers region, northern Queensland. Geol. Soc. Aust., Queensland division, 49-59.

Haslett P.G., 1976. Lower Cambrian stromatolites from open and sheltered intertidal environments, Wirrealpa, South Australia. In: Walter, M. R. (ed.) Stromatolites. Elsevier, 656-584.

Haymon R.M., Koski R.A. and Sinclair C., 1984. Fossils of hydrothermal vent worms from Cretaceous sulfide ores of the Samail ophiolite, Oman. Science, 223: 1407-1409.

Haymon R.M., Fornari D.J., Von Damm K.L., Lilley M.D., Perfit M.R., Edmond J.M., III W.C.S., Lutz R.A., Grebmeier J.M., Carbotte S., Wright D., McLaughlin E., Smith M., Beedle N. and Olson E., 1993. Volcanic eruption of the mid-ocean ridge along the East Pacific Rise crest at 9°45-52'N: Direct submersible observations of seafloor phenomena associated with an eruption event in April, 1991. Earth and Planetary Science Letters, 119: 85-101.

Heiken G. and Wohletz K., 1985. Volcanic ash. University of California Press, Berkeley, 246 pp.

Hekinian R. and Fouquet Y., 1985. Volcanism and metallogenesis of axial and off-axial structures on the East Pacific Rise near 13°N. Econ. Geol., 80: 221-249.

Hekinian R., Francheteau J., Renard V., Ballard R.D., Choukroune P., Cheminee J.L., Albarede F., Minster J.F., Charlou J.L., Marty J.C. and Boulegue J., 1983. Intense hydrothermal activity at the axis of the East Pacific Rise near 13°N: submersibe witnesses the growth of sulfide chimney. Marine Geophysical Researches, 6: 1-14.

Hekinian R., Hoffert M., Larqué P., Cheminéé J.L., Stoffers P. and Bideau D., 1993. Hydrothermal Fe and Si oxyhydroxide deposits from South Pacific intraplate volcanoes and East Pacific Rise axial and off-axial regions. Econ. Geol., 88: 2099-2121.

Henderson R.A., 1980. Structural outline and summary geological history for northeastern Australia. In: Henserson, R. A. and Stephenson, P. J. (eds.) The geology and geophysics of northeastern Australia. Geol. Soc. Aust., Queensland division: 1-27.

Henderson R.A., 1983. Early Ordovician faunas from the Mount Windsor Subprovince, northeastern Queensland. Memoirs Association Australasian Palaeontologists, 1: 145-175.

Henderson R.A., 1986. Geology of the Mt Windsor Subprovince-a Lower Proterozoic volcano-sedimentary terrane in the northern Tasman Orogenic Zone. Aust. J. Earth Sci., 33: 343-364.

Henderson R.A. and Nind M.A.P., 1994. Tertiary units, landscape and regolith of the Charters Towers Region. In: Henderson R.A. and Davis B.K. (eds.) New developments in geology and metallogeny: Northern Tasman Orogenic Zone, Townsville, Queensland: 17-21.

Herrmann W., 1995. Geochemical aspects of the Thalanga massive sulfide deposit, Mt Windsor Subprovince. In: Beams S.D. (ed.) 17th International Geochemical Exploration Symposium. Mineral deposits of northeast Queensland: Geology and geophysics, Townsville, Queensland, 155-170.

Herzig P.M., Becker K.P., Stoffers P., Backer H. and Blum N., 1988. Hydrothermal silica chimney fields in the Galapagos spreading center at 86° W. Earth and Planetary Science Letters, 89: 261-272.

Hill A.P., 1991. Structure and metal zonation of the Thalanga VMS-deposit, north Queensland. SGEG ore fluid conference, Canberra, Abstracts, 36.

Hill A.P., 1993. Synchronous felsic volcanism and sea-floor base-metal sulphide mineralisation at East Thalanga, north Queensland, Australia. IAVCEI General Assembly, Canberra, Australia, Abstracts, 48.

Hill A.P., 1996. Structure, volcanic setting, hydrothermal alteration and genesis of the Thalanga massive sulfide deposit [Ph.D]. University of Tasmania, 404 pp.

Hofmann H.J. and Jackson G.D., 1987. Proterozoic ministromatolites with radial-fibrous fabric. Sedimentology, 34: 963-971.

Holm N.G., 1987. Biogenic influences on the geochemistry of certain ferruginous sediments of hydrothermal origin. Chem. Geol., 63: 45-57.

Holm N.G., 1989. The $^{13}C/^{12}C$ ratios of siderite and organic matter of a modern metalliferous hydrothermal sediment and their implications for banded iron formations. Chem. Geol., 77: 41-45.

Horikoshi E., 1969. Volcanic activity related to the formation of the Kuroko-type deposits in the Kosaka district, Japan. Mineral. Deposita, 4: 321-345.

Houghton B.F. and Landis C.A., 1989. Sedimentation and volcanism in a Permian arc-related basin, southern New Zealand. Bull. Volc., 51: 433-450.

Houghton B.F. and Wilson C.J.N., 1989. A vesicularity index for pyroclastic deposits. Bull. Volc., 51: 451-462.

Houghton B.F., Wilson C.J.N., McWilliams M.O., Lanphere M.A., Weaver S.D., Briggs R.M. and Pringle M.S., 1995. Chronology and dynamics of a large silicic magmatic system: central Taupo Volcanic Zone, New Zealand. Geology, 23: 13-16.

Howells M.F., Reedman A.J. and Campbell S.D.G., 1986. The submarine eruption and emplacement of the Lower Rhyolitic Tuff Formation (Ordovician), N Wales. J. Geol. Soc. London, 143: 411-423.

Humphris S.E., Herzig P.M., Miller D.J., Alt J.C., Becker K., Brown D., Brügmann G., Chiba H., Foquet Y., Gemmell J.B., Guerin G., Hannington M.D., Holm N.G., Honnorez J.J., Iturrino G.J., Knott R., Ludwig R., Nakamura K., Petersen S., Reysenbach A.-L., Rona P.A., Smith S., Sturz A.A., Tivey M.K. and Zhao X., 1995. The internal structure of an active sea-floor massive sulphide deposit. Nature, 377: 713-716.

Hunns S.R., 1994 Geology of the Mount Chalmers volcanic-hosted massive sulfide, and implications for its formation. In: Holcombe, R., Stephens, C. and Fielding, C. (eds.) 1994 Field Conference: Capricorn region central coastal Queensland. Geol. Soc. Aust., Queensland division, 80-92.

Hunns S.R., Zaw K., Large R.R., Dean J.A., Ryan C.G. and McPhie J., 1994 Preliminary geochemical results constraining the formation of the Mount Chalmers volcanic-hosted massive sulfide deposit. In: Henderson, R. and Davis, B. (eds.) New developments in geology and metallogeny: Northern Tasman Orogenic Zone. EGRU Contribution 50, 117-124.

Huston D.L., 1988. Aspects of the geology of massive sulfide deposits from the Balcooma district, Northern Queensland and Rosebery, Tasmania: Implications for ore genesis [Unpublished Ph.D thesis]. University of Tasmania, 380 pp.

Huston D.L., 1992. Geological and geochemical controls on mineralisation at the Reward deposit: detailed studies of the Highway pipe. [unpub.] CODES, University of Tasmania. 31 pp.

Huston D.L., 1993. The effect of alteration and metamorphism on wall rocks to the Balcooma and Dry River South volcanic-hosted massive sulfide deposits, Queensland, Australia. J. Geoch. Explor., 48: 277-307.

Huston D.L., Taylor T., Fabray J. and Patterson D.J., 1992. A comparison of the geology and mineralisation of the Balcooma and Dry River South volcanic-hosted massive sulfide deposits, northern Queensland. Econ. Geol., 87: 785-811.

Huston D.L., Kuronen U. and Stolz J., 1995. Waterloo and Arincourt prospects, northern Queensland: contrasting styles of mineralisation within the same volcanogenic hydrothermal system. Aust. J. Earth Sci., 42: 203-221.

Hutton L.J. and Crouch S.B.S., 1993. New and revised igneous units in the Charters Towers and Dotswood 1:100 000 sheet areas. Queensland Government Mining Journal, 23-26.

Hutton L.J., Perkins I.P. and Wyborn D., 1990. A reinterpretation of the Ravenswood Batholith, North Queensland. Pacific Rim Congress '90, Proceedings: 179-185.

Hutton L.J., Hartley J.S. and Riekins I.P., 1993. Geology of the Charters Towers region. In: Henderson, R. A. (ed.) Guide to the economic geology of the Charters Towers region, northeastern Queensland. Geol. Soc. Aust., Queensland division, 1-12.

Hutton L.J., Jenkins I.P., Woods K.T., Hartley J.S. and Crouch S.B.S., 1994. A geochemically and structurally based reinterpretation of the Ravenswood Batholith. In: Henderson R.A. and Davis B.K. (eds.) New developments in geology and metallogeny: Northern Tasman Orogenic Zone, Townsville, Queensland, 3-5.

Jack D.J., 1989. Hellyer host rock alteration [Unpub. M.Sc. thesis]. University of Tasmania, 182 pp.

Jagodzinski E.A. and Cas R.A.F., 1993. Preserved remnants of the original pyroclastic flow in subaqueous, crystal-rich volcaniclastic deposits of the Big Sunday Formation: genetic implications. IAVCEI General Assembly, Canberra, Australia, Abstracts, 53.

James H.L., 1954. Sedimentary facies of iron formations. Econ. Geol., 49: 235-293.

Janecky D.R. and Seyfried W.E.J., 1984. Formation of massive sulfide deposits on oceanic ridge crests: Incremental reaction models for mixing between hydrothermal solutions and seawater. Geochim Cosmochim Acta, 48: 2723-2738.

Johnson A.C., 1991. Mount Windsor EPM 3380: Geological compilation (sheet 1 and 2). Barrack Mine Management Pty. Ltd. [unpub.]

Johnson H.D. and Baldwin C.T., 1996. Shallow clastic seas. In: Reading, H. G. (ed.) Sedimentary environments: processes, facies and stratigraphy. Blackwell Sciences, Cambridge, 232-280.

Jones J.G., 1969. Pillow lavas as depth indicators. Am. J. Sci., 267: 181-195.

Juniper S.K. and Fouquet Y., 1988. Filamentous iron-silica deposits from modern and ancient hydrothermal sites. Canadian Mineralogist, 26: 859-869.

Kah L.C. and Grotzinger J.P., 1992. Early Proterozoic (1.9 Ga) Thrombolites of the Rocknest Formation, Northwest Territories, Canada. Palaios, 7: 305-315.

Kalogeropoulos S.I. and Scott S.D., 1983. Mineralogy and geochemistry of tuffaceous exhalites (Tetsusekiei) of the Fukazawa mine, Hokuroku district, Japan. Econ. Geol. Mon., 5: 412-432.

Kalogeropoulos S.I. and Scott S.D., 1989. Mineralogy and geochemistry of an Archean tuffaceous exhalite: the Main Contact Tuff, Millenbach mine area, Noranda, Quebec. Can. J. Earth Sci., 26: 88-105.

Kano K.I., 1989. Interactions between andesitic magma and poorly consolidated sediments: examples in the Neogene Shirahama Group, South Izu, Japan. J. Volcanol. Geotherm. Res., 37: 59-75.

Kano K., Takeuchi K., Yamamoto T. and Hoshizumi H., 1991. Subaqueous rhyolite block lavas in the Miocene Ushikiri Formation, Shimane Peninsula, SW Japan. J. Volcanol. Geotherm. Res., 46: 241-253.

Kano K., Orton G.J. and Kano T., 1994. A hot Miocene subaqueous scoria-flow deposit in the Shimane Peninsula, SW Japan. J. Volcanol. Geotherm. Res., 60: 1-14.

Kato Y., 1987. Woody pumice generated with submarine eruption. J. Geol. Soc. Japan, 93: 11-20.

Kay J.R., 1982. Notes on the geology of the Highway gold mine, Charter Towers. In: Withnall I.W. (ed.) Geol. Soc. Aust. 1982 Field Conference, Charters Towers-Greenvale area.

Kay J.R., 1987. The Highway gold mine, Charters Towers-submarine volcanogenic gold-barite stringer mineralisation, modified by lateritic weathering. University of Queensland, Department of Geology Paper, 12: 111-125.

Khin Zaw and Large R.R., 1992. The precious metal-rich South Hercules mineralisation, western Tasmania: A possible subsea-floor replacement volcanic-hosted massive sulfide deposit. Econ. Geol., 87: 931-952.

Knoll A.H. and Simonson B., 1981. Early Proterozoic microfossils and penecontemporaneous quartz cementation in the Sokoman Iron Formation, Canada. Science, 211: 478-480.

Kohn B.P. and Glasby G.P., 1978. Tephra distribution and sedimentation rates in the Bay of Plenty, New Zealand. NZ J. Geol. Geophys., 21: 49-70.

Kokelaar B.P., 1982. Fluidization of wet sediments during emplacement and cooling of various igneous bodies. J. Geol. Soc. London, 139: 21-33.

Kokelaar P., 1986. Magma-water interactions in subaqueous and emergent basaltic volcanism. Bull. Volc., 48: 275-289.

Kokelaar P., 1993. Volcaniclastic density currents: basic concepts and definitions. In: McPhie, J. (ed.) Explosive volcanism: processes and products. CEV short course, Canberra, 7.1-7.7.

Kokelaar B.P. and Durant G.P., 1983a. The submarine eruption and erosion of Surtla (Surtsey), Iceland. J. Volcanol. Geotherm. Res., 19: 239-246.

Kokelaar B.P. and Durant G.P., 1983b. The petrology of basalts from Surtla (Surtsey), Iceland. J. Volcanol. Geotherm. Res., 19: 247-253.

Kokelaar P. and Romangnoli C., 1995. Sector collapse, sedimentation and clast population evolution at an active island-arc volcano: Stromboli, Italy. Bull. Volc., 57: 240-262.

Kokelaar B.P., Bevins R.E. and Roach R.A., 1985. Submarine silicic volcanism and associated sedimentary and tectonic process, Ramsey Island, SW Wales. J. Geol. Soc. London, 142: 591-613.

Koski R.A., Clague D.A. and Oudin E., 1984. Mineralogy and chemistry of massive sulfide deposits from the Juan de Fuca Ridge. Geol. Soc. Am. Bull., 95: 930-945.

Krynauw J.R., Hunter D.R. and Wilson A.H., 1988. Emplacement of sills into wet sediments at Grunehogna, western Dronning Maud Land, Antarctica. J. Geol. Soc. London, 145: 1019-1032.

Kurokawa A., 1991. Formation of felsic pumiceous hyaloclastites: a case study from Tadami district, Fukushima Prefecture, Japan. Ganko Journal of mineralogy, petrology and economic geology, 86: 439-458.

Kurokawa A., 1992. Felsic pumiceous hyaloclastite in central Japan. 29th International Geological Congress, Kyoto, Japan, Abstracts: 499.

Lackschewitz K.S., Dehn J. and Wallrabe-Adams H.J., 1994. Volcaniclastic sediments from mid-oceanic Kolbeinsey Ridge, north of Iceland: Evidence for submarine volcanic fragmentation processes. Geology, 22: 975-978.

Laing W.P., 1988. Structure of the Reward deposit, north Queensland. Unpublished report to Terra Search Pty. Ltd.

Large R.R., 1977. Chemical evolution and zonation of massive sulfide deposits in volcanic terrains. Econ. Geol., 72: 549-572.

Large R.R., 1991. Ore deposit models and exploration criteria for VMS deposits in the Mt Windsor Volcanics. In: Pongratz, J. P. and Large, R. R. (eds.) Geological controls on VMS mineralisation in the Mt Windsor Volcanic Belt-research report No. 2 [unpub.], 181-198.

Large R.R., 1992. Australian volcanic-hosted massive sulfide deposits: features, styles, and genetic models. Econ. Geol., 87: 471-510.

Large R.R. and Both R.A., 1980. The volcanogenic ores at Mount Chalmers, eastern Queensland. Econ. Geol., 75: 992-1009.

Large R.R., McGoldrick P.J., Berry R.F. and Young C.H., 1988. A tightly folded, gold-rich, massive sulfide deposit: Que River mine, Tasmania. Econ. Geol., 83: 681-693.

Large R.R., Huston D., McGoldrick P.J., Ruxton R.A. and McArthur G., 1989. Gold distribution and genesis in Australian volcanogenic massive sulfide deposits, and their significance for gold transport models. Econ. Geol. Mon., 6: 520-536.

Lawson D.E., 1972. Torridonian volcanic sediments. Scott J Geol, 4: 345-362.

Leat P.T. and Thompson R.N., 1988. Miocene hydrovolcanism in NW Colorado, USA, fuelled by explosive mixing of basic magma and wet unconsolidated sediment. Bull. Volc., 50: 229-243.

Ledbetter M.T. and Sparks R.S.J., 1979. Duration of large-magnitude explosive eruptions deduced from graded bedding in deep-sea ash layers. Geology, 7: 240-244.

Letouzey J. and Kimura M., 1985. Okinawa Trough genesis: Structure and evolution of a back-arc basin developed in a continent. Marine and Petroleum Geology, 2: 111-130.

Levingston K.R., 1981. Geological evolution and economic geology of the Burdekin River region, Queensland. Bureau of Mineral Resources, Geology and Geophysics. Bulletin 208: 48 pp.

Lewis K.B. and Pantin H.M., 1984. Intersection of a marginal basin with a continent: structure and sediments of the Bay of Plenty, New Zealand. In: Kokelaar, B. P. and Howells, M. F. (eds.) Marginal Basin Geology. Geol. Soc. London, Spec. Pub., 16: 121-135.

Lilley M.D., Feely R.A. and Trefry J.H., 1995 Chemical and biochemical transformations in hydrothermal plumes. In: Humphris, S., Zierenberg, R., Mullineaux, L. and Thomson, R. (eds.) Seafloor hydrothermal systems: physical, chemical, biological and geological interactions. Geophysical Monograph, 91: 369-391.

Lock B.E., 1972. A lower Palaeozoic rheo-ignimbrite from White Bay, Newfoundland. Can. J. Earth Sci., 9: 1495-1503.

Logan B.W., Rezak R. and Ginsburg R.N., 1964. Classification and environmental significance of algal stromatolites. J. Geol., 72: 68-83.

Lonsdale P. and Batiza R., 1980. Hyaloclastite and lava flows on young seamounts examined with a submersible. Geol. Soc. Am. Bull., 91: 545-554.

Lorenz B.E., 1984. Mud-magma interactions in the Dunnage Mélange, Newfoundland. In: Kokelaar, B. P. and Howells, M. F. (ed.) Marginal Basin geology - volcanic and associated sedimentary and tectonic processes in modern and ancient marginal basins. Geol. Soc. Lond. Spec. Pub., 16: 271-277 pp.

Lottermoser B.G., 1989. Rare earth element study of exhalites within the Willyama Supergroup, Broken Hill Block, Australia. Mineral. Deposita, 24: 92-99.

Lowe D.R., 1982. Sediment gravity flows: II. Depositional models with special reference to the deposits of high density turbidity currents. Journal of Sedimentology, 52: 279-297.

Lydon J.W., 1988a. Volcanogenic massive sulfide deposits part 1: a descriptive model. In: Roberts, R. G. and Sheahan, P. A. (eds.) Ore deposit models. Geoscience Canada, Reprint series 3: 145-153.

Lydon J.W., 1988b. Volcanogenic massive sulfide deposits part 2: genetic models. In: Roberts, R. G. and Sheahan, P. A. (eds.) Ore deposit models. Geoscience Canada, Reprint series 3: 155-181.

Macdonald G.A., 1972. Volcanoes. Prentice Hall, New Jersey, 510 pp.

McBirney A.R., 1963. Factors governing the nature of submarine volcanism. Bull. Volc., 26: 455-469.

MacLean W.H. and Kranidiotis P., 1987. Immobile elements as monitors of mass transfer in hydrothermal alteration: Phelps Dodge massive sulfide deposit, Matagami, Quebec. Econ. Geol., 82: 951-962.

McLennan S.M. and Taylor S.R., 1979. Rare earth element mobility associated with uranium mineralisation. Nature, 282: 247-250.

McPhie J., 1993. The Tennant Creek porphyry revisited: a syn-sedimentary sill with peperite margins, early Proterozoic, Northern Territory. Aust. J. Earth Sci., 40: 545-558.

McPhie J. and Allen R.L., 1992. Facies architecture of mineralised submarine volcanic sequences: Cambrian Mount Read Volcanics, western Tasmania. Econ. Geol., 87: 587-596.

McPhie J. and Large R., 1992. The Highway-Reward prospect: a brief description of the volcanic facies and nature of mineralisation. CODES, University of Tasmania. [Unpub.] Report to Aberfoyle Resources Ltd. 11 pp.

McPhie J. and Hunns S.R., 1995. Secondary welding of submarine, pumice-lithic breccia at Mount Chalmers, Queensland, Australia. Bull. Volc., 57: 170-178.

McPhie J., Doyle M.G. and Allen R.L., 1993. Volcanic Textures. CODES, University of Tasmania, Hobart, 198 pp.

Messenger P.R. and Taube A., 1994 The northern part of the Calliope Volcanic Assemblage, Mt Morgan-Dee Range area. In: Holcombe, R., Stephens, C. and Fielding, C. (eds.) 1994 Field Conference: Capricorn region, central coastal Queensland. Geol. Soc. Aust., Queensland division, 46-63.

Michard A., 1989. Rare earth element systematics in hydrothermal fluids. Geochemica et Cosmochimica acta, 53: 745-750.

Michard A., Albarède F., Michard G., Minister J.F. and Chalou J.L., 1983. Rare-earth elements and uranium in high-temperature solutions from the East Pacific Rise hydrothermal vent field (13° N). Nature, 303: 795-797.

Michard A. and Albarède F., 1986. The REE content of some hydrothermal fluids. Chem. Geol., 55: 51-60.

Miller C.R., 1996. Geological and geochemical aspects of the Liontown VHMS deposit, NE Queensland [M. Econ. Geol.]. University of Tasmania, 90 pp.

Monty C.L., 1977. Evolving concepts on the nature and ecological significance of stromatolites. In: Flugel, E. (ed.) Fossil algae: recent results and developments. Springer Verlag, 14-35.

Moore D.G., 1962. Bearing strength and other physical properties of some shallow and deep-sea sediments from the North Pacific. Geol. Soc. Am. Bull., 73: 1163-1166.

Moore J.G., Phillips R.L., Grigg R.W., Peterson D.W. and Swanson D.A., 1973. Flow of lava into the sea, 1969-1971, Kilauea Volcano, Hawaii. Geol. Soc. Am. Bull., 84: 537-546.

Morrison G.W., 1988. Palaeozoic gold deposits of northeast Queensland. Bicentenial Gold 88, Melbourne, Abstracts, 91-101.

Mueller W. and White J.D.L., 1992. Felsic fire-fountaining beneath Archean seas: pyroclastic deposits of the 2730 Ma Hunter Mine Group, Quebec, Canada. J. Volcanol. Geotherm. Res., 54: 117-134.

Murase T. and McBirney A.R., 1973. Properties of some common igneous rocks and their melts at high temperatures. Geol. Soc. Am. Bull., 84: 3563-3592.

Murray C.G., 1986. Metallogeny and tectonic development of the Tasman Fold Belt System in Queensland. Ore Geology Reviews, 1: 315-400.

Murray C.G., 1990. Tasman Fold Belt in Queensland. In: Hughes, F. E. (ed.) Geology of the mineral deposits of Australia and Papua New Guinea. The Australasian Institute of Mining and Metallurgy. Monograph, 14: 1431-1450.

Nairn I.A. and Beanland S., 1989. Geological setting of the 1987 Edgecumbe earthquake, New Zealand. NZ J. Geol. Geophys., 32: 1-13.

Niem A.R., 1977. Mississippian pyroclastic flow and ash-fall deposits in the deep-marine Ouachita flysch basin, Oklahoma and Arkansas. Geol. Soc. Am. Bull., 88: 49-61.

Ninkovich D., Sparks R.S.J. and Ledbetter M.T., 1978. The exceptional magnitude and intensity of the Toba eruption, Sumatra: an example of the use of deep-sea tephra layers as a geological tool. Bull. Volc., 41: 286-298.

Nishimura A. and Murakami F., 1988. Sedimentation of the Sumisu Rift, Izu-Ogasawara Arc. Bull. Geol. Surv. Japan, 39: 39-61.

Normark W.R., Morton J.L., Koski R.A. and Clague D.A., 1983. Active hydrothermal vents and sulfide deposits on the southern Juan de Fuca Ridge. Geology, 11: 158-163.

Norrish K. and Hutton J.T., 1969. An accurate X-ray spectrographic method for analysis of a wide range of geologic samples. Geochim Cosmochim Acta, 33: 431-454.-

Norrish K. and Chappell B.W., 1977. X-ray fluorescence spectrography. In: Zussman, J. (eds.) Physical methods in determinative mineralogy. New York, Academic Press, 161-214.

Oehler J.H., 1976a. Experimental studies in Precambrian paleontology: Structural and chemical changes in blue-green algae during simulated fossilization in synthetic chert. Geol. Soc. Am. Bull., 87: 117-129.

Oehler J.H., 1976b. Hydrothermal crystallization of silica gel. Geol. Soc. Am. Bull., 87: 1143-1152.

Ohmoto H., 1978. Submarine calderas: A key to the formation of volcanogenic massive sulfide deposits? Mining Geology, 28: 219-231.

Ohmoto H. and Skinner B.J., 1983. The Kuroko and related volcanogenic massive sulfide deposits: introduction and summary of new findings. Econ. Geol. Mon., 5: 1-8.

Ohmoto H. and Takahashi T., 1983. Geological setting of the kuroko deposits, Japan: Part III. Submarine calderas and kuroko genesis. Econ. Geol. Mon., 5: 39-54.

Ohmoto H., Mizukami M., Drummond S.E., Eldridge C.S., Pisutha-Arnond V. and Lenagh T.C., 1983 Chemical processes of Kuroko Formation. In: Ohmoto, H. and Skinner, B. (eds.) The Kuroko deposits and related volcanogenic massive sulfide deposits. Econ. Geol. Mono., 5: 433-438.

Olivarez A.M. and Owen R.M., 1991. The europium anomaly of seawater: implications for fluvial versus hydrothermal REE inputs to the oceans. Chem. Geol., 92: 317-328.

Oliver N.H.S., 1996. Review and classification of structural controls on fluid flow during regional metamorphism. J. Metamorphic Geol, 14: 477-492.

Oudin E. and Constantinou G., 1984. Black smoker chimney fragments in Cyprus sulphide deposits. Nature, 308: 349-353.

Paine A.G.L., Harding R.R. and Clarke D.E., 1971. Geology of the Northeastern part of the Hugheden 1:250,000 sheet area, Queensland. Bureau of Mineral Resources, Geology and Geophysics, Report 126.

Park R.K., 1977. The preservation potential of some recent stromatolites. Sedimentology, 24: 485-506.

Perkins C., McDougall I. and Walshe J.L., 1993. Isotopic dating of precious and base metal deposits and their host rocks in eastern Australia. [unpub.] AMIRA project P334.

Pichler H., 1965. Acid hyaloclastites. Bull. Volc., 28: 293-310.

Pike J.E.N., 1983. Composition of Tertiary volcanic rocks, Mohave Mountains, Arizona. Geol. Soc. Am. Abst. with Programs, 15(5), 304.

Pollard D.D., Mullar O.H. and Dockstader D.R., 1975. The form and growth of fingered sheet intrusions. Geol. Soc. Am. Bull., 86: 351-363.

Pottorf R.J. and Barnes H.L., 1983 Mineralogy, geochemistry, and ore genesis of hydrothermal sediments from the Atlantis II Deep, Red Sea. In: Ohmoto, H. and Skinner, B. (eds.) The Kuroko and related volcanogenic massive sulfide deposits. Econ. Geol. Mono. 5, 198-223.

Preiss W.V., 1976. Basic field and laboratory methods for the study of stromatolites. In: Walter, M. R. (ed.) Stromatolites. Developments in sedimentology. Elsevier, 5-13.

Rawlings D.J., 1993. Mafic peperite from the Gold Creek Volcanics in the Middle Proterozoic McArthur Basin, Northern Territory. Aust. J. Earth Sci., 40: 109-113.

Renaut R.W. and Owen R.B., 1988. Opaline cherts associated with sublacustrine hydrothermal springs at Lake Bogoria, Kenya Rift valley. Geology, 16: 699-702.

Reynolds M.A. and Best J.G., 1976. Summary of the 1953-57 eruption of Tuluman Volcano, Papua New Guinea. In: Johnson, R. W. (ed.) Volcanism in Australasia. Elsevier, 287-296.

Reynolds M.A., Best J.G. and Johnson R.W., 1980. 1953-57 eruption of Tuluman volcano: rhyolitic volcanic activity in the northern Bismarck Sea. Geol. Surv. Papua New Guinea Mem., 7: 44.

Ridler R.H., 1971. Analysis of Archean volcanic basins in the Canadian Shield using the exhalite concept. Can. Min. Metall. Bull., 64: 20.

Rimstidt J.D. and Barnes H.L., 1980. The kinetics of silica-water reactions. Geochim. Cosmochim. Acta, 44: 1683-1699.

Rogan M., 1982. A geophysical study of the Taupo Volcanic Zone, New Zealand. J. Geophys. Res., 87, B5: 4073-4088.

Rollinson H., 1993. Using geochemical data: evaluation, presentation, interpretation. Longman scientific and technical, 352 pp.

Romagnoli C., Kokelaar P., Rossi P.L. and Sodi A., 1993. The submarine extension of Scaria del Fuoco feature (Stromboli isl.): morphologic characterization. Acta Vulcanologica, 3: 91-98.

Rona P.A., 1984. Hydrothermal mineralization at seafloor spreading centres. Earth Sci. Rev, 20: 1-104.

Rona P.A., Hannington M.D., Raman C.V., Thompson G., Tivey M.K., Humphris S.E., Lalou C. and Petersen S., 1993. Active and relict sea-floor hydrothermal mineralisation at the TAG hydrothermal field, Mid-Atlantic Ridge. Econ. Geol., 88: 1989-2017.

Ross C.S. and Smith R.L., 1955. Water and other volatiles in volcanic glasses. American Mineralogist, 40: 1071-1089.

Sainty R.A., 1992. Shallow-water stratigraphy at the Mount Chalmers volcanic-hosted massive sulfide deposit, Queensland, Australia. Econ. Geol., 87: 812-824.

Sanders I.S. and Johnston J.D., 1989. The Torridonian Stac Faud Member: an extrusion of fluidised peperite? Trans. Royal Soc. Edinburgh. Earth Sciences, 80: 1-4.

Sato Y., Ohmori Y. and Miyamoto H., 1979. Recent exploration of the Fukazawa kuroko deposit and some interesting modes of occurrences of the ores. Mining Geology, 29: 175-185.

Schandl E.S. and Gorton M.P., 1991. Postore mobilisation of rare earth elements at Kidd Creek and other Archean massive sulfide deposits. Econ. Geol., 86: 1546-1553.

Schmincke H.-U., 1967. Fused tuff and peperites in south central Washington. Geol. Soc. Am. Bull., 78: 319-330.

Schmincke H.-U. and Sunkel G., 1987. Carboniferous submarine volcanism at Herbornseelbach (Lahn-Dill area, Germany). Geol. Rund., 76: 709-734.

Schubel K.A. and Simonson B.M., 1990. Petrography and diagenesis of cherts from Lake Miagadi, Kenya. J. Sediment. Petrol., 60: 761-776.

Scott M.R., Scott R.B., Morse J.W., Betzer P.R., Butler L.W. and Rona P.A., 1978. Metal-enriched sediments from the TAG hydrothermal field. Nature, 276: 811-813.

Scott S.D., 1992. Polymetallic sulfide riches from the deep: fact or fallacy? In: Hsü, K. J. and Thiede, J. (ed.) Use and missuse of the seafloor. John Willey & Sons Ltd., New York, 87-115.

Self S., Sparks R.S.J., Booth B. and Walker G.P.L., 1974. The 1973 Heimaey Strombolian scoria deposit, Iceland. Geol. Mag., 111: 539-548.

Self S., Kienle J. and Huot J.P., 1980. Ukinrek maars, Alaska, II. Deposits and formation of the 1977 craters. J. Volcanol. Geotherm. Res., 7: 39-65.

Siebert L., 1984. Large volcanic debris avalanches: characteristics of source areas, deposits and associated eruptions. J. Volcanol. Geotherm. Res., 22: 163-197.

Sigurdsson H., 1977. Chemistry of the crater lake during the 1971-72 Soufriére eruption. J. Volcanol. Geotherm. Res., 2: 165-186.

Smith G.A., 1986. Coarse-grained nonmarine volcaniclastic sediment: terminology and depositional processes. Geol. Soc. Am. Bull., 97: 1-10.

Smith T.L. and Batiza R., 1989. New field and laboratory evidence for the origin of hyaloclastite flows on seamount summits. Bull. Volc., 51: 96-114.

Solomon M., 1976. "Volcanic" massive sulfide deposits and their host rocks-a review and an explanation. In: Wolf, K. A. (ed.) Handbook of strata-bound and stratiform ore deposits, II. Regional studies and specific deposits. Elsevier, 21-50.

Sparks R.S.J. and Walker G.P.L., 1977. The significance of vitric-enriched airfall ashes associated with crystal-enriched ignimbrites. J. Volcanol. Geotherm. Res., 2: 329-341.

Sparks R.S.J. and Huang T.C., 1980. The volcanological significance of deep-sea ash layers associated with ignimbrites. Geol. Mag., 117: 425-436.

Stanton W.I., 1960. The lower Palaeozoic rocks of south-west Murrisk, Ireland. J. Geol. Soc. London, 116: 269-296.

Staudigel H. and Schmincke H.U., 1984. The Pliocene seamount series of La Palma, Canary Islands. J. Geophys. Res., 89: 11195-11215.

Stolz A.J., 1989. Stratigraphic relationships and geochemistry of the Mount Windsor Volcanics. Mount Windsor Project-Research Report No. 1 [unpub.]. Centre for Ore Deposit and Exploration Studies, University of Tasmania, 1-50.

Stolz A.J., 1991. Stratigraphy and geochemistry of the Mt Windsor Volcanics and associated exhalites. In: Pongratz, J. and Large, R. (eds.) Geological controls on VMS mineralisation in the Mt Windsor Volcanic Belt-Research [unpub.] Report No. 2. Centre for Ore Deposit and Exploration Studies, University of Tasmania, 23-83.

Stolz A.J., 1994. Geochemistry and Nd isotope character of the Mt Windsor Volcanics: implications for the tectonic setting of Cambro-Ordovician VHMS mineralisation. In: Henderson R.A. and Davis B.K. (eds.) New developments in geology and metallogeny: Northern Tasman Orogenic Zone, Townsville, Queensland: 13-16.

Stolz A.J., 1995. Geochemistry of the Mount Windsor Volcanics: Implications for the Tectonic setting of the Cambro-Ordovician volcanic-hosted massive sulfide mineralisation in Northeastern Australia. Econ. Geol., 90: 1080-1097.

Sverjensky D.A., 1984. Europium equilibria in aqueous solutions. Earth and Planetary Science Letters, 67: 70-78.

Taube A., 1986. The Mount Morgan gold-copper mine and environment, Queensland: A volcanogenic massive sulfide deposit associated with penecontemporaneous faulting. Econ. Geol., 81: 1322-1340.

Taube A. and Messenger P., 1994 Volcanic stratigraphy of the Dee Range: a new prospective on Mt Morgan. In: Henderson, R. and Davis, B. (eds.) New developments in geology and metallogeny: Northern Tasman Orogenic Zone. 85-87.

Taylor B., Klaus A., Brown G.R. and Moore G.F., 1991. Structural development of Sumisu Rift, Izu-Bonin arc. J. Geophys. Res., 96, B10: 16113-16129.

Tivey M.K. and Delaney J.R., 1986. Growth of large sulfide structures on the Endeavour segment of the Juan de Fuca Ridge. Earth and Planetary Science Letters, 77: 303-317.

Trudinger P.A. and Mendelsohn F., 1976. Biological processes and mineral deposition in stromatolites. In: Walter, M. R. (ed.) Stromatolites: developments in stromatolites. Elsevier, 5-13.

Tsutsumi M. and Ohmoto H., 1983 A preliminary oxygen isotope study of Tetsusekiei ores associated with the Kuroko deposits in the Hokuroku district, Japan. In: Ohmoto, H. and Skinner, B. (eds.) The Kuroko deposits and related volcanogenic massive sulfide deposits. Econ. Geol. Mono., 5: 433-438.

Ui T., Metsugi H., Suzuki K. and Walker G.P.L., 1983. Flow lineations of Koya low aspect-ratio ignimbrite, south Kyushu, Japan. EOS, 64: 876.

Van Eck M., 1994. The geology and lithogeochemistry of the Lower Palaeozoic Seventy Mile Range Group at Mt Farrenden, Charters Towers, North Queensland, Australia. [M. Econ. Geol]. University of Tasmania, 41 pp.

Vine R.R. and Paine A.G.L., 1974. 1:250 000 Geological series-explanatory notes: Hughenden, Queensland. Bureau of Mineral Resources, Geology and Geophysics.

Vivallo W., 1985. The geology and genesis of the Proterozoic massive sulfide deposit at Garpenberg, central Sweden. Econ. Geol., 80: 17-32.

Von der Borch C.C., 1971. Glassy objects in Tertiary deep-sea clays cored by the Deep Sea Drilling Project. Marine Geol., 10: 5-14.

Walker G.P.L., 1972. Crystal concentration in ignimbrites. Contrib. Mineral. Petrol., 36: 135-146.

Walker G.P.L., 1973a. Explosive volcanic eruptions - a new classification scheme. Geol. Rund., 62: 431-446.

Walker G.P.L., 1979. A volcanic ash generated by explosions where ignimbrite entered the sea. Nature, 281: 642-646.

Walker G.P.L., 1989a. Gravitational (density) controls on volcanism, magma chambers and intrusions. Aust. J. Earth Sci., 36: 149-165.

Walker G.P.L. and Croasdale R., 1972. Characteristics of some basaltic pyroclastics. Bull. Volc., 35: 303-317.

Walker R.G., 1984. Shelf and shallow marine sands. In: Walker, R. G. (ed.) Facies Models. Geoscience Canada, Toronto, 141-170 pp.

Walter M.R., Goode A.D.T. and Hall W.D.M., 1976. Microfossils from a newly discovered stromatolitic iron formation in Western Australia. Nature, 261: 221-223.

Walter M.R., Grotzinger J.P. and Schopf J.W., 1982. Proterozoic stromatolites. In: Schopf, J. W. and Klein, C. (eds.) The Proterozoic biosphere - a multidisciplinary study. Cambridge University Press, 252-260.

Walter M.R. and Hoffman H.J., 1983. The paleontology and palaeoecology of Precambrian iron-formations. In: Trendall, A. F. and Morris, R. C. (eds.) Iron Formations: Facts, problems. Elsevier, 373-400.

Waters J.C. and Wallace D.B., 1992. Volcanology and sedimentology of the host succession to the Hellyer and Que River volcanic-hosted massive sulfide deposits, northwestern Tasmania. Econ. Geol., 87: 650-666.

Webb A.W., 1970a. Appendix-Isotopic age determinations from the Townsville 1:250 000 sheet area. In: Wyatt, D. H., Paine, A. G. L., Clarke, D. E., Gregory, C. M. and Harding, R. R. (eds.) Geology of the Townsville 1:250 000 sheet area, Queensland. Bureau of Mineral Resources, Geology and Geophysics, Australia, Report 127.

Webb A.W., 1970b. Appendix 2-Isotopic age determinations. In: Wyatt, D. H., Paine, A. G. L., Clarke, D. E., Gregory, C. M. and Harding, R. R. (eds.) Geology of the Charters Towers 1:250 000 sheet area, Queensland. Bureau of Mineral Resources, Geology and Geophysics, Australia, Report 137.

Webb A.W., 1971. Appendix-Isotopic dating of the Lolworth Complex, Hughenden and Charters Towers sheet areas. In: Paine, A. G. L., Harding, R. R. and Clarke, D. E. (eds.) Geology of the northeastern part of the Hughenden 1:250 000 sheet area, Queensland. Bureau of Mineral Resources, Geology and Geophysics, Australia, Report 126.

Wellman P., 1995. Tasman Orogenic System: A model for its subdivision and growth history based on gravity and magnetic anomalies. Econ. Geol., 90: 1430-1442.

White J.D.L. and Busby-Spera C.J., 1987. Deep marine arc apron deposits and syndepositional magmatism in the Alistos group at Punta Cono, Baja California, Mexico. Sedimentology, 34: 911-927.

White M.J. and McPhie J., 1996. Stratigraphy and palaeovolcanology of the Cambrian Tyndall Group, Mount Read Volcanics, western Tasmania. Aust. J. Earth Sci., 43: 147-159.

White M.J., McPhie J., Corbett K.D. and Pemberton J., 1993. Welded ignimbrite emplaced below wave base: Cambrian examples in Tasmania. IAVCEI General Assembly, Canberra, Australia, Abstracts, 121.

Whitford D., McPherson W.P.A. and Wallace D.B., 1989. Geochemistry of the host rocks to the volcanogenic massive sulfide deposits at Que River, Tasmania. Econ. Geol., 84: 1-21.

Whitham A.G. and Sparks R.S.J., 1986. Pumice. Bull. Volc., 48: 209-223.

Williams H. and McBirney A.R., 1979. Volcanology. Freeman, Cooper and Company, San Francisco, 397 pp.

Williams L.A. and Parks G.A., 1985. Silica Diagenesis, I. Solubility controls. J. Sediment. Petrol., 55: 301-311.

Williams L.A. and Crerar D.A., 1985. Silica Diagenesis, II. General mechanisms. J. Sediment. Petrol., 55: 312-321.

Wilshire H.G. and Hobbs B.E., 1962. Structure, sedimentary inclusions, and hydrothermal alteration of a latite intrusion. J. Geol., 70: 328-341.

Wilson C.J.N., Houghton B.F., McWilliams M.O., Lanphere M.A., Weaver S.D. and Briggs R.M., 1995. Volcanic and structural evolution of Taupo Volcanic Zone, New Zealand: a review. J. Volcanol. Geotherm. Res., 68: 1-28.

Winchester J.A. and Floyd P.A., 1977. Geochemical discrimination of different magma series and their differentiation products using immobile elements. Chem. Geol., 20: 325-344.

Withnall I.W., Bultitude R.J., Lang S.C., Donchak P.J. and Hammond R.L., 1987. Geology and tectonic history of the Palaeozoic Hodgkinson and Broken River Provinces, North Queensland. Pacific Rim Congress 87, Queensland, 495-498.

Withnall I.W., Black L.P. and Harvey K.J., 1991. Geology and geochronology of the Balcooma area: part of an early Palaeozoic magmatic belt in north Queensland. Aust. J. Earth Sci., 38: 15-29.

Wohletz K.H., 1983. Mechanisms of hydrovolcanic pyroclast formation: grain size, scanning electron microscopy, and experimental studies. J. Volcanol. Geotherm. Res., 17: 31-63.

Wormald P.J., 1992. Sub-volcanic facies analysis within an intrusive breccia and igneous complex hosting the Mt Leyshon gold mine, NE Queensland. Geol. Soc. Aust., Abstracts, 32: 134-135.

Wormald P.J., Orr T.O.H. and Hodkinson I.P., 1991. The Mount Leyshon gold mine (NE Queensland), an intrusive breccia and igneous complex. World Gold Congress 1991, Proceedings, Aus I.M.M., Cairns, 223-232.

Wormald P.J., Orr T.O.H. and Hodkinson I.P., 1993. The Mount Leyshon Gold Mine (NE Queensland), an intrusive breccia and igneous complex. In: Henderson, R. A. (ed.) Guide to the economic geology of the Charters Towers region, northeastern Queensland. Geol. Soc. Aust., Queensland division, 61-74.

Wright I.C., 1992. Shallow structure and active tectonism of an offshore continental back-arc spreading system: the Taupo Volcanic Zone, New Zealand. Marine Geol., 103: 287-309.

Wright J.V. and Mutti E., 1981. The Dali Ash, Island of Rhodes, Greece: a problem in interpreting submarine volcanogenic sediments. Bull. Volc., 44: 153-168.

Wyatt D.H., Paine A.G.L., Clarke D.E. and Harding R.R., 1970. Geology of the Townsville 1:250,000 sheet area, Queensland. Bureau of Mineral Resources, Geology and Geophysics, Australia. Report 127.

Wyatt D.H., Paine A.G.L, Clarke D.E., Gregory C.M. and Harding R.R., 1971. Geology of the Charters Towers 1:250,000 sheet area, Queensland. Bureau Mineral Resources, Geology and Geophysics Australia, Report 137.

Yamagishi H., 1979. Classification and features of subaqueous volcaniclastic rocks of Neogene age in southwest Hokkaido. Geol. Surv. Hokkaido Rep., 51: 1-20.

Yamagishi H., 1982. Miocene subaqueous volcaniclastic rocks of the Oshoro peninsula, southwest Hokkaido, Japan. J. Geol. Soc. Japan, 88: 19-29.

Yamagishi H., 1985. Growth of pillow lobes - evidence from pillow lavas of Hokkaido, Japan, and North Island, New Zealand. Geology, 13: 499-502.

Yamagishi H., 1987. Studies on the Neogene subaqueous lavas and hyaloclastites in southwest Hokkaido. Geol. Surv. Hokkaido Rep., 59: 55-117.

Yamagishi H., 1991. Morphological features of Miocene submarine coherent lavas from the "Green Tuff" basins: examples from basaltic and andesitic rocks from the Shimokita Peninsula, northern Japan. Bull. Volc., 53: 173-181.

Yamagishi H. and Dimroth E., 1985. A comparison of Miocene and Archean rhyolite hyaloclastites: Evidence for a hot and fluid rhyolite lava. J. Volcanol. Geotherm. Res., 23: 337-355.

Yamagishi H. and Matsuda Y., 1991. The Neogene submarine felsic rocks of Yoichi Beach, Shakotan Peninsula. J. Geol. Soc. Japan, 97: 269-277.

Yamagishi H. and Goto Y., 1992. Cooling joints of subaqueous rhyolite lavas at Kuroiwa, Yaumo, southern Hokkaido, Japan. Bull. Volcanol. Soc. Japan, 37: 205-207.

Yamamoto T., Soya T., Suto S., Uto K., Takada A., Sakaguchi K. and Ono K., 1991. The 1989 submarine eruption off eastern Izu Peninsula, Japan: ejecta and eruption mechanisms. Bull. Volc., 53: 301-308.

Zierenberg R.A., Shanks III W.C., Seyfried Jr W.E., Koski R.A. and Strickler M.D., 1988. Mineralisation, alteration, and hydrothermal metamorphism of the ophiolite-hosted Turner-Albright sulfide deposit, southwestern Oregon. J. Geophys. Res., 93, B5: 4657-4674.

Appendix A

Clast shape and textural associations in peperite as a guide to hydromagmatic interactions: Late Permian basaltic and basaltic andesite examples from Kiama, Australia

Clast shape and textural associations in peperite as a guide to hydromagmatic interactions: Late Permian basaltic and basaltic andesite examples from Kiama, Australia

Introduction

Interaction between magma or lava and wet unconsolidated sediment is common in environments where sedimentation accompanies volcanism, especially in subaqueous settings where large volumes of magma are emplaced sub-seafloor as syn-sedimentary intrusions. A variety of processes and products attributable to magma-wet sediment interaction have been recorded, including intrusive pillows (Snyder and Fraser 1963a,b; Kano 1991), effusive magma-sediment slurries (Lawson 1972, Leat and Thompson 1988, Sanders and Johnston 1989), and peperite (Fisher 1960, Schmincke 1967, Williams and McBirney 1979, Brooks et al. 1982, Kokelaar 1982, Busby-Spera and White 1987, Brooks 1995). Peperite is a genetic term for a rock formed by the mixing of magma or lava with wet sediment. Peperite occurs at contacts between intrusions and the host sediment (Hanson and Schweickert 1982, Branney and Suthren 1988), along basal contacts of lavas (Schmincke 1967) or surrounds burrowing parts of lavas. Here I describe peperite and related structures in basaltic and basaltic andesite lavas and syn-sedimentary intrusions from the Late Permian Broughton Formation, Kiama, New South Wales. Because of continuous coastal exposure at this locality it has been possible to interpret from field observations the significance of textures and structures in peperite.

Peperite is useful for demonstrating contemporaneous volcanism and sedimentation, and because it preserves evidence of progressive stages in hydrovolcanic interactions (non-explosive mixing, steam explosions). Busby-Spera and White (1987) identified two textural types of peperite: in blocky peperite, clasts derived from the magma have polyhedral blocky shapes and commonly fit together like a jigsaw puzzle, whereas in globular peperite, juvenile clasts are bulbous. In this study variations in clast shapes and interrelationships are interpreted in terms of changing hydrovolcanic interactions during magma-sediment mixing. In particular, the role of host-sediment properties in determining peperite type is assessed and associations between peperitic, autoclastic and coherent facies are examined.

Terminology and description of peperite

Peperite can be identified, described and interpreted on the basis of (1) igneous clast shape; (2) fabric; and (3) location with respect to the margin of an igneous body. Clast shapes described in this study are present in many other examples of peperite (e.g. Busby-Spera and White 1987, Branney and Suthren 1988, Hanson 1991, Hanson and Wilson 1993, McPhie 1993, Rawlings 1993, Brooks 1995). Important insights into hydromagmatism, and intrusive and mixing processes might be gained from the investigation of the complex relationships between different clast types and textural associations, so it is important that complexities are recorded. Peperite consisting of one clast type is termed blocky, globular, ragged or platy peperite following on from Busby-Spera and White (1987). Peperite containing a high proportion of clasts from more than one textural group is here classified as mixed peperite and the clast shapes indicated (e.g. mixed ragged-globular peperite). In peperite with a closely packed fabric (Hanson and Wilson 1993), sediment fills joints and fractures that define pseudo-pillows (Watanabe and Katsui 1976; Yamagishi 1987, 1991), and columns and polyhedral joint blocks (Brooks et al., 1982) in the coherent facies. Peperite with dispersed fabric (Hanson and Wilson 1993) is a sediment matrix-rich breccia with clasts and tongues of the igneous component. Peperite occurs at the margins of lavas and intrusions and is present as pods, sheets and dykes in massive coherent facies within the interior of the units.

Geological Setting

Peperite examined in coastal exposures at Kiama, New South Wales occurs in the upper part of the Late Permian Broughton Formation. The Broughton Formation and overlying coal-bearing Pheasants Nest Formation form part of a conformable regressive sedimentary succession within the Permo-Triassic Sydney Basin (Cas and Bull 1993).

The Broughton Formation and the lower part of the Pheasants Nest Formation include both sedimentary and volcanic facies associations (Raam 1969). The sedimentary facies association is dominated by thin to thickly bedded immature sandstone, pebble conglomerate and mudstone of volcanic provenance, and occurs as four intervening units between volcanic facies of the Broughton Formation. Units are interpreted as high-density turbidity current and tractional current deposits emplaced in a storm- and tide-dominated, shallow marine environment (Bull and Cas 1989). Dropstones within the lower part of the Broughton Formation suggest that periodic coastal sea ice and/or icebergs were present during deposition. Dips of bedding rarely exceed 2°. The volcanic facies association comprises nine shoshonitic basaltic to basaltic andesite lavas and syn-sedimentary intrusions, previously termed latites, and associated autoclastic breccia and peperite (Carr 1985). Three of the lowermost members of Broughton Formation are relevant to this study. They are, from oldest to youngest, the Blow Hole Latite Member, the Kiama Sandstone Member and the Bumbo Latite Member (Fig. 1). The Blow Hole Latite Member is holocrystalline and porphyritic, containing euhedral to subhedral plagioclase and pyroxene phenocrysts, and chloritic pseudomorphs of olivine phenocrysts, in a fine-grained pilotaxitic groundmass. The groundmass consists of plagioclase microlites, pyroxene microlites, chlorite, an unidentified opaque phase (magnetite?), and interstitial potassium feldspar. The petrography of the Bumbo Latite Member is similar, although olivine phenocrysts are absent and the groundmass is finer grained. Volcanic and sedimentary facies associations are well exposed in coastal cliffs at Kiama. However, outcrop inland is restricted to quarries and road cuts.

Contact Relationships

The Blow Hole Latite Member is a 50 m thick basaltic andesite sheet which was initially interpreted as a tripartite intrusion (Raam 1964). However, Bull and Cas (1989) considered that only the middle unit of the sheet was partly intrusive, and regarded it as a lava which locally burrowed into wet sediment. This study demonstrates that the Blow Hole Latite Member can be divided into two flow units with peperitic contacts suggesting their intrusion into wet unconsolidated sediments. A thin, poorly exposed horizon of bedded sandstone (Rifle Range Tuff Member, Raam 1964) exposed at Rifle Range Point (Fig. 1) separates the upper and lower flow units. The middle flow unit proposed by previous authors is a peperitic facies of the lower flow unit. The upper and lower units are interpreted as syn-sedimentary intrusions, due to the volume and extent of peperite development. However, critical facies relationships required to discount a burrowing flow are absent due to poor exposure inland.

The Bumbo Latite is a 150 m thick massive, columnar jointed basalt sheet above the Kiama Sandstone Member (Fig. 1). The base of the member is locally peperitic and the upper contact was not examined in this study. The Bumbo Latite also has been interpreted as a tri-composite extrusion (Bowman 1974).

At map scale the sheets are broadly concordant with bedding in the enclosing sedimentary rocks. However, at outcrop scale contacts vary from relatively planar to complex and highly irregular. Unmixed lower contacts vary from smooth to undulating with 10-20 cm amplitude load casts of coherent basaltic andesite separated by flames of sandstone. Underlying sedimentary rocks are relatively undisturbed except for minor soft-sediment deformation attributable to the loading effect of the sheets.

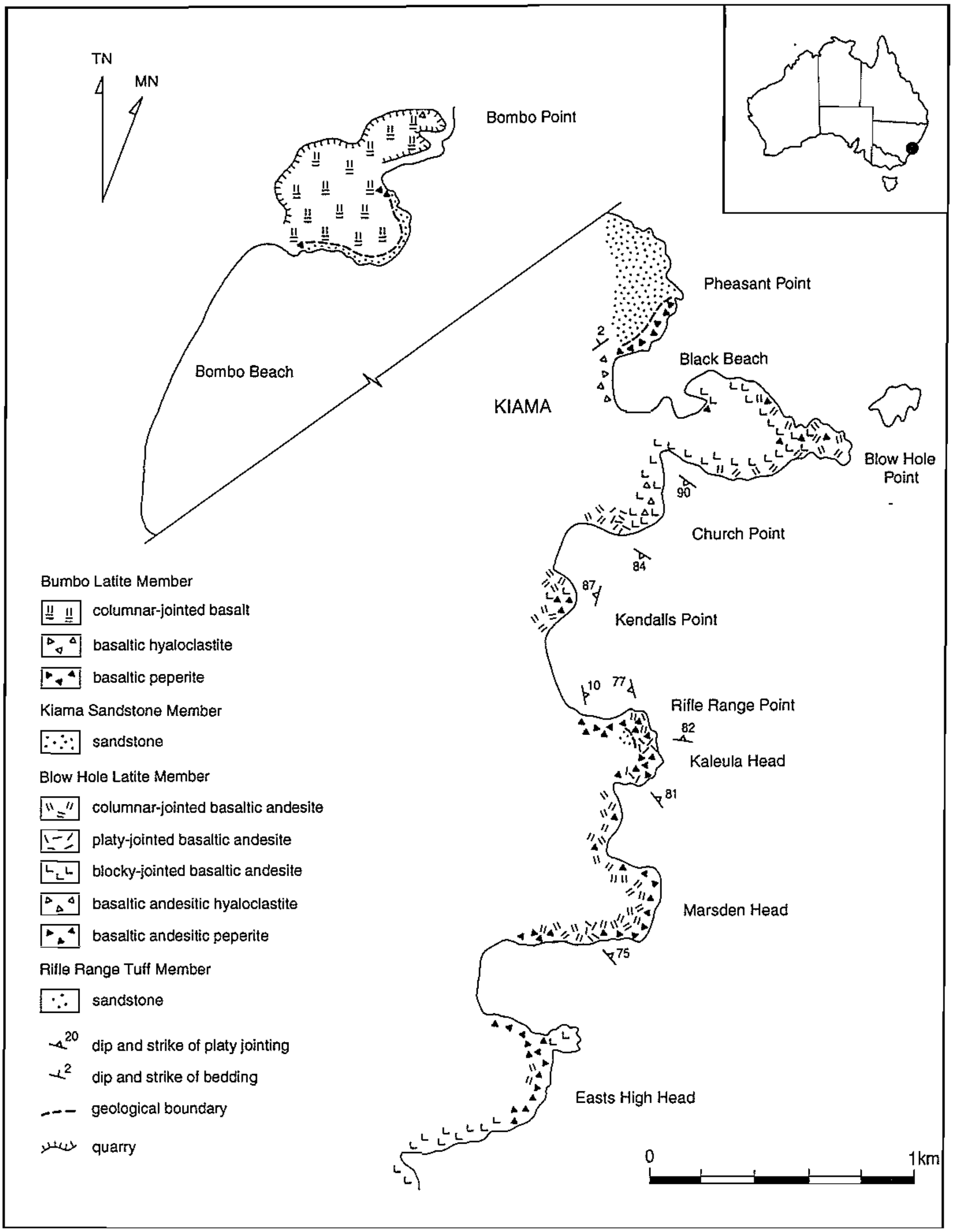

Figure 1. Geology of the Permian Broughton Formation at Kiama, showing complex relationships between peperite, hyaloclastite and coherent facies in the Blow Hole and Bumbo Latite Members.

Facies of the Blow Hole and Bumbo Latite Members

Coherent Facies

Regular, well developed, wide (to 1 m) columnar joints characterise the massive interiors of the Bumbo and Blow Hole Latite Members. In places (e.g. Kaleula Point) column faces are dissected by interconnected, broadly curved tortoise shell joints which, in three dimensions, define equant polyhedral blocks. More often columns are cut by less regular, curved and planar joints. Column axes are generally subvertical and perpendicular to sheet margins. However, along contacts with some dyke-like peperitic domains in the Blow Hole Latite Member, column axes are subhorizontal at contacts, but progressively steepen and become subvertical a few metres into massive basaltic andesite (Fig. 2, 3A). Along the top of peperite dykes, columns are subvertical, but are cut at right angles by concentric joints spaced a few 10' s of centimetres apart (Fig. 2). Concentric joints mirror the upper margin of the peperite domains, forming a wavy pattern where peperite dykes are closely spaced.

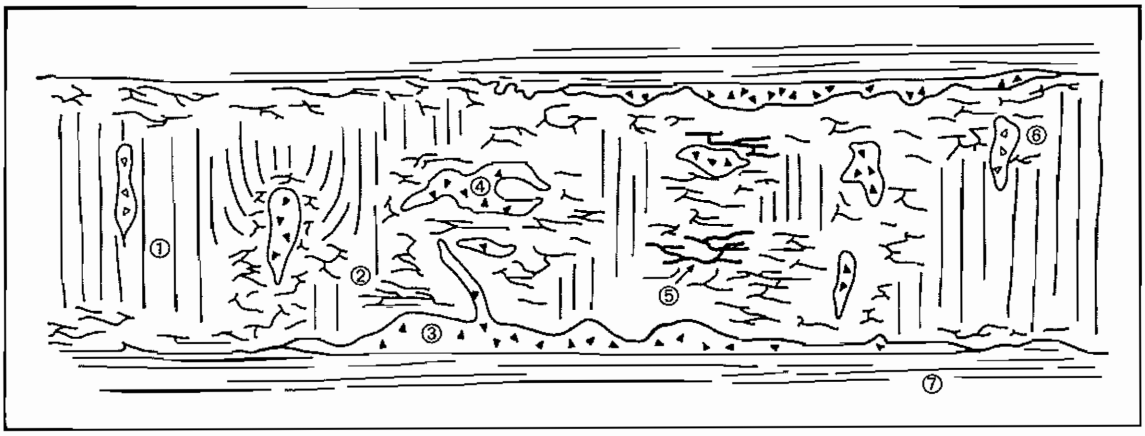

Figure 2. Cartoon illustrating the facies and facies relationships of lower flow unit in the Blow Hole Latite intrusion. 1 — columnar jointed coherent facies; 2 — blocky jointed coherent facies with pseudo-lobes and pseudo-pillows; 3 —dispersed peperite facies; 4 — dispersed peperite in the interior of the sheet; 5— closely-packed peperite; 6 — hyaloclastite; 7 — undisturbed sediment.

Near contacts with sedimentary facies or peperitic zones, columnar joints merge into a several metre wide interval of blocky jointing. Widely spaced, smoothly curved, intersecting joints outline polyhedral blocks, 2-6 metres in length (pseudo-pillows, Watanabe and Katsui 1976; Yamagishi 1987, 1991), many of which are internally jointed. Joints are progressively more closely spaced within a metre or two of contacts (cf. Brooks et al., 1982) dissecting the rock into small blocks, 5 to 30 cm across. Some blocks are defined by intersecting radial and concentric joints which diverge outward from small (20-30 cm) discontinuous apophysis-like tongues of peperite (Fig. 3B). Blocky jointed basalt or basaltic andesite is in direct contact with peperite along part or all of some contacts and elsewhere grades into hyaloclastite.

Locally in the Blow Hole Latite Member, subvertical platy joints form an intervening zone between columnar jointed and blocky jointed coherent facies. Platy joints are laterally continuous, spaced up to 1.5 metres apart, dissected by crude blocky jointing, and conform to contacts with peperitic and blocky jointed domains. Subhorizontal joints up to 10' s of metres in length form bifurcating networks in both platy- and blocky-jointed domains.

Hyaloclastite Facies

Exposures of hyaloclastite are monomictic and characterised by jigsaw-fit of polyhedral blocky and cuneiform clasts separated by minor amounts of finely comminuted magmatic rock. In the Blow Hole Latite Member, in situ hyaloclastite may be the brecciated equivalent of large parts of the coherent facies or form a narrow selvedge between blocky jointed coherent facies and peperite. Often, clasts decrease in size approaching peperitic contacts and some fractures have been invaded by sediment, forming peperite.

At Blow Hole Point, small pods of hyaloclastite are enclosed by massive columnar and blocky jointed basaltic andesite. Almost continuous outcrop between Blow Hole Point, Black Beach and Pheasant Point (Fig. 1) provides a section through the outer interior to the margin of the upper Blow Hole Latite Member, and suggests that it is a sill. The hyaloclastite facies can be regarded as an intermediate facies between the massive columnar- and blocky-jointed coherent facies and marginal peperite. Features which characterise this transition are, from the margin inward, a rapid decrease in peperite to hyaloclastite, reduction in the degree of brecciation, and replacement of blocky jointing by columnar jointing as the major joint style.

Closely-packed peperite

Peperite with closely-packed fabric occurs only within the interior of the Blow Hole Latite Member. Blocky jointed coherent facies merge into domains of closely-packed peperite where sediment is present between widely spaced, smoothly curved, intersecting joints which define polyhedrally jointed blocks (Fig. 2). More continuous sediment-filled subhorizontal joints, up to 30 m in length, outline pseudo-pillows (Fig. 3C). Pseudo-pillows are dissected by internal joints, which are free of sediment, or else separated by a thin or thick infill of sediment (cf. Yamagishi et al. 1989). Basaltic andesite in the interior and margins of pseudo-pillows is texturally equivalent to that of the massive facies.

Figure 3.

Outcrop features of the Blow Hole Latite Member (A-D, F) and Bumbo Latite Member (E).

(A) Transition from blocky jointing (b) to columnar jointing (c) passing out from the margin of a dyke-like body of dispersed peperite within the interior of the intrusion (p). Columns are sub-horizontal at the contact with the dyke but progressively steepen and become subvertical. Pack for scale. Marsden Head.

(B) Lobate incursions (arrow) of peperite (p) into blocky jointed coherent facies (b). Within the coherent facies, trails of ellipsoidal vesicles conform to the shape of some parts of the contact. Scale 10 cm long. Kendalls Point.

(C) Closely-packed peperite showing progressive dismembering of coherent basalt into pseudo-pillows (p). Sediment fills fractures between subhorizontal fractures (arrow) and fractures in pseudo-pillows. Kaleula Head.

(D) Cross section through lobes (l) dissected by incipient columnar and blocky jointing and partially enclosed in altered dispersed peperite (p). Clasts in the breccia and adjacent to lobe margins display jigsaw-fit texture demonstrating that the lobe and breccia are cogenetic. Marsden Head.

(E) Detailed drawing from photograph. Type D lobes (l) enclosed in cogenetic peperite have altered margins (a) and unaltered jointed (j) and cores (u). Parts of some lobe margins are strongly vesicular (v). Peperite with vesicular clasts (vp) contrasts with peperite-dominated by poorly vesicular polyhedral blocky clasts (bp). Scale 10 cm long. Bombo Point.

(F) Lamination (arrow) and concentration of lithic clasts (l) on the ?lee side of a juvenile clast (j) derived from the walls of the enclosing sheet fracture in closely-packed peperite. Juvenile clast is 2.5 cm long. Kaleula Head.

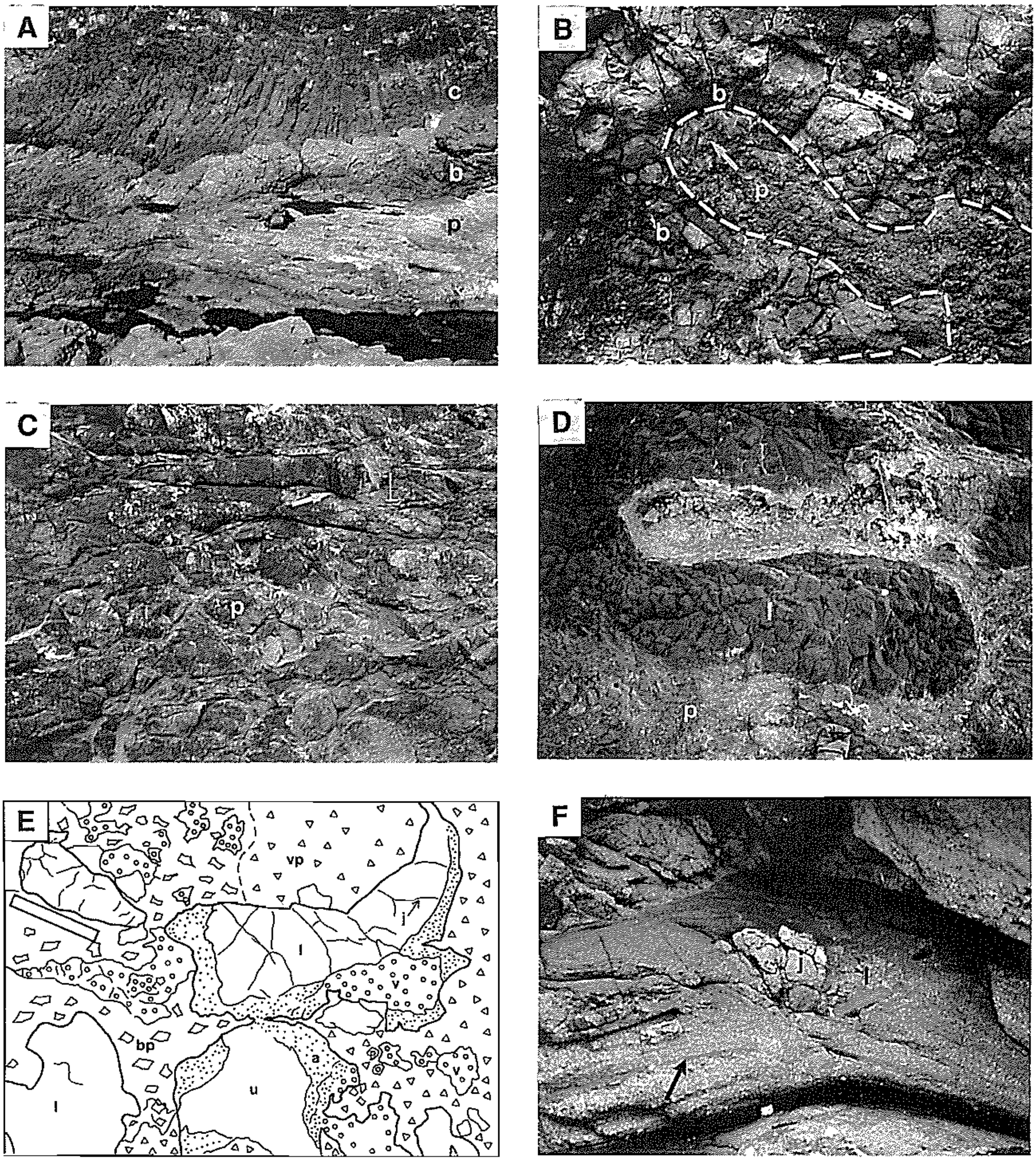
A
c
b
p
B
b
p
b
C
p
D
l
p
E
vp
j
l
v
bp
a
u
l
v
F
j
l

However, along some contacts with sediment less than a millimetre of the groundmass is black in colour and charged with a fine unidentified opaque phase.

Subhorizontal fractures in closely-packed peperite are filled with up to 10 cm of siltstone to sandstone. However, thicknesses of sediment vary considerably along their length. Towards fracture terminations, infills decrease to a sub-millimetre film which is present along the whole length of the fracture, or else fractures are sediment free. In some cases, segments or the terminations of subhorizontal fractures comprise stacked sets of interconnected, sediment-filled, en-echelon fractures. Similar, but subvertical en-echelon fractures characterise some outcrops of the polyhedrally jointed coherent facies. En-echelon fractures are interpreted as tensile fractures formed by non-rotational, dilational strain during the invasion of overpressured sediment (cf. Beach 1975, Francis 1982). The surfaces of subhorizontal fractures are sharp, but have an irregular form which reflects small-scale steps in the direction of fracture propagation and incomplete exfoliation of incipient clasts from some walls. Platy clasts (cf. Brooks 1995) liberated from fracture surfaces form jigsaw-fit aggregates separated by minor amounts of sediment matrix. Apophyses of sediment extend a few centimetres in from some sheet fracture walls and locally have formed peperite comprising globular-shaped clasts.

Close to domains of dispersed peperite, outlines of pseudo-pillows are masked as the proportion of sediment-filled fractures increases. Remnants of large pseudo-pillows enclose multiple smaller pseudo-pillows which, with increasing brecciation, disintegrate into aggregates of blocky to ellipsoidal clasts separated by sediment matrix. Wedge-shaped, sediment filled fractures penetrate the pseudo-pillows. The largest fractures are over 1 m in length and, where closely spaced, generate complex serrated margins to pseudo-pillows. Thinner wedges extending in from the surfaces of larger fractures locally merge, outlining platy clasts surrounded by sediment.

At Marsden Head, well developed, subvertical columnar joints, cut at right angles by subhorizontal joints, extend upward from a subhorizontal sheet-like body of dispersed peperite in the interior of the sheet. An irregular, roughly ellipsoidal section of columnar jointing, 10 m wide and 5 m high, that occurs 1m above the peperite is dissected by blocky joints and sediment-filled fractures. Ghosts of former columnar joints are visible towards the centre of the zone, but are best observed along gradational contacts with intact columnar jointed basaltic andesite. Domains of blocky jointed basaltic andesite are dissected by fine sediment-filled fractures that are connected to the underlying peperite by a network of sediment veins (cf. Brooks et al., 1982). Some veins follow the margins of column faces, but most form bifurcating networks within the blocky jointed interiors of remnant columns. Farther to the south, sediment fills the space between some column faces. Relationships at these two localities suggest that columnar jointing was initiated synchronous with peperite formation.

Dispersed Peperite

Peperite with dispersed fabric passes into massive blocky jointed coherent facies, or grades through an intervening zone of closely-packed peperite as the proportion of sedimentary matrix between clasts decreases. Contacts with the enclosing facies are highly irregular.

Dispersed peperite occurs from the base to top of the Blow Hole Latite and does not appear to be restricted to a specific level. In map view, this facies forms elliptical pods and interconnected peperite tongues, a few metres wide and up to 10 m long, isolated in blocky jointed coherent facies. Tongues separate lobe-like, blocky jointed, coherent domains which extend in from the surrounding coherent facies. In cross-section, dyke-like bodies, irregular branching networks, and sheets of peperite are surrounded by coherent facies or extend up from the base of the sheets to more than 10 m into coherent facies. Pods and tongues of peperite apparently isolated within coherent facies are interpreted as cross-sections through dykes (cf. Brooks et al., 1982). However, others are evidently rootless and direct connections to the enclosing sedimentary package are not apparent. Elliptical domains of coherent basalt or basaltic andesite partially or completely enclosed in peperite resemble cross-sections through lava-lobes (Figs. 3D, 4, 5A-B).

Most peperitic domains include poorly- and strongly-vesicular parts, resulting in apparent polymictic breccias in which pods and fingers of contrasting vesicularity are juxtaposed. Clasts contain a uniform to heterogeneous distribution of vesicles ranging from 0.1 to 3.5 cm in diameter, and vary from non-vesicular to containing around 15% vesicles; some are nearly scoriaceous. At the margins of some poorly vesicular coherent facies, a coherent vesicular rind passes out into peperite comprising vesicular clasts (Fig. 4), demonstrating that the facies are cogenetic. Along some contacts within the Blow Hole Latite Member, lobate apophyses of peperite (10-20 cm across) comprising vesicular clasts are enclosed in weakly-vesicular coherent facies (Fig. 3B). Aligned ellipsoidal vesicles in the weakly-vesicular coherent basalt-andesite mirror the broad shape of some of these contacts. In many apophyses, sediment is concentrated at the top of the structure, possibly trapped there as expanded pore water cooled, preventing further advance into the still plastic basaltic andesite. Clasts associated with vesicular domains have fluidal and globular shapes although some clasts in poorly vesicular domains also have these shapes. In some outcrops (e.g. Kendalls Point, Marsden Head), in situ hyaloclastite at the margins of the coherent facies passes into dispersed peperite containing jigsaw-fit aggregates of polyhedral blocky clasts. Within the peperite, groups of poorly vesicular clasts with jigsaw-fit texture are enclosed by areas where clast rotation and separation are evident. In some exposures (e.g. Kendalls Point), wide (5-40 cm) subhorizontal sediment-filled fractures can be traced through the breccia. Fracture walls are irregular and stepped.

Occurrences of dispersed peperite at the margins of the Blow Hole and Bumbo Latite Members consistently have a dispersed fabric. This is best illustrated along the contact between the Bumbo Latite Member and the underlying Kiama Sandstone Member at Bombo Point. Vesicular domains occur as small pods in coherent poorly vesicular basalt and as peperite which encloses small lobe-like bodies of poorly vesicular basalt up to 0.8 m in length (Figs. 3E, 5D). Away from contacts, there is a transition from tube-vesicles to round and ellipsoidal vesicles in coherent vesicular basalt. Margins of large lobes and all of the smallest lobes are light green in colour and altered, whereas lobe interiors are black and unaltered. Lobe-like bodies show progressive disintegration into jigsaw-fit aggregates of blocky clasts. Jigsaw-fit texture is poorly preserved in peperite containing vesicular clasts. Contacts between poorly- and strongly-vesicular domains are mostly sharp. However, mixing of vesicular and non-vesicular clast types has locally generated texturally complex peperite. Sandstone containing juvenile vesicular clasts fills some fractures in the poorly vesicular lobe-like bodies, so that the lobes appear to intrude earlier, texturally distinct peperite.

The upper contact of the upper Blow Hole Latite Member is extensively exposed on the shore platform at Pheasants Point. Pods, tongues and sheets of massive to blocky jointed basaltic andesite up to 5 m in length are enclosed in cogenetic peperite (Fig. 5C). Parts of some tongues are cut by wide to narrow sediment-filled fractures which dissect them into smaller bodies and irregular blocks with jigsaw-fit geometry. Small digitate apophyses of basaltic andesite up to 5 cm in length extend out from lobe margins. In detail, much of the peperite consists of interconnected, bulbous, entrail-like domains of basaltic andesite which are separated by sediment, but which can be traced back to coherent facies of the lobes. Peperite at the margins of some lobes encloses pods comprising clasts which are more vesicular and/or have different shapes, and are separated by greater amounts of sediment. Bedding in sandstone above the contact zone is undisturbed, in contrast to the near complete destruction of bedding in the peperitic facies.

Lobes

Lobe-like bodies of coherent basalt and basaltic andesite are isolated in the peperite or connected to coherent facies by wide stems of the same composition. On the basis of size, shape and relationships with associated peperite, lobes are divided into four types; A to D (Fig. 5). Peperite in the interior of the sheets incorporates types A-D, whereas peperite at

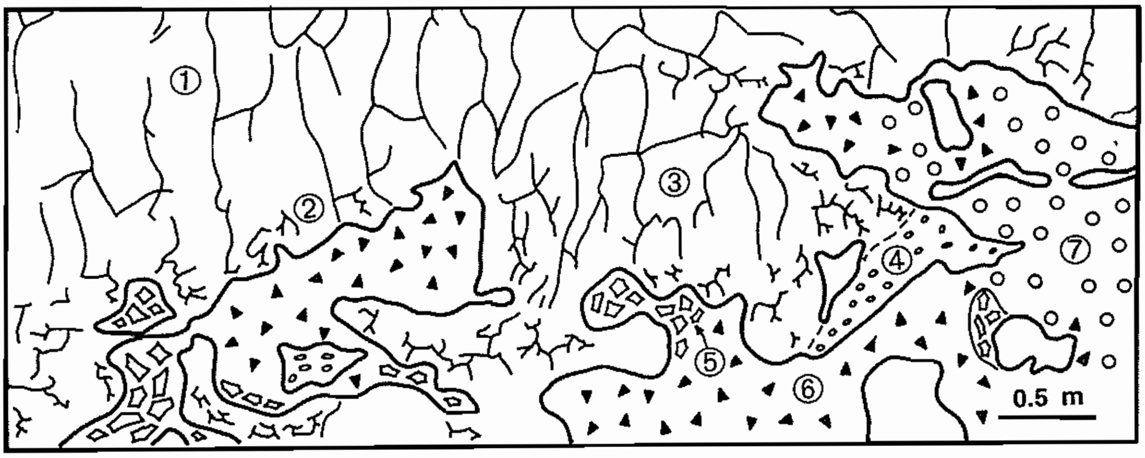

Figure 4. Simplified field sketch of textures and structures in dispersed peperite at Kendalls Point. 1—coherent basaltic andesite dissected by widely spaced curved joints; 2— equant joint blocks; 3—lobe-like coherent domain; 4—vesicular coherent basaltic-andesite; 5— peperite (polyhedral blocky clasts); 6—peperite (polyhedral and irregular blocky clasts); 7— peperite (irregular blocky clasts).

contacts with then enclosing sediments contains only types C and D. In peperitic facies of the Bumbo Latite Member, only type D lobes have been recognised.

Type A lobes — are elliptical- to pendant-shaped when viewed in cross-section (Figs. 3D, 5A), and tongue -shaped to elliptical in map view. They are up to 25 m in length and 20 m wide. Lobe interiors are unaltered and dissected by intersecting polyhedral joints, or polyhedral-jointed basaltic andesite encloses an inner zone of incipient radial columnar jointing. Pale green, in situ hyaloclastite (± peperite) forms a selvedge along segments of some lobe margins. Parts of some margins are vesicular and grade out into peperite comprising vesicular clasts. Rarely, vesicular pods to 15 cm wide occur in the lobes. Lobe interiors are penetrated by sediment-filled fractures. Fractures are planar along contacts with poorly vesicular domains, but have more irregular shapes when cutting numerous vesicles.

Type B lobes — Fractures at the margins of the type B lobes are penetrated by sediment, whereas lobe interiors are sediment-free (Fig. 5B). Sediment-filled fractures cut across some larger lobes producing trains of progressively smaller remnant coherent domains, which become more widely spaced as larger segments of the lobes are brecciated. Jigsaw-fit aggregates of clasts separated by sediment outline former large lobes which have undergone complete brecciation. Clasts become smaller and separated by greater amounts of sediment forming a matrix between the lobes. Slight modification of jigsaw-fit textures by rotation and separation of clasts, to complete loss of jigsaw-fit texture is widespread in the matrix.

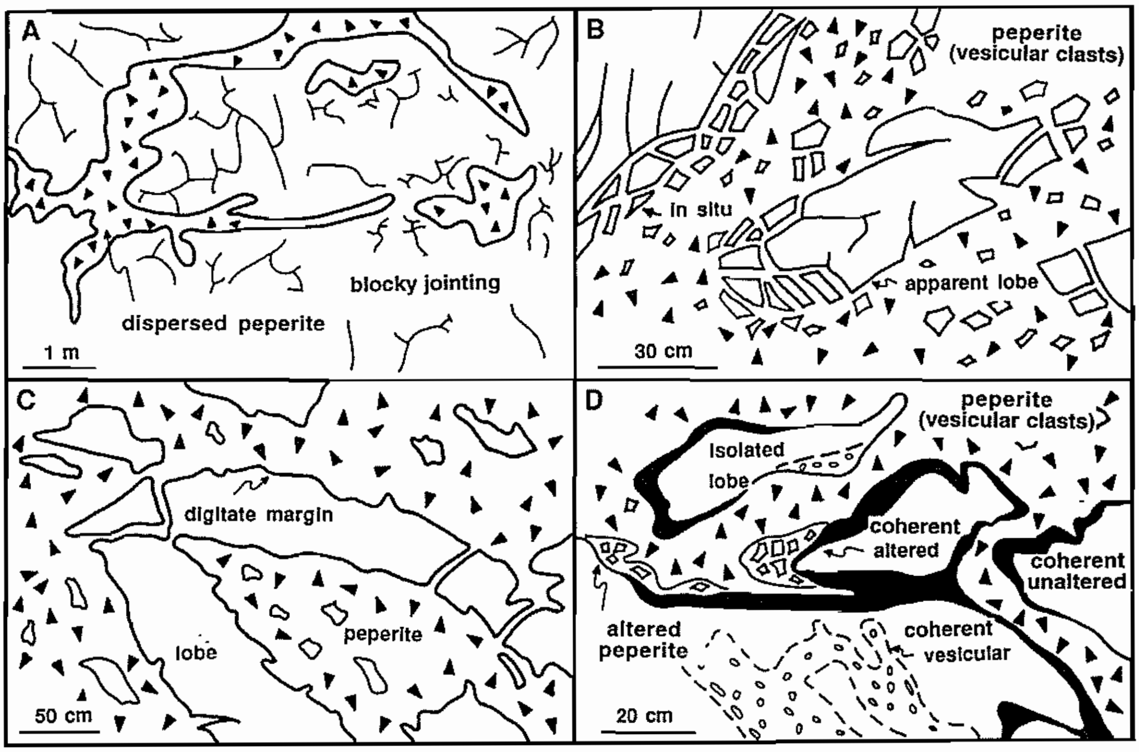

Figure 5. Field sketches of lobes formed by incomplete brecciation in peperite facies of the Blow Hole Latite (A-C) and dispersed peperite facies of the Bumbo Latite (D). A— Cross section of a type A lobe; Kaleula Head. B— Plan view of a type B lobe in peperite displaying in situ and clast-rotated textures; Marsden Head. C— Type C lobe gradational into peperite containing clasts varying from poorly to strongly vesicular and from blocky to globular in shape; Pheasant Point. D— Type D lobes enveloped by an altered margin and enclosed in peperite containing domains of poorly and strongly vesicular clasts. Coherent facies show an equivalent range in vesicularity to clasts in peperite. Bumbo Point.

Type C lobes — Type C lobes characterise the peperitic upper margin of the upper Blow Hole Latite Member. Sheets of relatively coherent jointed basaltic andesite enclose pods and large domains of peperite (e.g. Marsden Head). Outlines of lobes become distinct as the proportion of peperite increases, enclosing relic pods of polyhedrally jointed basaltic andesite to 1 metre in size (Fig. 5C). Sediment-filled fractures dissect large lobes into groups of blocky clasts and small lobes which are separated by sediment matrix-rich domains. Clasts fit together along some margins but others have moved following fragmentation. Variation in clast shapes and vesicularity produces texturally complex peperite.

Type D lobes — Within some peperitic domains, poorly vesicular coherent basalt or basaltic andesite is interleaved with strongly vesicular intervals to 1m across (Fig. 5D). In strongly vesicular domains, there is a gradation between coherent basalt or basaltic andesite, hyaloclastite and sediment matrix-rich and sediment matrix-poor peperite. All facies contain isolated pods and finger-like protrusions of poorly vesicular coherent or polyhedrally jointed basaltic andesite (Figs. 3E, 5D). Those pods and fingers in peperitic domains resemble concentric pillows (cf. Yamagishi 1987) and small pillow lobes. Some lobes are enveloped by a hyaloclastite (± peperite) sheath comprising poorly vesicular blocky clasts. Similar clasts are isolated in the surrounding peperite which is dominated by vesicular clasts.

Clast types and shapes

Peperite contains igneous clasts that can be divided into six main textural types on the basis of clast shape and relationships between clasts (Fig. 6).

Globular clasts — Globular clasts have bulbous, globular shapes ("entrail globular" clasts) or are roughly equant but are bound by finely digitate, fluidal margins ("equant globular" clasts). There is a progression in clast shapes between entrail- and equant-globular. In detail, most "clasts" are connected by fluidally-shaped stems a few millimetres to several centimetres wide; they are incipient clasts formed through fragmentation mechanisms which did not go to completion.

Entrail globular

Interconnected incipient clasts with rounded globular shapes form complex branching entrail-like interdigitations with sediment (Fig. 6A). Digits terminate in the surrounding sediment or connect small subrounded patches of relatively coherent igneous component. The patches are up to several tens of centimetres across and many contain small, centimetre-sized blebs of sediment. Pinching off of branches along the bifurcating digits has delivered discrete clasts to the surrounding sediment. Only a thin film of homogenised sediment separates some clasts from their parent digit, whereas others are surrounded by large amounts of sediment.

Equant globular

In peperite comprising equant globular clasts there is less disruption of the igneous component as incipient clasts are larger and interpenetration with sediment is largely restricted to their margins (Fig. 6B). Incipient clasts are cut by bifurcating sinuous seams of sediment which propagate in from clast margins or outward from the interior. Other clast margins are planar and have sharp or finely serrated margins which imply that they are quench fractures.

Mesoblocky clasts — Mesoblocky clasts are an important but relatively minor component of some vesicular and poorly vesicular closely-packed and dispersed peperite facies. Along margins of mesoblocky domains, jagged sediment-filled fractures dissect the igneous component, defining progressively smaller fragments. Remnant finger-like projections of coherent and in situ fragmented igneous component extend out from margins of the coherent facies into clouds of mesoblocky fragments (Fig. 6C). Fragments are angular with finely serrate margins, and are mostly 1-5 mm across. Adjacent to fingers, many fragments display jigsaw-fit texture and are separated by only small amounts of sediment. Jigsaw-fit texture is absent in sediment matrix-rich breccia only a small distance into the breccia. Large clasts with shapes similar to mesoblocky clasts are an important component of incompletely fragmented domains.

Polyhedral blocky clasts — Polyhedral blocky clasts have angular, blocky and cuneiform shapes bounded by curviplanar margins (Fig. 6D). In some outcrops, broadly curved first-order fractures outline large blocky clasts which are dissected by second-order fractures into jigsaw-fit aggregates of progressively smaller polyhedral blocky clasts. Jigsaw-fit textures are disturbed in some parts of the breccia. Disturbance produces results which range from the slight modification of jigsaw-fit, by rotation and translation of fragments, to large scale separation of clasts.

Irregular blocky clasts — Strongly vesicular domains of dispersed peperite are characterised by a high proportion of clasts with irregular blocky shapes. Clasts are equant in shape, but bound by irregular to feathered margins which are in part the former walls of vesicles (Fig. 6E). Strongly vesicular clasts are bound mostly by vesicle walls and have feathered terminations. Highly irregular clast margins reflect rapid changes in the direction of fractures as they cut vesicles. Along contacts with coherent vesicular domains, clasts commonly display jigsaw-fit texture. Jigsaw-fit texture is lost as more sediment separates clasts.

Platy clasts — Platy clasts (Brooks 1995) are common in both closely-packed and dispersed peperite facies but are the principal clast type of closely-packed peperite. Platy clasts are several times longer than they are wide and show planar or irregular margins. They reflect the propagation of planar sediment-filled fractures (e.g. sheet, en-echelon) within relatively coherent facies.

Some clasts in peperite are bound by both globular to spongy margins and sharp planar-curviplanar margins, so that they do not fall into any one of the main textural groups (Fig. 6F).

Figure 6.

Clast types in peperite associated with the Blow Hole and Bumbo Latite Members.

(A) Discrete and interconnected incipient clasts with entrail globular shapes (light) enclosing and enclosed by sandstone (s).

(B) Incipient equant globular clasts with bulbous digitate margins invaded by thin fluidally-shaped sediment seams (arrow).

(C) Finger-like projection of basaltic andesite (f) showing progressive disintegration into mesoblocky fragments with finely serrate margins. Jigsaw-fit between fragments (arrow) is lost as sediment (s) penetrates fractures.

(D) In this example of polyhedral blocky peperite, clasts are separated by small amounts of sandstone matrix (s). Groups of clasts with jigsaw-fit contrast with domains where clasts have rotated and moved (arrow).

(E) Irregular blocky clasts bound by margins which are in part the former walls of vesicles (arrow) and enclosed in sandstone (s).

(F) In this domain of dispersed peperite, margins of clasts vary from planar-curviplanar to delicately fluidal (skeletal/spongy). These clasts imply a change in fragmentation mechanism during magma-sediment interaction.

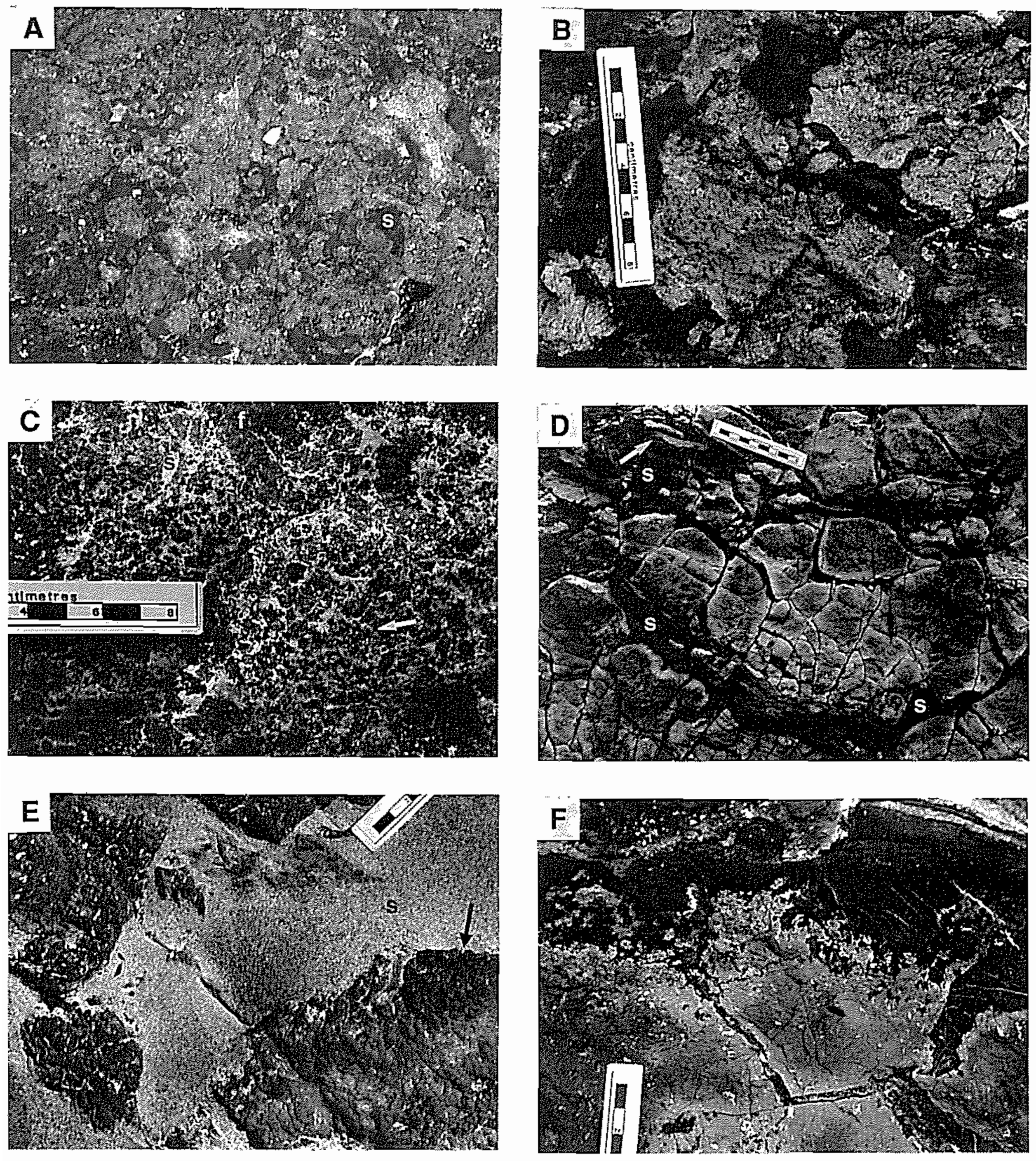
A
S
B
centimetres
C
f
S
ntimetres
4
6
8
D
S
S
S
E
S
F

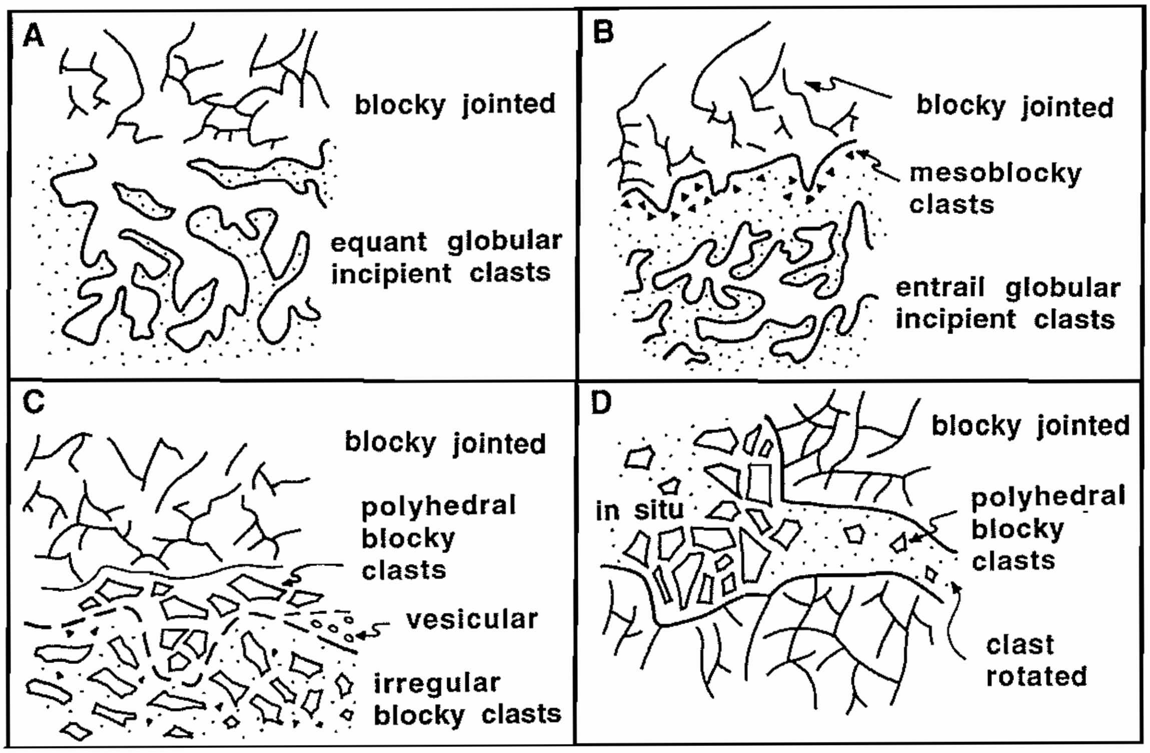

Figure 7. Associations of different clast shapes in peperitic domains. A— Peperite consisting entirely of discrete and incipient clasts with equant globular shapes. B— Textural association involving clasts with mesoblocky and entrail globular shapes. C— Transition from blocky jointed facies into peperite with zones of polyhedral blocky clasts and irregular blocky clasts. D— Blocky-jointed coherent and hyaloclastite facies pass into polyhedral blocky peperite with in situ and clast-rotated texture. No scale is implied as the relative proportion and extent of each textural zone varies considerably.

Textural associations

The foregoing discussion highlights the wide variation in clast types in peperite. The distribution of clast types is not random. Textural zones are defined here as a domain of one clast type in hyaloclastite or peperite. Peperite may consist entirely of one textural zone or of multiple textural zones, arranged geometrically in recurrent textural associations. Variation in vesicularity is a principal determinant of clast types and textural associations. In closely-packed peperite, the magmatic component is consistently poorly vesicular, observed clast types are restricted to platy, globular and mesoblocky types, and textural associations are less diverse. Only short segments of a few fractures have mesoblocky and globular textures. In dispersed peperite, four principal associations have been recognised: (1) blocky jointed - equant globular; (2) blocky jointed - mesoblocky - entrail globular; (3) polyhedral blocky - irregular blocky; and (4) hyaloclastite - polyhedral blocky (Fig. 7).

Sediment matrix

Sediment forms the matrix to clasts, partially surrounds incipient clasts, and fills fractures and joints. The three principal sediment types, from most to least abundant, are: reddish-brown sandstone and minor siltstone, yellow-brown sandstone and granular to pebbly sandstone. Wisps and laminae of one grain size are enclosed by sediment of another grain size. Discontinuous planar- and rare cross-lamination are common to all peperitic facies, but best developed and most continuous in sediment-filled subhorizontal fractures in closely-packed peperite facies. Within the fractures, lamination is broadly concordant to walls but locally terminates against steps in the fractures. At one locality, laminae partially mantle a clast-supported lens of well-rounded granules which are concentrated on the ?lee side of a juvenile clast derived from the walls of the sheet fracture (Fig. 3F). Concentration of lithic clasts and fines depletion are interpreted to reflect local turbulence as fluids (water and steam) and sediment streamed through the fracture. Similarly, elutriation of fine sediment from some parts of the peperite is suggested by their sediment matrix-poor, clast-supported, but disrupted character. In some of these cases, wide subhorizontal fractures in blocky jointed coherent facies have sediment-poor, juvenile clast-supported breccia at their bases and sediment-rich upper parts which support large juvenile clasts. The distribution of sediment and juvenile clasts is similar to reverse coarse-tail grading.

Discussion

Emplacement and cooling

Contraction that accompanied cooling of the Bumbo and Blow Hole Latite sheets produced a variety of joint styles which are zonally arranged relative to peperitic and sedimentary facies, and record unequal rates of cooling. There is a transition from columnar jointed facies, through blocky jointed facies, into hyaloclastite along contacts with the enclosing sediments and/or peperite.

Columnar joints developed as intersecting contraction cracks nucleated within the blocky jointed zone and migrated towards the interior of the sheets, perpendicular to surfaces of equal tensile stress (Spry 1962, Long and Wood 1986). The pattern of columnar jointing suggests that, in most domains, surfaces of equal stress were parallel to isothermal surfaces at the contacts of the sheets, and columns formed perpendicular to both. Cooling of the igneous component along contacts with some dyke-like peperitic domains produced a distinctive style of columnar jointing. Initially, columns formed perpendicular to subvertical isothermal surfaces at the dyke margin but progressively steepened away from the dykes under a greater influence of isothermal surfaces parallel to sheet margins.

Sediment fills the space between some columns and other columns are dissected by blocky joints filled with sediment. These relationships suggest that columnar joints acted as pathways for the infiltration of wet sediment into the interior of the sheets. In blocky jointed zones, similar fractures may have provided access for fluids (± sediment) to move in and fragment the margins of the sheets (cf. Watanabe and Katsui 1976, Yamagishi 1987, 1991, Yamagishi and Goto 1992). The inward progression from blocky jointing to pseudo-pillow structure reflects a decrease in the degree of fragmentation and decrease in the cooling rate. In places, blocky jointed coherent facies developed along peperitic contacts, but more often, blocky jointing formed in a distinct zone inward from the hyaloclastite zone. In the hyaloclastite zone, quench fractures dissected joint blocks into jigsaw-fit aggregates of polyhedral blocky clasts (cf. Dimroth et al. 1978, Yamagishi 1979).

Vesiculation

Vesicle distributions in the Bumbo and Blow Hole Latite sheets are interpreted to reflect both primary magmatic vesiculation and vesiculation due to injection of steam from external water prior to complete solidification (cf. Fuller 1931, Waters 1960, Macdonald 1972, Walker 1987). Vesicles in poorly vesicular, coherent and peperitic facies probably reflect degassing of primary magmatic volatiles. Strongly vesicular zones are sparse, invariably associated with peperite and are localised and discontinuous. Isolated strongly vesicular pods in otherwise dense, massive, poorly vesicular basalt and basaltic andesite have not been observed (cf. Dimroth et al. 1978, Sahagian et al. 1989, McMillan et al. 1987, 1989). The association of peperite and domains of strong vesicularity suggest that the lava incorporated limited amounts of steam from the wet sediment in the initial stages of peperite formation (cf. Smedes 1956). Vesicular domains are interpreted as a form of vesicle cylinder. Wet sediment was heated and pore water vaporised as it moved into the magmatic component in dispersed peperite. A vesicular front may have propagated out into the magmatic component as sediment entered peperitic domains. Vesiculation was complete prior to brecciation, as sediment-filled fractures cut across vesicles and no clasts are zoned with respect to vesicularity. Vesiculation of fracture walls in closely-packed peperite did not occur, as the sediment was partially dewatered or the fluid was not vaporised, or the magmatic component had cooled sufficiently to resist vesiculation, or the lava had already degassed. Fraser (1976) attributes vesicle cylinders (2-20 cm across) in high-alumina basalts of the Cascade Mountains and Modoc Plateau to segregation of bubbles and residual melt into regularly spaced vertical cylinders. Although this mechanism cannot be discounted, the association of peperite and strong vesicularity in the Bumbo and Blow Hole Latite sheets favours the interpretation of vesiculation by steam.

Stress waves generated by high-pressure vaporisation of pore water at the melt-sediment interface can induce vesiculation of the melt (Wohletz 1983). Steam explosions are interpreted to have played a minor role in generating peperite in the Blow Hole and Bumbo Latite Members, suggesting that stress wave induced vesiculation was insignificant.

Relatively few vesicles are filled with sediment, even in nearly scoriaceous peperite facies of the Bumbo and Blow Hole Latite Members (cf. Branney and Suthren 1988, Brooks et al. 1982). This may reflect a lack of interconnection between vesicles or that particles were too large to move through interconnections.

Lobes

Lobe types A-D lobes may simply be isolated coherent patches within otherwise strongly brecciated material. Alternatively, they could be interpreted as fractured and dismembered lava lobes, extruded into and partially or completely enclosed by their own or earlier peperite and hyaloclastite. Along some contacts, coherent facies pass through peperite containing jigsaw-fit clasts into lobes, demonstrating that type A-D lobes have formed through incomplete brecciation of coherent facies. Along contacts and in peperite where jigsaw-fit textures are not preserved, formation of lobes through extrusion/intrusion cannot be discounted. Type D lobes formed as vesicular pods in the sheet fragmented and mixed with sediment, leaving poorly vesicular domains. Complete loss of jigsaw-fit texture is widespread in the breccia surrounding type D lobes, so that they appear to invade earlier peperite. However, poorly vesicular coherent facies along the margins of peperitic facies enclose strongly vesicular pods which are coherent analogues of the matrix to type D lobes in peperite.

Fluidisation of the host sediment

The ability of sediment to penetrate even the finest fractures and large spaces in the interior of the basalt-andesite sheets to distances of tens of metres from the base, indicates that the sediment was highly mobile during peperite formation. Kokelaar (1982) ascribed similar features in peperitic facies of Ordovician andesitic and rhyolitic sills from Scotland and Wales to fluidisation of sediment by heating of pore water at sediment-magma contacts. In the present case, water at contacts was vaporised and some sediment injected up into the sheets, forming domains of peperite. Injection was driven by the relatively low density of the fluid-sediment mix compared with the magma and undisturbed sediment, and possibly by fluid over-pressure. The density inversion requires a disturbance to initiate flow of the low density layer, so that vapour expansion driven by the transition of water to steam may be more important, at least initially. The fluid-sediment slurries may have moved along fractures formed by contraction and/or quenching, or as propagating sediment dykes. Vesiculation of the magma by steam preceded the formation of peperite by mixing with the fluidised sediment. Some parts of the surrounding magma remained sufficiently plastic to deform around mushroom-shaped tongues of sediment which penetrated up from contacts with peperitic domains.

Irregularities, fractures or peperitic domains at the margins of the sheets may have been preferred sites for the injection of fluid-sediment slurries (cf. Brooks 1995). Invasion of the sediment was probably vigorous but was not obviously explosive as jigsaw-fit textures between clasts and incipient clast are widely preserved, and contacts between vesicular and non-vesicular peperite are sharp with little mixing of clast types. Also, igneous clasts in the peperite commonly have bulbous, feathered or irregular outlines, rather than the angular blocky shapes typical of phreatomagmatic brecciation.

Remnant sedimentary lamination in sediment filling space between clasts in peperite has been described by many authors (e.g. Hanson and Wilson 1993, Kokelaar 1982, Branney and Suthren 1988, Hanson 1991, Brooks 1995). In the present case, wisps, seams or planar and cross laminae of one grain size are enclosed in, or alternate with, sediment of another grain size, producing extremely complex relationships in some cases. Lamination could be interpreted as: (i) relic primary bedding rotated and disrupted during intrusion; (ii) laminated sediment which infiltrated from above; or (iii) non-primary lamination. Structures are often subhorizontal, consistent with regional bedding, but are interpreted as non-primary sedimentary lamination because: (1) lamination is well developed within peperite facies completely enclosed by massive coherent lava; (2) lamination filling fractures in closely-packed peperite is parallel to fracture walls and could only be introduced along the length of the fractures (up to 30 m) through fluidisation; (3) structures in the sediment (e.g. cross lamination and lithic lenses in closely-packed peperite; reverse coarse-tail grading) are not consistent with washing-in processes. Layering reflects the repeated streaming of highly mobile sediment through fractures, and the intrusion of initial fracture- or space-filling sediment by coarser grain sizes. Vapour pressure was building, equilibrating and waning rapidly and unevenly in the invading sediment as it streamed to fill propagating fractures and open spaces. Rapid changes in sediment paths, superposition of sediments with different grains during the merging of fractures, and propagation of fractures at different rates all may have all been important in affecting vapour pressure and generating layering.

Relative timing

Figure 8 illustrates the relative timing of development of textures and structures in the Blow Hole and Bumbo Latite Members. Degassing of the sheets occurred both during emplacement, as evidenced by elongate vesicles, and after flow ceased, as indicated by spherical vesicles. Formation of vesicle cylinders clearly must have occurred while the sheets were still ductile, but probably after emplacement. Mixing of the lava and fluidised sediment formed domains of dispersed peperite. The general restriction of hyaloclastite and blocky jointed facies to the margins of peperitic domains suggests that fractures developed concurrent with peperite in these domains. Columnar joints developed over a large part of the cooling history. Incipient columns dissected by blocky joints formed early concurrent with peperite. Long, well developed columnar joints in the massive interior of the sheets reflect slow cooling, largely following fragmentation and peperite formation. Sediment penetrating columnar joints at the base of the Blow Hole Latite Member, and filling brittle (en-echelon) fractures, suggest that sediment was moving through the sheet even in the late part of the cooling history.

Mechanisms of brecciation

The shape of clasts and contacts between sediment and the igneous component in peperite is a guide to fragmentation processes. Experimental and theoretical studies of magma-water interaction (e.g. Sheridan and Wohletz 1983, Wohletz 1986, Kokelaar 1986) have produced textures, structures and clasts with shapes which are similar to those observed in peperite, suggesting the mechanisms of magma-water interaction and magma-water-sediment interaction may be similar. Four primary clast forming processes are currently recognised to occur during magma-water interaction; magmatic explosivity, steam explosivity, cooling-contraction granulation, and dynamic stressing (e.g. Wohletz 1983, Kokelaar 1986). Steam explosivity is divisible into contact-surface interaction and bulk interaction (Kokelaar 1986).

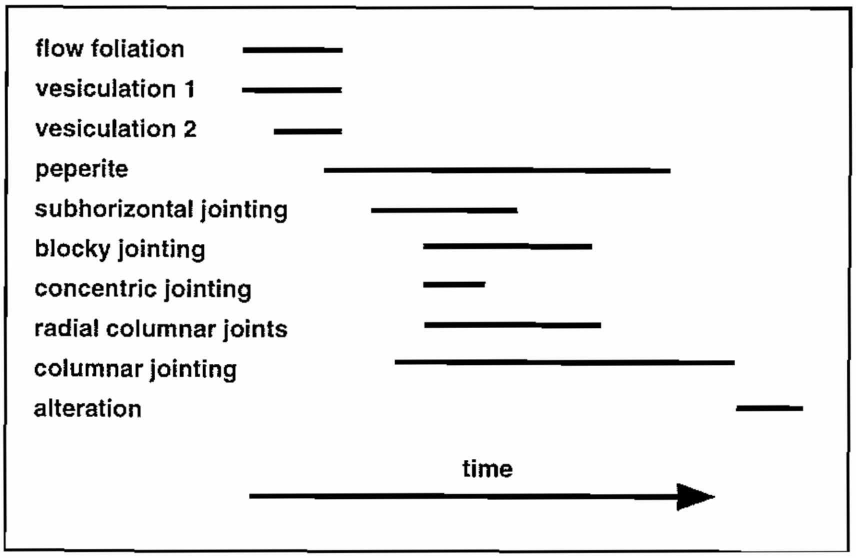

Figure 8. Relative timing of development of textures and structures in the Blow Hole and Bumbo Latite Members. Exsolution of magmatic volatiles (vesiculation 1) was probably initiated in the vent and continued through vesiculation by heating of pore water during interaction between magma and wet sediment (vesiculation 2).

Peperite comprising globular clasts indicates that non-explosive, contact-surface interaction and bulk interaction are probably important in the formation of peperite. Good evidence for contact-surface interaction is seen where tongues and apophyses of the igneous component transect undisturbed laminated or bedded host sediment, implying the passive removal of sediment during emplacement (cf. Branney and Suthren 1988). This was achieved by film boiling of pore water (Leidenfrost effect; Mills 1984), causing fluidisation of sediment at the magma-sediment interface. Sediment is displaced along and away from the contact zone until cooling below a critical temperature (Leidenfrost temperature) causes steam to condense and the sediment to be deposited. Oscillations in the vapour film can distort the magma surface into delicate bulbous fluidal shapes which detach, generating small fluidally-shaped fragments (Sheridan and Wohletz 1983, Wohletz 1986). Vapour films insulated the magma from direct contact with sediment and suppressing both steam explosions and quench fragmentation.

A case for bulk interaction in peperite formation is suggested where pods and seams of sediment are enclosed in the igneous component or occur between incipient clasts (cf. Kokelaar 1986, Branney and Suthren 1988, Brooks 1995). The main clast-forming process is the tearing-apart of the igneous component around invading and expanding steam-sediment slurries. Propagation of sediment seams promotes the disintegration of relatively coherent igneous material into progressively smaller clasts. Initially only a thin film of sediment, a few millimetres or centimetres wide, fills the seams. Walls of clasts are progressively wedged apart as sediment penetrates the seams. Vaporisation of pore water may have generated pressure waves causing disintegration of the magma. Kokelaar (1986) suggests that heat exchange between the magma and sediment through convective heat transfer may be more important than by direct contact mixing during bulk interaction. However, fluidally-shaped margins to incipient clasts with entrail and equant globular shapes suggest that direct contact mixing is in some cases important, and implies that bulk interaction and contact-surface interaction have combined to fragment the magma. Conductive heat transfer, a function of surface area and time of heat transfer, may increase as margins are "roughened" and the melt fragmented by contact-surface interaction, but will be limited by the insulating effects of a continuous vapour film. Concurrent bulk- and contact-surface-interaction combined to fragment the greatest percentage of the Blow Hole Latite Member.

In examples of peperite comprising ragged clasts, higher yield strengths at the strain rates which accompanied fragmentation are suggested by finely serrated, ragged clast margins. Again, bulk interaction during magma-sediment interaction may be indicated by textures in these domains. However, clasts with ragged shapes formed during bulk interaction (e.g. Branney and Suthren 1988) are similar to those produced by dynamic stressing.

Dynamic stress fragmentation is ascribed to brecciation of the chilled parts of lavas or intrusions by the continued movement of fluid magma in the interior.

In peperite comprising polyhedral blocky clasts, fractures define equant blocks, whereas platy clasts form by intersecting subparallel planar fractures and more widely spaced short cross fractures (cf. Brooks 1995). Clast shapes reflect different local stress fields, and may represent end members of a spectrum of clast shapes formed by quenching. Small scale changes in the direction of propagation of quench fractures in response to internal heterogeneities in the igneous component (e.g. phenocrysts) form jagged blocky/platy clasts bounded by serrated margins rather than sharp planar and curviplanar margins characteristic of polyhedral blocky clasts and some platy clasts (cf. Brooks 1995).

It remains unclear what the mechanism of formation of mesoblocky clasts was. Brittle failure may have resulted from propagation of stress waves through the melt in response to the collapse or explosive expansion of vapour films (cf. Wohletz 1983), or through cooling-contraction granulation. Turbulent mixing following quenching of the resulting fragments promoted the movement of fragments out of the zone of interaction and loss of jigsaw-fit texture.

Vesicles strongly influence the character of peperite formed when magma or lava invades wet, unconsolidated sediment. Fractures which cut across vesicles generate irregular blocky clasts with margins which are in part the former walls of vesicles. Vesiculation which occurs concurrent with fragmentation is likely to play a more active role in determining clast shape, but will be limited because bubbles will be entrapped as cooling proceeds and viscosity increases. An insulating sheath of vapour which forms at the contact between the magma and enclosing wet sediment may allow some bubbles to reach the magma-sediment interface (Mills 1984). Vapour bubbles which reach, form at, or penetrate the melt-film interface will probably interact with it, creating local pressure gradients which will influence vapour flow and hence also the shape of the contact surface and clasts.

Textural associations: evidence for controls on peperite formation

Textural associations of more than two clast types, and individual clasts with both bulbous and planar margins, imply a change in fragmentation mechanism. In many cases, initial magma fragmentation and mixing with sediment is thought to have resulted mainly from the tearing apart of the magma (bulk interaction) and shaping of the magma-sediment interface into fluidal globular shapes by contact-surface interaction. In other cases, globular surfaces and clasts developed first. Planar fractures reflect fragmentation by cooling-contraction granulation and/or by propagating stress waves. Planar fractures which cut across and displace fluidal globular surfaces in the igneous component formed later (cf. Goto and McPhie 1996). The relationship between some planar fractures and globular surfaces is ambiguous and both may have formed simultaneously with viscosity and/or temperature being the control.

Bulk physical properties, such as the density and viscosity of the magma and sediment will in part control their behaviour during interaction. Difficulties in determining the physical properties driving transitions in fragmentation mechanism result from the complex and rapidly changing states of the components. For example, the magmatic component will become more viscous with time, and steam together with volatiles can promote multi-stage vesiculation of the melt. The sediment may be progressively dewatered during interaction, with intergranular fluids ranging in temperature from cold to boiling or superheated steam. Also, the host sediment is itself a many-phase system.

Busby-Spera and White (1987) concluded that host sediment properties strongly influence magma-sediment interaction, and hence the shapes of clasts. They suggest that fluidal globular peperite is more likely to develop in fine-grained, well sorted, loosely packed sediment, as it is more easily fluidised and vapour films can be maintained at the melt-sediment interface. Coarser, poorly sorted sediment is associated with blocky-shaped clasts (blocky peperite) at Punta China, Baja, California. In these, greater permeability was interpreted to inhibit the development of vapour films, and only a small percentage of the sediment grain size is amenable to fluidisation. In the absence of insulating vapour films, quench fragmentation and steam explosions are the main fragmentation processes. At Kiama, different clast types occur within sediment of constant grain size (Fig. 6F). Similarly, clasts with the same shape occur in sediment with different grain sizes. These examples suggest that factors other than sediment grain size are also important in determining fragment shape (cf. Goto and McPhie 1996). However, sediment surrounding clasts in peperite represents the final grain size distribution at the time of fragmentation and not necessarily that which was present at the time of fragmentation.

Fragmentation processes are complexly dependent on external confining pressure. In cases where the lithostatic and hydrostatic pressure exceed the critical pressure (about 31.2 Mpa for seawater; Kokelaar 1982), the degree of expansion of heated pore water is impeded, steam explosions are suppressed and fluidisation may be inhibited. At lower confining pressures steam may expand explosively. The character of peperite examined in this study suggests that confining pressures were insufficient to suppress fluidisation of the host sediment along magma-sediment contacts or to prevent vesiculation of the magma, but large enough to inhibit steam explosivity.

Experimental and theoretical studies (Sheridan and Wohletz 1981, 1983; Wohletz 1983, 1986) suggest that changes in the water/magma ratio may lead to changes in eruption style. In peperite, it is possible that both short and long term variations in water (and sediment)-melt ratios may be responsible for the changing fragmentation mechanisms, and so clast shapes. Direct application of results from experimental and theoretical studies of magma-water interaction to magma-slurry systems involving peperite is probably not possible. Also, changes in the water/melt ratio may occur due to varying volume rate of magma or sediment supply and fluxing of sediment with varying pore water contents during fragmentation.

Viscosity reduces growth rates of instabilities at the magma-sediment interface (Wohletz 1986), so that high viscosity magmas may mix more slowly with sediment than would low viscosity magmas. One might expect clasts with fluidally-shaped margins to be more common in peperite involving magma of mafic rather than silicic composition. The spectrum of clast shapes recognised in peperite span magma compositions ranging from basaltic to rhyolitic, suggesting that this may not be the case. However, changes in the rheological behaviour of a given magma from ductile to brittle, most likely in response decreasing viscosity, are clearly important in cases where peperite contains single clasts bound by both globular and planar surfaces. Planar fractures displace fluidal globular surfaces suggesting that they formed later. During the globular clast-forming stage, the magma had a relatively low viscosity and sediment was displaced by fluidisation. Planar and curviplanar fractures formed as the magma became more viscous, most likely in response to decreasing temperature and/or the breakdown of insulating vapour films at the magma-sediment interface (cf. Goto and McPhie 1996)

Viscosity profiles in some lavas and intrusions are likely to be complex, varying in response to, for example, pulsatory flow or intrusion (cf. Goto and McPhie 1996), and differing volatile contents, crystallinity and temperature. If magma rheology fluctuates then different parts of an intrusion or lava may be associated with peperite with different clast types and/or textural associations. Fluidal contacts and clasts will be generated early or in domains where the magma temperature is highest and viscosity is at a minimum. Continued flow will stress those parts that have already begun to cool and solidify, promoting brittle disintegration along contraction fractures, and clasts with blocky or ragged shapes are more likely to form. Also, if wet sediment injects the magma in pulses, then magma rheology at the time or site of interaction might fluctuate and different clasts form.

Conclusions

Peperites associated with basaltic to basaltic andesite lavas and intrusions in the Late Permian Broughton Formation, Kiama, New South Wales have been described on the basis of (1) igneous clast shape; (2) fabric; and (3) location with respect to the margins of the lava or intrusion. The complexities of peperite, in terms of clast types and their relative abundances and distribution, as well as textures and structures in the host sediment, indicate that a spectrum of fragmentation and mixing processes may occur together and thus interact.

Examples of peperite with more than one clast type, involving magma of the same composition and sediment of constant grain size, are common. In many examples, globular surfaces formed during an early, low viscosity phase of magma emplacement into wet sediment. Planar and curviplanar fractures truncate some fluidal surfaces suggesting that these, at least in part, formed slightly later as the magma became more viscous (cooler) and/or vapour films at the magma-sediment interface broke down (cf. Goto and McPhie 1996).

The intimate mixing of magma and wet sediment recorded by peperite is commonly a precursory step towards explosive hydromagmatism. At Kiama, peperite has developed by one or a combination of (1) non-explosive oscillation of vapour films at the magma-sediment interface (contact-surface interaction); (2) non-explosive expansion of pore water following enclosure of sediment in the magma or entrapment of sediment at the magma-sediment contacts (bulk interaction), (3) cooling-contraction granulation; and (4) brecciation of the chilled parts of an intrusion-extrusion by flow of the hotter interior (dynamic stressing).

Fluidisation of the host sediment during mixing with the melt is common to peperite involving clasts from all of the textural groups. Lamination in sediment within peperite can include remnants of original stratification (e.g. Kokelaar 1982) and layering formed by the streaming of fluid-sediment slurries through fractures and between clasts.

References

Beach A., 1975. The geometry of en-echelon vein arrays. Tectonophysics, 28: 245-263.

Bowman H.N., 1974. Geology of the Wollongong, Kiama, and Robertson 1;50 000 sheets. Geol. Surv. New South Wales, 179 pp.

Branney M.J. and Suthren R.J., 1988. High-level peperitic sills in the English Lake District: distinction from block lavas, and implications for Borrowdale Volcanic Group stratigraphy. Geol. J., 23: 171-187.

Brooks E.R., 1995. Paleozoic fluidization, folding, and peperite formation, northern Sierra Nevada, California. Can. J. Earth Sci., 32: 314-324.

Brooks E.R., Wood M.M. and Garbutt P.L., 1982. Origin and metamorphism of peperite and associated rocks in the Devonian Elwell Formation, northern Sierra Nevada, California. Geol. Soc. Am. Bull., 93: 1208-1231.

Bull S.W. and Cas R.A.F., 1989. Volcanic influences in a storm and tide dominated shallow marine depositional system: the Late Permian Broughton Formation, southern Sydney Basin, Kiama, NSW, Australia. Aust. J. Earth Sci., 36: 569-584.

Busby-Spera C.J. and White J.D.L., 1987. Variation in peperite textures associated with differing host-sediment properties. Bull. Volc., 49: 765-775.

Carr P.F., 1985. Geochemistry of Late Permian shoshonitic lavas from the southern Sydney Basin. Publication of the Geological Society of Australia, New South Wales Division, 165-183.

Cas R. and Bull S., 1993. Influence of environment on contrasting styles of volcanism: the Devonian Boyd Volcanic Complex, Southeastern Australia. Aust. Geol. Surv., 68 pp.

Dimroth E., Cousineau P., Leduc M. and Sanschagrin Y., 1978. Structure and organisation of Archean basalt flows, Rouyn-Noranda area, Quebec, Canada. Can. J. Earth Sci., 15: 902-918.

Fisher R.V., 1960. Classification of volcanic breccias. Geol. Soc. Am. Bull., 71: 973-982.

Francis E.H., 1982. Magma and sediment-I Emplacement mechanism of late Carboniferous tholeiite sills in northern Britain. Geol. Soc. London, 139: 1-20.

Frazer G.E., 1976. Vesicle cylinders formed in vapour-differentiated basalt flows. In: Geological Society of America. Abstracts with Programs, Denver, Colorado, 887-888.

Fuller R.E., 1931. The aqueous chilling of basaltic lava on the Columbia River plateau. Am. J. Sci., 221: 281-300.

Goto Y. and McPhie J., 1996. A Miocene basanite peperitic dyke at Stanley, northwestern Tasmania, Australia. J. Volcanol. Geotherm. Res., 74: 111-120.

Hanson R.E., 1991. Quenching and hydroclastic disruption of andesitic to rhyolitic intrusions in an submarine island-arc sequence, northern Sierra Nevada, California. Geol. Soc. Am. Bull., 103: 804-816.

Hanson R.E. and Schweickert R.A., 1982. Chilling and brecciation of a Devonian rhyolitic sill intruded into wet sediments, northern Sierra Nevada, California. J. Geol., 90: 717-724.

Hanson R.E. and Wilson T.J., 1993. Large-scale rhyolite peperites (Jurassic, southern Chile). J. Volcanol. Geotherm. Res., 54: 247-264.

Kano K., 1991. Miocene pillowed sills in the Shimane Peninsula, SW Japan. J. Volcanol. Geotherm. Res., 48: 359-366.

Kokelaar B.P., 1982. Fluidization of wet sediments during emplacement and cooling of various igneous bodies. J. Geol. Soc. London, 139: 21-33.

Kokelaar P., 1986. Magma-water interactions in subaqueous and emergent basaltic volcanism. Bull. Volc., 48: 275-289.

Lawson D.E., 1972. Torridonian volcanic sediments. Scott. J. Geol., 4: 345-362.

Leat P.T. and Thompson R.N., 1988. Miocene hydrovolcanism in NW Colorado, USA, fuelled by explosive mixing of basic magma and wet unconsolidated sediment. Bull. Volc., 50: 229-243.

Long P.E. and Wood B.J., 1986. Structures, textures, and cooling histories of Columbia River basalt flows. Geol. Soc. Am. Bull., 97: 1144-1155.

Macdonald G.A., 1972. Volcanoes. Prentice Hall, New Jersey, 510 pp.

McMillan K., Cross R.W. and Long P.E., 1987. Two-stage vesiculation in the Cohassett flow of the Grande Ronde Basalt, south-central Washington. Geology, 15: 809-812.

McMillan K., Long P.E. and Cross R.W., 1989. Vesiculation in Columbia River basalts. Geol. Soc. Am. Spec. Pub., 239: 157-167.

McPhie J., 1993. The Tennant Creek porphyry revisited: A syn-sedimentary sill with peperitic margins, Early Proterozoic, Northern Territory. Aust. J. Earth Sci., 40: 545-558.

Mills A.A., 1984. Pillow lavas and the Leidenfrost effect. J. Geol. Soc. London, 141: 183-186.

Raam A., 1964. Geology of the Minamurra-Geroa area, Sydney [BSc. Hons. thesis]. University of Sydney

Raam A., 1969 Gerringong Volcanics. In: Packham, G. M. (ed.) The geology of New South Wales. J. Geol. Soc. Aust., 16: 366-368.

Rawlings D.J., 1993. Mafic peperite from the Gold Creek Volcanics in the Middle Proterozoic McArthur Basin, Northern Territory. Aust. J. Earth Sci., 40: 109-113.

Sahagian D.L., Anderson A.T. and Ward B., 1989. Bubble coalescence in basalt flows: comparison of a numerical model with natural examples. Bull. Volc., 52: 49-56.

Sanders I.S. and Johnston J.D., 1989. The Torridonian Stac Faud Member: an extrusion of fluidised peperite? Trans. Royal Soc. Edinburgh Earth Sciences, 80: 1-4.

Schmincke H., 1967. Fused tuff and peperites in south central Washington. Geol. Soc. Am. Bull., 78: 319-330.

Sheridan M.F. and Wohletz K.H., 1981. Hydrovolcanic explosions: The systematics of water-pyroclast equilibration. Science, 212: 1387-1389.

Sheridan M.F. and Wohletz K.H., 1983. Hydrovolcanism: Basic considerations and review. J. Volcanol. Geotherm. Res., 17: 1-29.

Smedes H.W., 1956. Peperites as contact phenomena of sills in the Elkhorn Mountains, Montana. Geol. Soc. Am. Bull., 67: 1783.

Snyder G.L. and Fraser G.D., 1963a. Pillowed lavas I: Intrusive layered lava pods and pillowed lavas, Unalaska Island, Alaska. US Prof. Pap., 454-B: B1-B23.

Snyder G.L. and Fraser G.D., 1963b. Pillowed lavas, II: A review of selected recent literature. US Prof. Pap., 454-C: C1-C7.

Spry A.H., 1962. The origin of columnar jointing particularly in basalt flows. J. Geol. Soc. Aust., 8: 191-216.

Walker G., 1987. Pipe vesicles in Hawaiian basaltic lavas: Their origin and potential as paleoslope indicator. Geology, 15: 84-87.

Watanabe K.K. and Katsui Y., 1976. Pseudo-pillow lavas in the Aso Caldera, Kyushu, Japan. J. Jap. Assoc. Min. Pet. Econ. Geol., 71: 44-49.

Waters A.C., 1960. Determining direction of flow in basalts. Am. J. Sci., 258A: 350-366.

Williams H. and McBirney A.R., 1979. Volcanology. Freeman, Cooper and Company, San Francisco, 397 pp.

Wohletz K.H., 1983. Mechanisms of hydrovolcanic pyroclast formation: grain size, scanning electron microscopy, and experimental studies. J. Volcanol. Geotherm. Res., 17: 31-63.

Wohletz K.H., 1986. Explosive magma-water interactions: thermodynamics, explosion mechanisms, and field studies. Bull. Volc., 48: 245-264.

Yamagishi H., 1979. Classification and features of subaqueous volcaniclastic rocks of Neogene age in southwest Hokkaido. Geol. Surv. Hokkaido Rep., 51: 1-20.

Yamagishi H., 1987. Studies on the Neogene subaqueous lavas and hyaloclastites in southwest Hokkaido. Geol. Surv. Hokkaido Report, 59: 55-117.

Yamagishi H., 1991. Morphological features of Miocene submarine coherent lavas from the "Green Tuff" basins: examples from basaltic and andesitic rocks from the Shimokita Peninsula, northern Japan. Bull. Volc., 53: 173-181.

Yamagishi H. and Goto Y., 1992. Cooling joints of subaqueous rhyolite lavas at Kuroiwa, Yaumo, southern Hokkaido, Japan. Bull. Volcanol. Soc. Japan, 37: 205-207.

Yamagishi H., Kawachi S., Goto Y., Miyasaka S. and Koitabashi S., 1989. A Miocene submarine volcano - The Rekifune volcanic rocks in southern Tokachi, Hokkaido. Bulletin of the Volcanological Society of Japan, Ser. 2, 34: 251-261.

Appendix B

Geological cross-sections for the Highway-Reward deposit

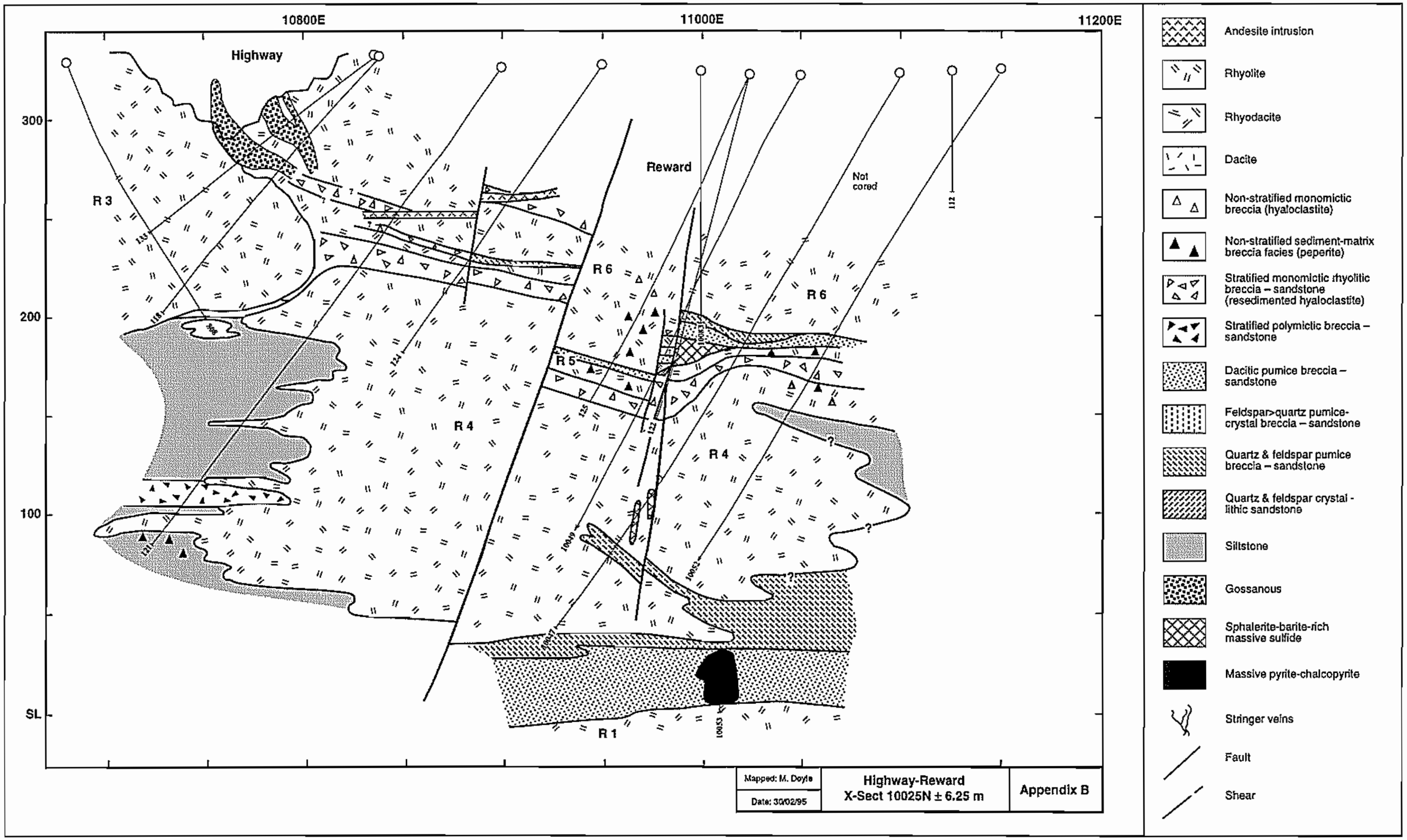
10800E
11000E
11200E
300
200
100
SL
Highway
Reward
Not cored
R 3
R 4
R 5
R 6
R 1
Andesite intrusion
Rhyolite
Rhyodacite
Dacite
Non-stratified monomictic breccia (hyaloclastite)
Non-stratified sediment-matrix breccia facies (peperite)
Stratified monomictic rhyolitic breccia – sandstone (resedimented hyaloclastite)
Stratified polymictic breccia – sandstone
Dacitic pumice breccia – sandstone
Feldspar>quartz pumice-crystal breccia – sandstone
Quartz & feldspar pumice breccia – sandstone
Quartz & feldspar crystal - lithic sandstone
Siltstone
Gossanous
Sphalerite-barite-rich massive sulfide
Massive pyrite-chalcopyrite
Stringer veins
Fault
Shear
Mapped: M. Doyle
Date: 30/02/95
Highway-Reward
X-Sect 10025N ± 6.25 m
Appendix B

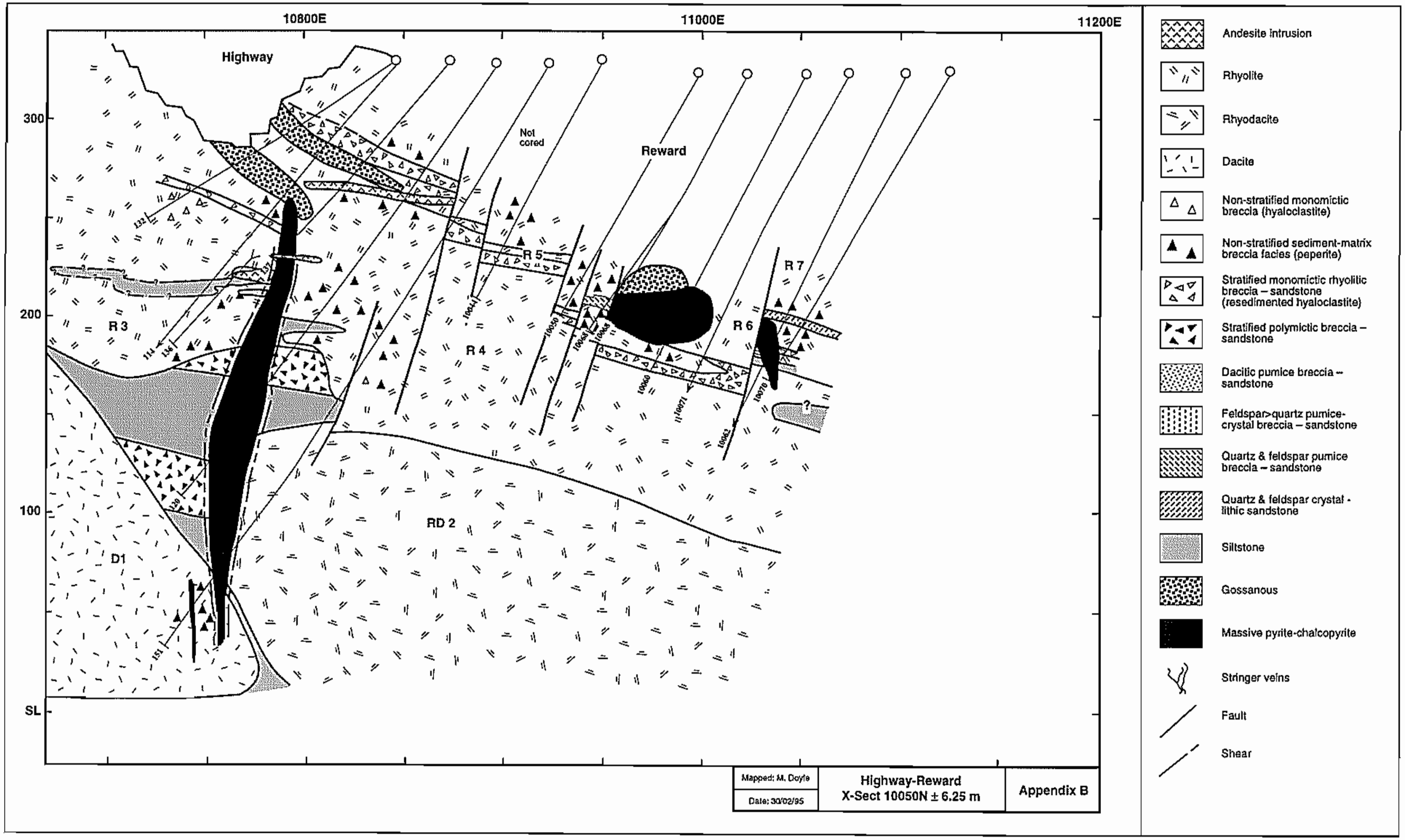
10800E
11000E
11200E
300
200
100
SL
Highway
Reward
Not cored
R 3
R 4
R 5
R 6
R 7
RD 2
D1
Andesite intrusion
Rhyolite
Rhyodacite
Dacite
Non-stratified monomictic breccia (hyaloclastite)
Non-stratified sediment-matrix breccia facies (peperite)
Stratified monomictic rhyolitic breccia – sandstone (resedimented hyaloclastite)
Stratified polymictic breccia – sandstone
Dacitic pumice breccia – sandstone
Feldspar>quartz pumice-crystal breccia – sandstone
Quartz & feldspar pumice breccia – sandstone
Quartz & feldspar crystal - lithic sandstone
Siltstone
Gossanous
Massive pyrite-chalcopyrite
Stringer veins
Fault
Shear
Mapped: M. Doyle
Date: 30/02/95
Highway-Reward
X-Sect 10050N ± 6.25 m
Appendix B

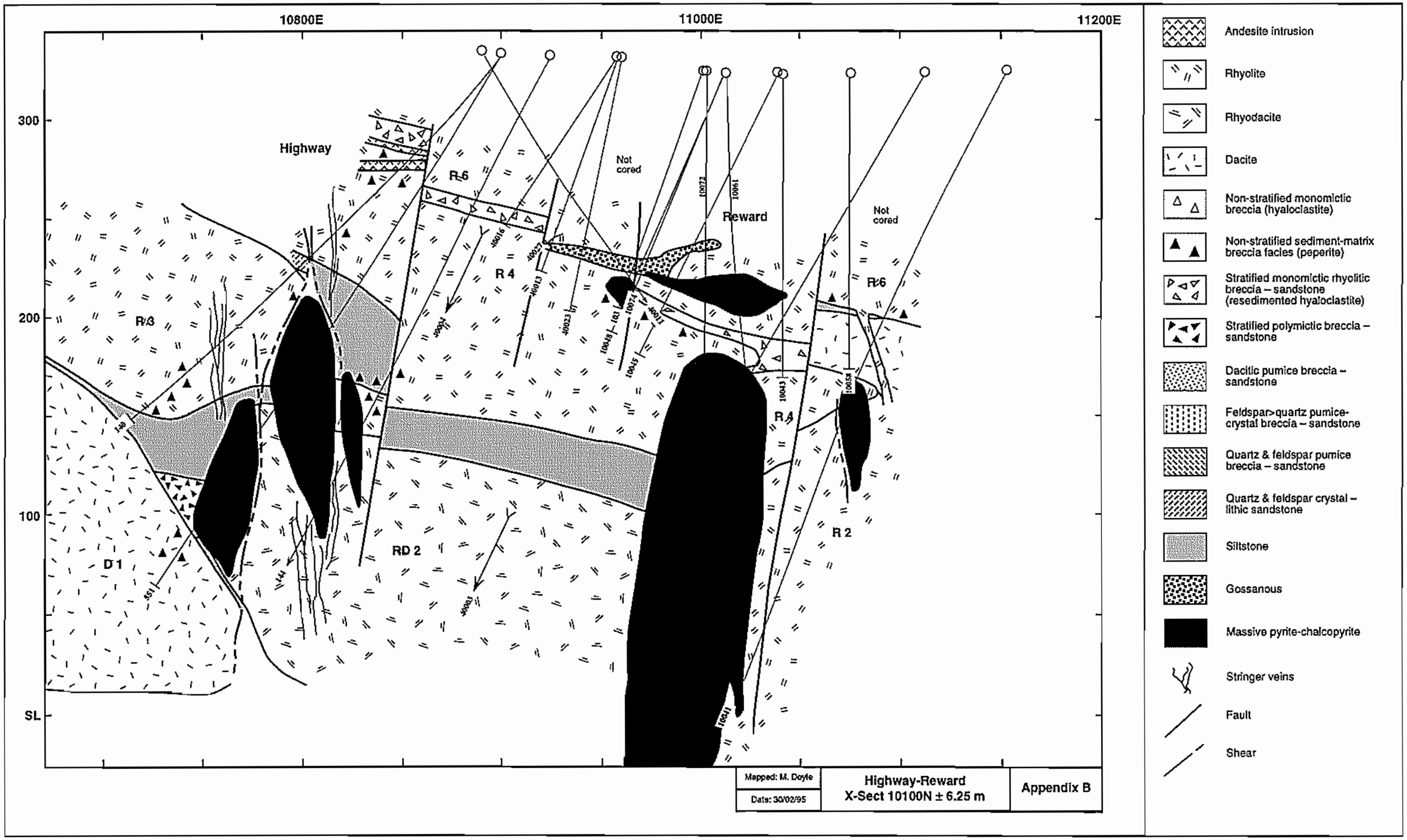
10800E
11000E
11200E
300
200
100
SL
Highway
Reward
Not cored
Not cored
R6
R4
R3
R2
RD 2
D 1
Andesite intrusion
Rhyolite
Rhyodacite
Dacite
Non-stratified monomictic breccia (hyaloclastite)
Non-stratified sediment-matrix breccia facies (peperite)
Stratified monomictic rhyolitic breccia – sandstone (resedimented hyaloclastite)
Stratified polymictic breccia – sandstone
Dacitic pumice breccia – sandstone
Feldspar>quartz pumice-crystal breccia – sandstone
Quartz & feldspar pumice breccia – sandstone
Quartz & feldspar crystal – lithic sandstone
Siltstone
Gossanous
Massive pyrite-chalcopyrite
Stringer veins
Fault
Shear
Mapped: M. Doyle
Date: 30/02/95
Highway-Reward
X-Sect 10100N ± 6.25 m
Appendix B

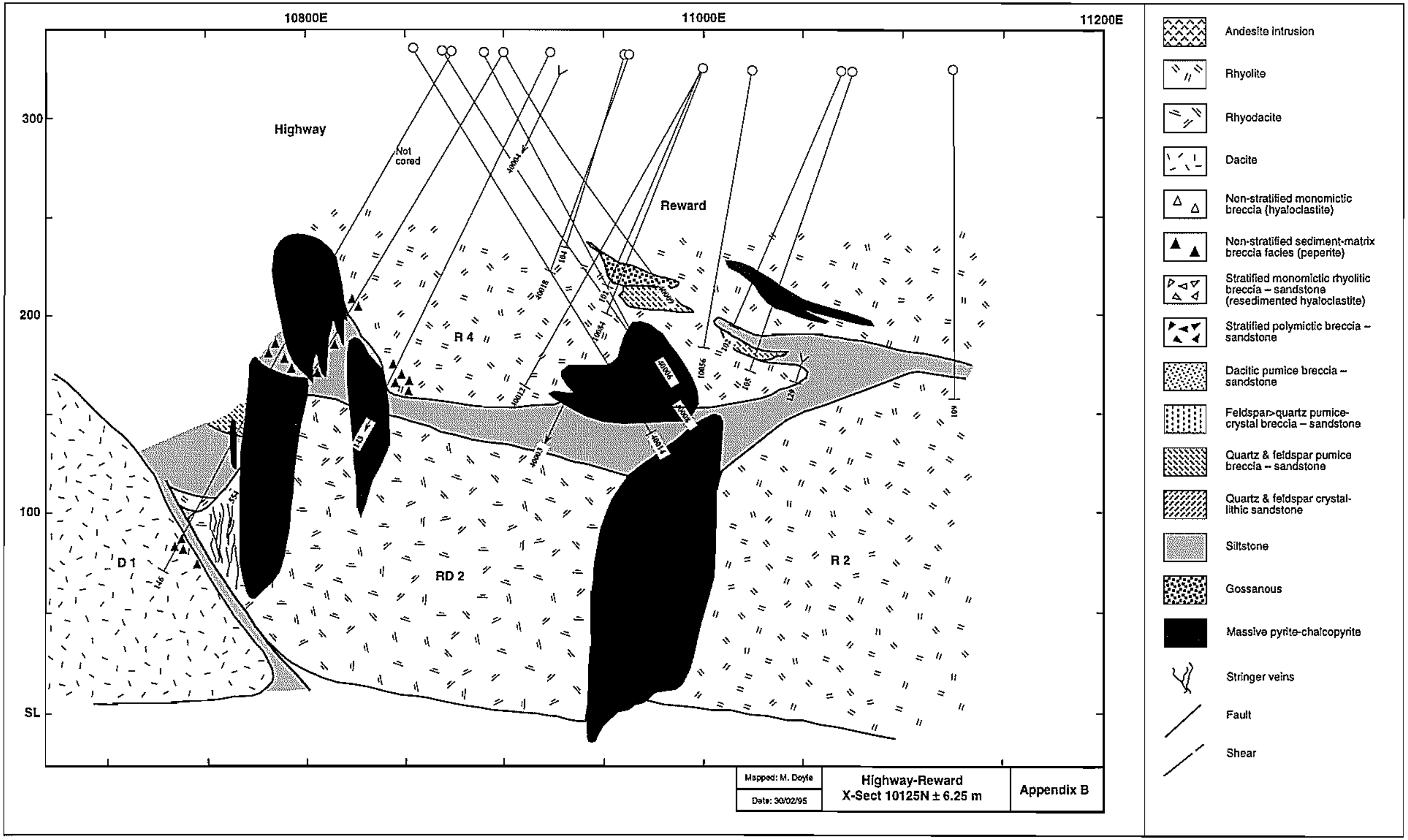
10800E
11000E
11200E
300
200
100
SL
Highway
Reward
Not cored
R 4
RD 2
R 2
D 1
Andesite intrusion
Rhyolite
Rhyodacite
Dacite
Non-stratified monomictic breccia (hyaloclastite)
Non-stratified sediment-matrix breccia facies (peperite)
Stratified monomictic rhyolitic breccia – sandstone (resedimented hyaloclastite)
Stratified polymictic breccia – sandstone
Dacitic pumice breccia – sandstone
Feldspar>quartz pumice-crystal breccia – sandstone
Quartz & feldspar pumice breccia – sandstone
Quartz & feldspar crystal-lithic sandstone
Siltstone
Gossanous
Massive pyrite-chalcopyrite
Stringer veins
Fault
Shear
Mapped: M. Doyle
Date: 30/02/95
Highway-Reward
X-Sect 10125N ± 6.25 m
Appendix B

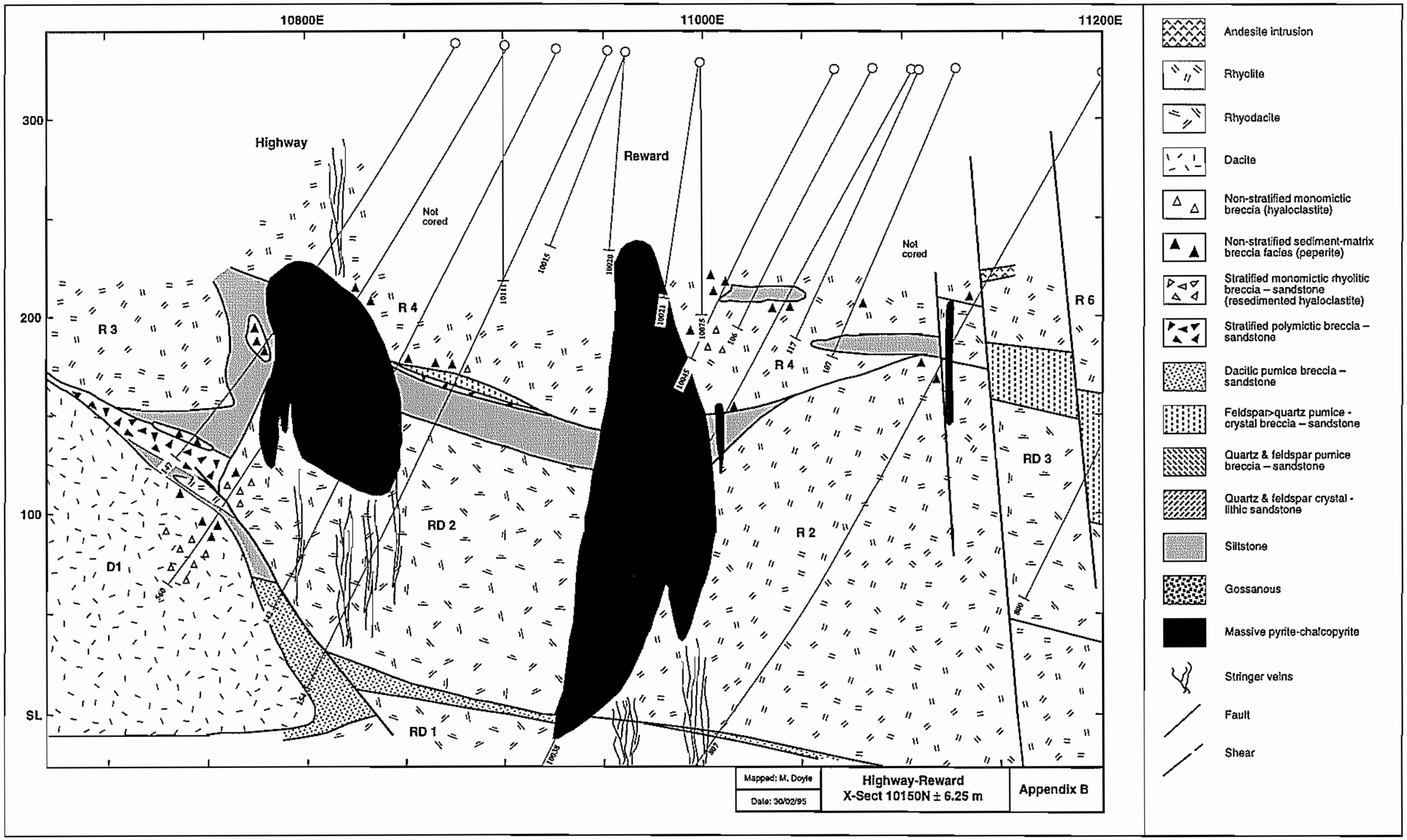
10800E
11000E
11200E
300
200
100
SL
Highway
Reward
Not cored
Not cored
R 3
R 4
R 4
R 6
RD 1
RD 2
RD 3
R 2
D1
10111
10015
10020
10021
10075
10045
10038
106
117
107
807
800
540
143
Andesite intrusion
Rhyolite
Rhyodacite
Dacite
Non-stratified monomictic breccia (hyaloclastite)
Non-stratified sediment-matrix breccia facies (peperite)
Stratified monomictic rhyolitic breccia – sandstone (resedimented hyaloclastite)
Stratified polymictic breccia – sandstone
Dacitic pumice breccia – sandstone
Feldspar>quartz pumice - crystal breccia – sandstone
Quartz & feldspar pumice breccia – sandstone
Quartz & feldspar crystal - lithic sandstone
Siltstone
Gossanous
Massive pyrite-chalcopyrite
Stringer veins
Fault
Shear
Mapped: M. Doyle
Date: 30/02/95
Highway-Reward
X-Sect 10150N ± 6.25 m
Appendix B

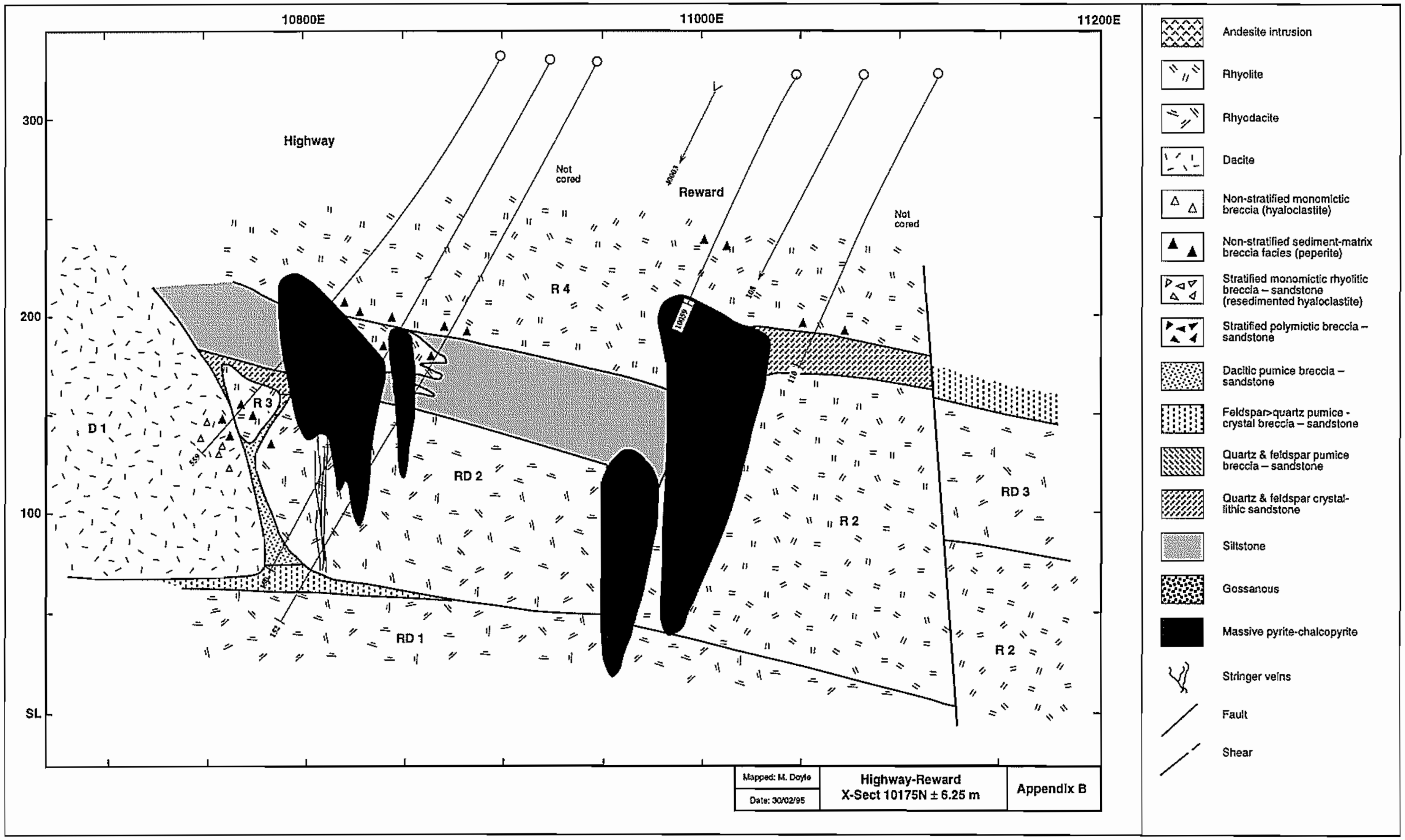
10800E
11000E
11200E
300
200
100
SL
Highway
Reward
Not cored
Not cored
R 4
R 3
D 1
RD 2
RD 1
R 2
RD 3
R 2
559
152
10059
108
110
40003
Andesite intrusion
Rhyolite
Rhyodacite
Dacite
Non-stratified monomictic breccia (hyaloclastite)
Non-stratified sediment-matrix breccia facies (peperite)
Stratified monomictic rhyolitic breccia – sandstone (resedimented hyaloclastite)
Stratified polymictic breccia – sandstone
Dacitic pumice breccia – sandstone
Feldspar>quartz pumice - crystal breccia – sandstone
Quartz & feldspar pumice breccia – sandstone
Quartz & feldspar crystal-lithic sandstone
Siltstone
Gossanous
Massive pyrite-chalcopyrite
Stringer veins
Fault
Shear
Mapped: M. Doyle
Date: 30/02/95
Highway-Reward
X-Sect 10175N ± 6.25 m
Appendix B

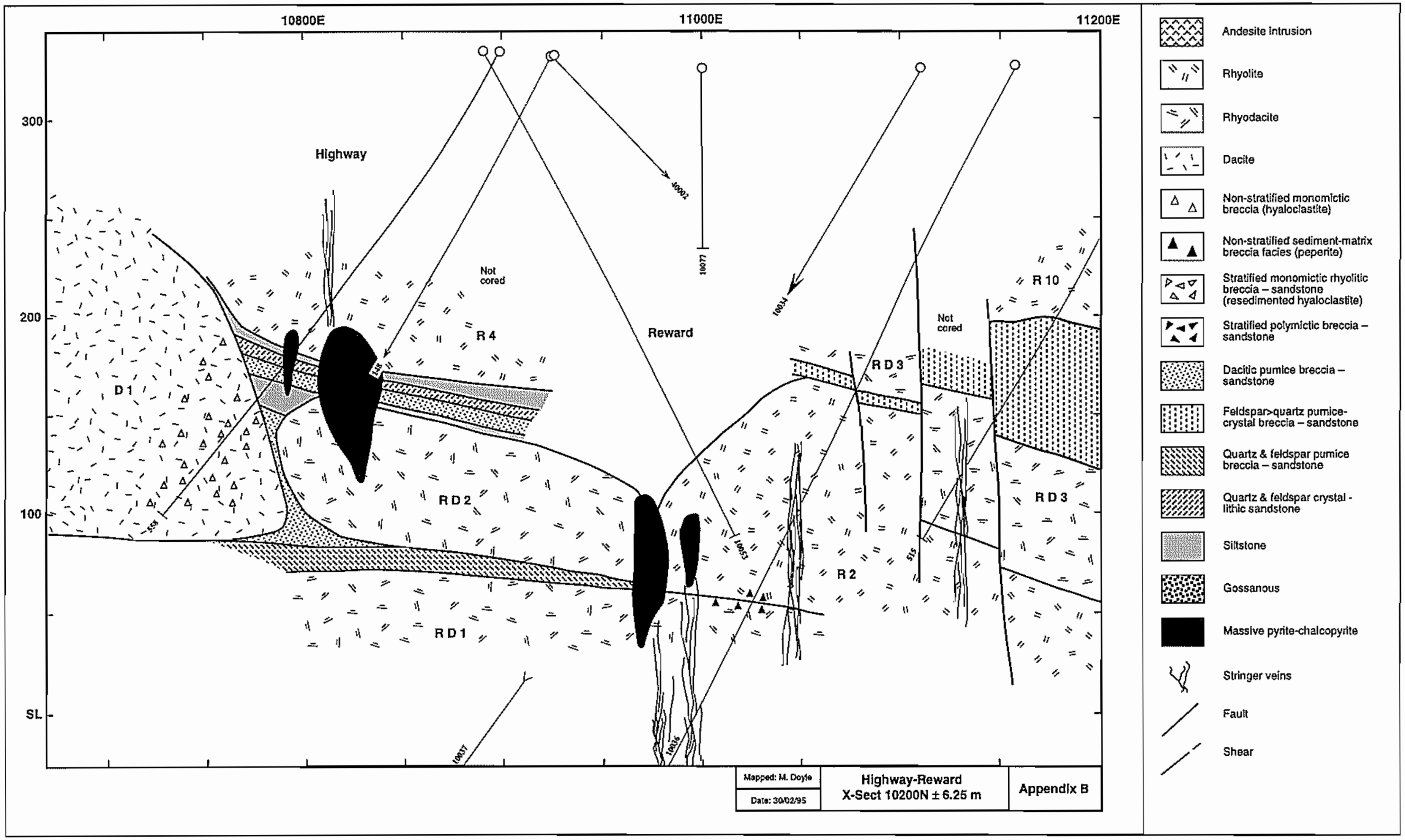
10800E
11000E
11200E
300
200
100
SL
Highway
Reward
Not cored
R 4
D 1
R D 2
R D 1
R 2
R D 3
R 10
Not cored
R D 3
40002
10077
10034
10053
10036
10037
555
515
Andesite intrusion
Rhyolite
Rhyodacite
Dacite
Non-stratified monomictic breccia (hyaloclastite)
Non-stratified sediment-matrix breccia facies (peperite)
Stratified monomictic rhyolitic breccia – sandstone (resedimented hyaloclastite)
Stratified polymictic breccia – sandstone
Dacitic pumice breccia – sandstone
Feldspar>quartz pumice-crystal breccia – sandstone
Quartz & feldspar pumice breccia – sandstone
Quartz & feldspar crystal - lithic sandstone
Siltstone
Gossanous
Massive pyrite-chalcopyrite
Stringer veins
Fault
Shear
Mapped: M. Doyle
Date: 30/02/95
Highway-Reward
X-Sect 10200N ± 6.25 m
Appendix B

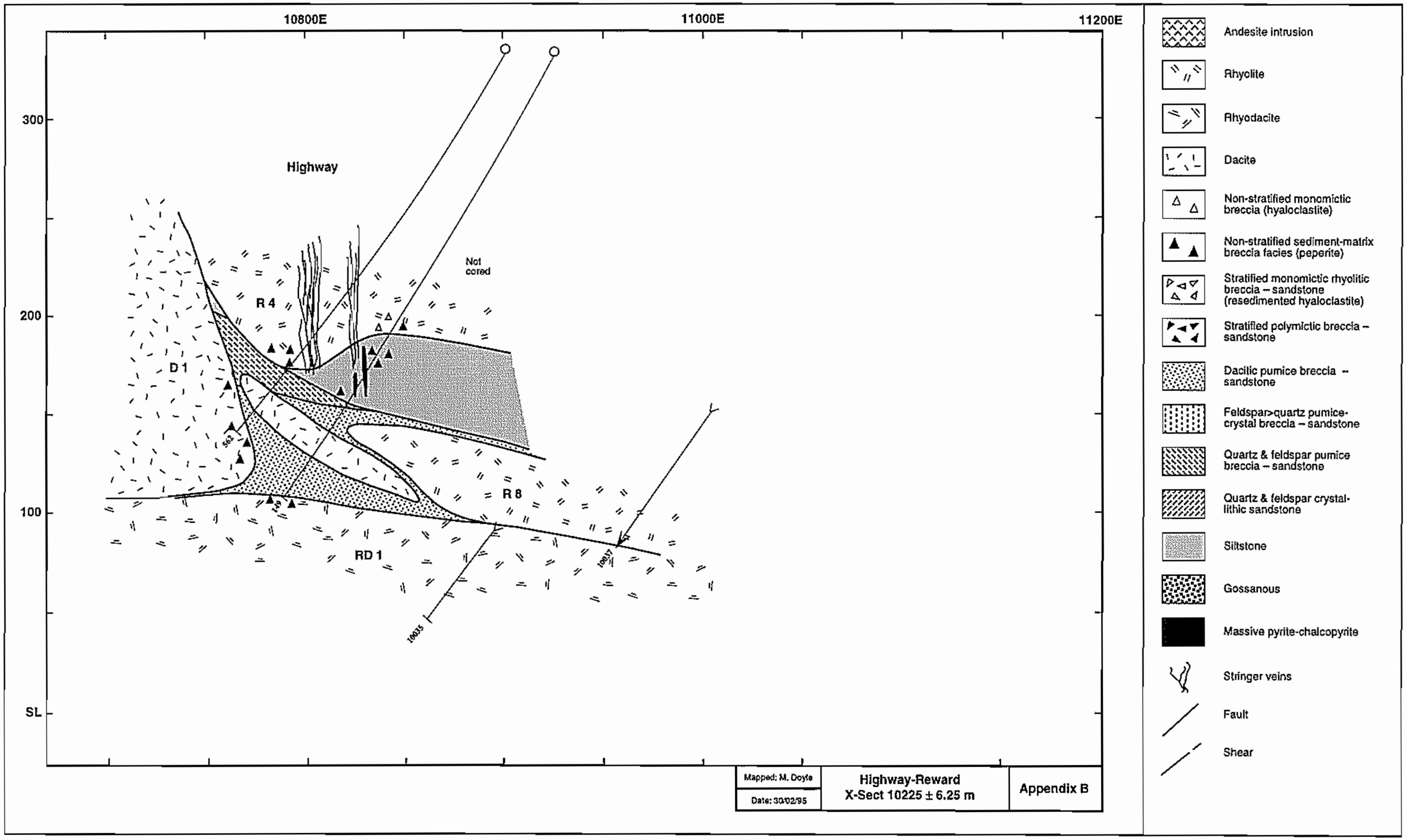
10800E
11000E
11200E
300
200
100
SL
Highway
Not cored
R 4
D 1
R 8
RD 1
562
149
10017
10035
Andesite intrusion
Rhyolite
Rhyodacite
Dacite
Non-stratified monomictic breccia (hyaloclastite)
Non-stratified sediment-matrix breccia facies (peperite)
Stratified monomictic rhyolitic breccia – sandstone (resedimented hyaloclastite)
Stratified polymictic breccia – sandstone
Dacitic pumice breccia – sandstone
Feldspar>quartz pumice-crystal breccia – sandstone
Quartz & feldspar pumice breccia – sandstone
Quartz & feldspar crystal-lithic sandstone
Siltstone
Gossanous
Massive pyrite-chalcopyrite
Stringer veins
Fault
Shear
Mapped: M. Doyle
Date: 30/02/95
Highway-Reward
X-Sect 10225 ± 6.25 m
Appendix B

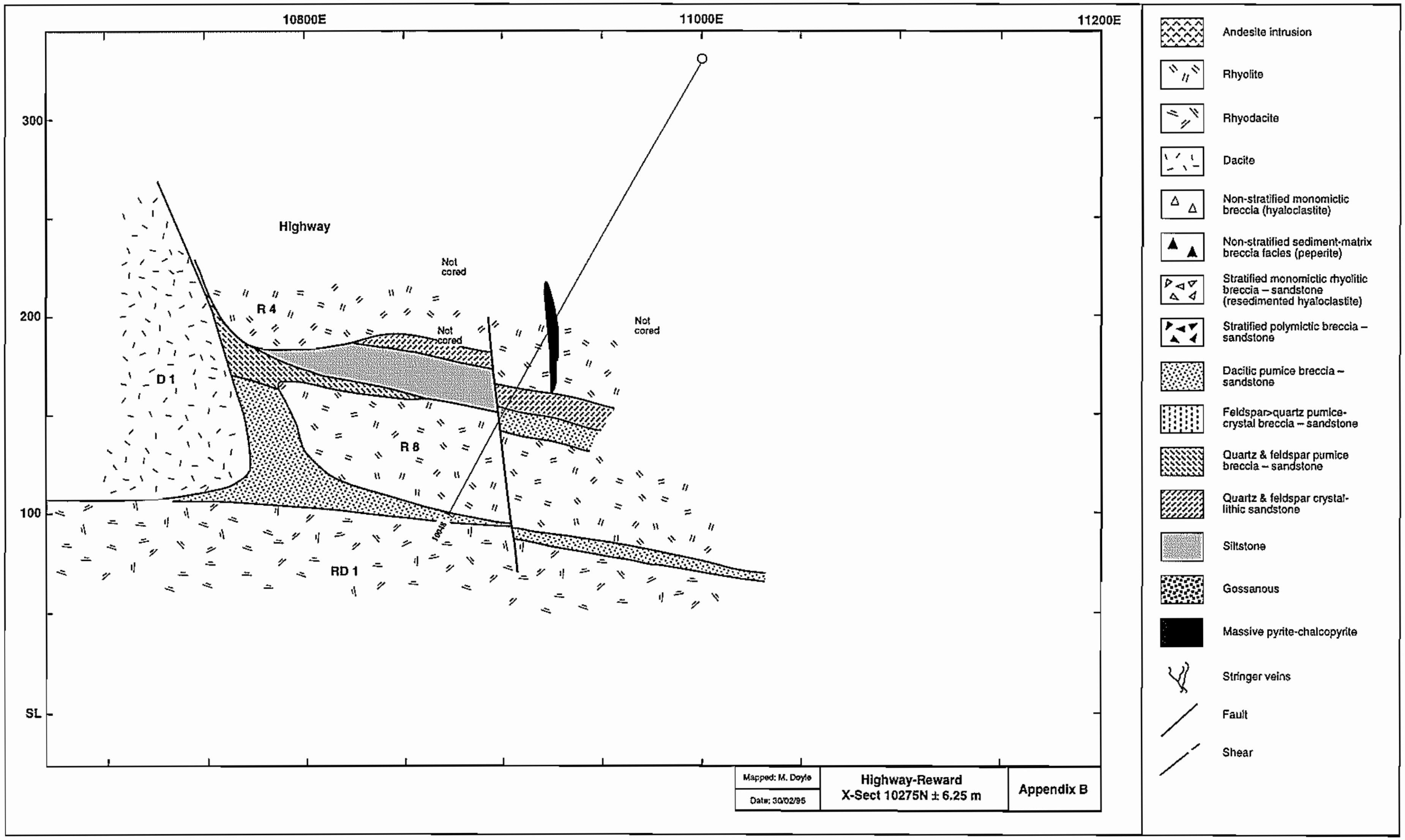

Mapped: M. Doyle
Date: 30/02/95

Highway-Reward
X-Sect 10275N ± 6.25 m

Appendix B

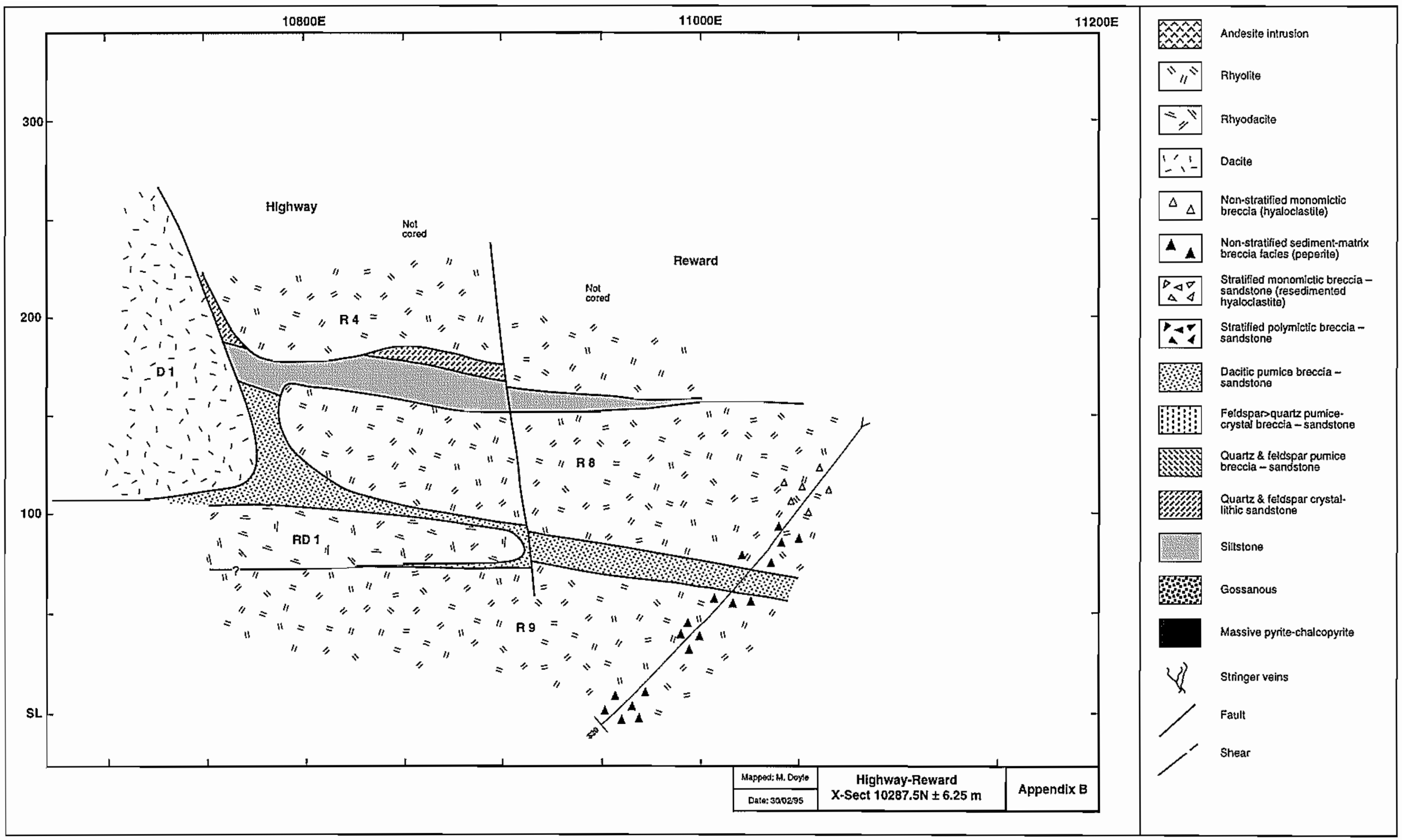
10800E
11000E
11200E
300
200
100
SL
Highway
Reward
Not cored
Not cored
R 4
R 8
R 9
RD 1
D 1
?
Andesite intrusion
Rhyolite
Rhyodacite
Dacite
Non-stratified monomictic breccia (hyaloclastite)
Non-stratified sediment-matrix breccia facies (peperite)
Stratified monomictic breccia – sandstone (resedimented hyaloclastite)
Stratified polymictic breccia – sandstone
Dacitic pumice breccia – sandstone
Feldspar>quartz pumice-crystal breccia – sandstone
Quartz & feldspar pumice breccia – sandstone
Quartz & feldspar crystal-lithic sandstone
Siltstone
Gossanous
Massive pyrite-chalcopyrite
Stringer veins
Fault
Shear
Mapped: M. Doyle
Date: 30/02/95
Highway-Reward
X-Sect 10287.5N ± 6.25 m
Appendix B

Appendix C

Summary graphic lithological logs

HMO 36	REM 142
HMO 39	REM 147
HMO 40	REM 148
HMO 52	REM 551
HMO 60	REM 558
HMO 86	REM 560
HMO 89	REM 600
REM 113	REW 800
REM 116	REW 801
REM 118	REW 803
REM 122	REW 804
REM 123	REW 805
REM 128	REW 807
REM 132	REW 809

Lithology

- Unaltered andesite
- Dacite
- Rhyolite
- Rhyodacite
- Flow banding
- Perlite
- Non-stratified monomictic breccia (hyaloclastite)
- Siltstone seams in coherent facies
- Siltstone-matrix-poor breccia (peperite)
- Siltstone-matrix-rich breccia (peperite)
- Stratified monomictic breccia-sandstone (resedimented hyaloclastite)
- Stratified polymictic breccia-sandstone
- Crystal-vitric sandstone
- Crystal-pumice breccia-sandstone
- Crystal-lithic breccia-sandstone
- Pumice breccia
- Siltstone
- Massive pyrite-chalcopyrite±sphalerite
- $ Semi-massive pyrite-chalcopyrite±sphalerite
- Massive/banded pyrite-sphalerite±barite
- Stringer veins
- ? Intensely altered volcanic
- F Feldspar-bearing
- F>Q Feldspar > quartz volcaniclastic unit
- Q&F Quartz & feldspar
- —— F Fault

Alteration

- Clay
- Sericite
- Sericite-quartz
- Quartz-sericite
- Quartz ± pyrite
- Sericite-quartz-chlorite
- Sericite-chlorite
- Chlorite
- Chlorite-sericite
- Chlorite-sericite-quartz
- Albite/K-feldspar-sericite-quartz-chlorite
- Hematite±quartz
- Hematite±sericite±chlorite
- Chlorite (± sericite)-carbonate
- Sericite-carbonate

Facies codes for alteration in volcanic rocks

(a) Phase(s)

• mineralogical and textural changes accompany hydrothermal alteration. Each alteration mineral can be referred to as a phase.

• each alteration domain comprises an area of rock that is characterised by a particular alteration mineral assemblage or by different proportions of similar minerals (phases) in similar mineral assemblages.

C	- chlorite	S	- sericite
SI	- quartz	K	- albite/K-feldspar
H	- hematite	CB	- carbonate
PY	- pyrite		

e.g. SI-S quartz-sericite (alteration domain comprising quartz and sericite)

(b) Relative abundance (phases - domains)

• the least abundant mineral within an alteration domain is presented on the right hand side (RHS) and the most abundant mineral on the left hand side (LHS).

e.g. S-SI (sericite-quartz) dominant phase - subordinate phase

• in a rock comprising two or more alteration domains, the phase(s) comprising the dominant domain are presented on the LHS and those of the remaining domains on the RHS in order of relative abundance

e.g. C / S-SI (chlorite & sericite-quartz domains) dominant - subordinate

(c) Intensity

• allocation of a number to describe the intensity of alteration within each domain

Weak (1-2) Moderate (3-4) Strong to intense (5-6)

• e.g. C^5 (strong chlorite alteration)
$S\text{-}SI^3$ (moderate sericite-quartz alteration)

(d) Controls/textures

The distribution of alteration minerals and domains can be controlled by the pre-alteration texture or superimposed structures. Alternatively, the alteration phases/ domains can generate a range of new textures and patterns in the rock.

x	- crystal	am	- apparent matrix
mx	- matrix	ac	- apparent clast
c	- clasts	mo	- mottled
fr	- fracture (perlite, quench)	w	- wash
hf	- hydraulic fracture	fi	- fiamme
fb	- flow banding	k	- fleck
sh	- shear	s	- spotty
v	- vein	pt	- patchy
d	- disseminated		

• e.g. Cp^5 (strong pervasive chlorite alteration)

• e.g. Cp^5 / SIf^3 (strong pervasive chlorite alteration and moderate, fracture-controlled quartz alteration)

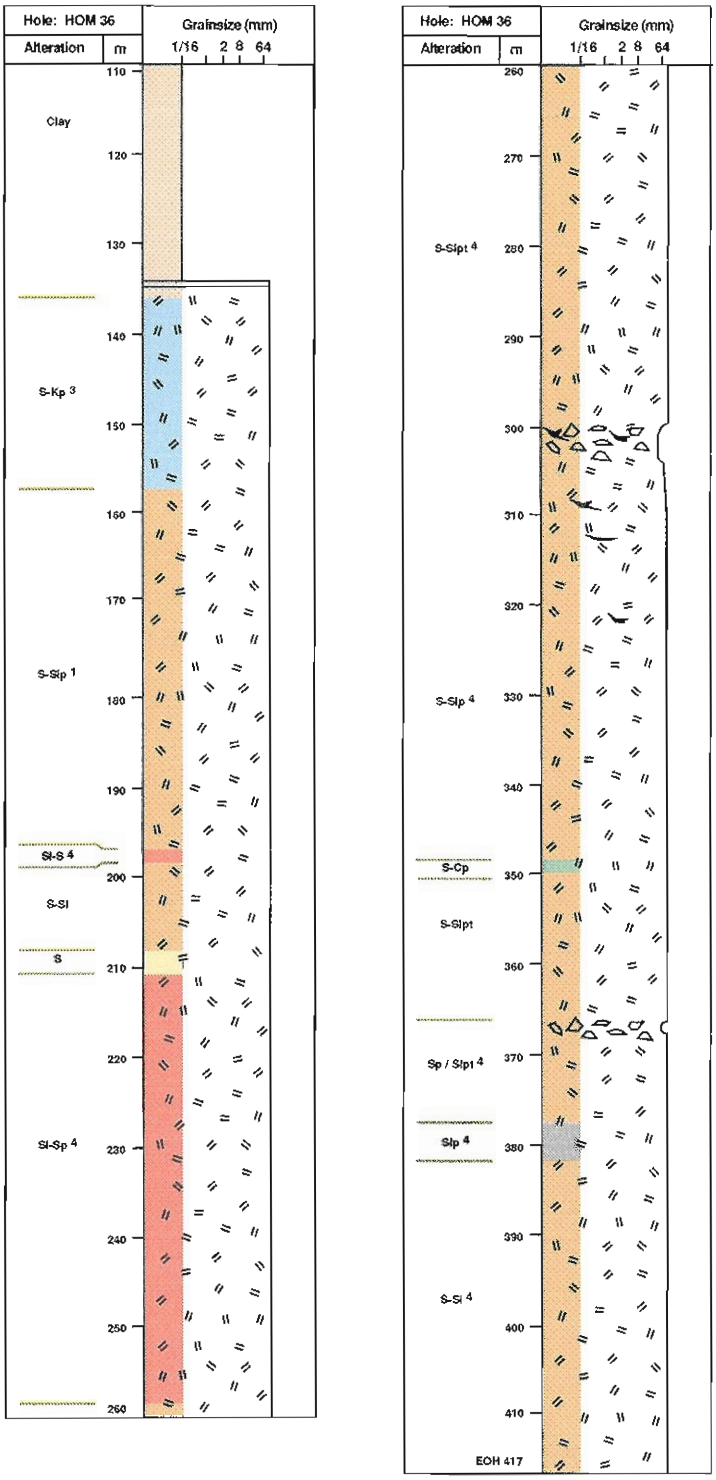
Hole: HOM 36
Grainsize (mm)
Alteration
m
1/16 2 8 64
Clay
S-Kp 3
S-Slp 1
SI-S 4
S-SI
S
SI-Sp 4
S-Slpt 4
S-Slp 4
S-Cp
S-Slpt
Sp / Slpt 4
Slp 4
S-SI 4
EOH 417

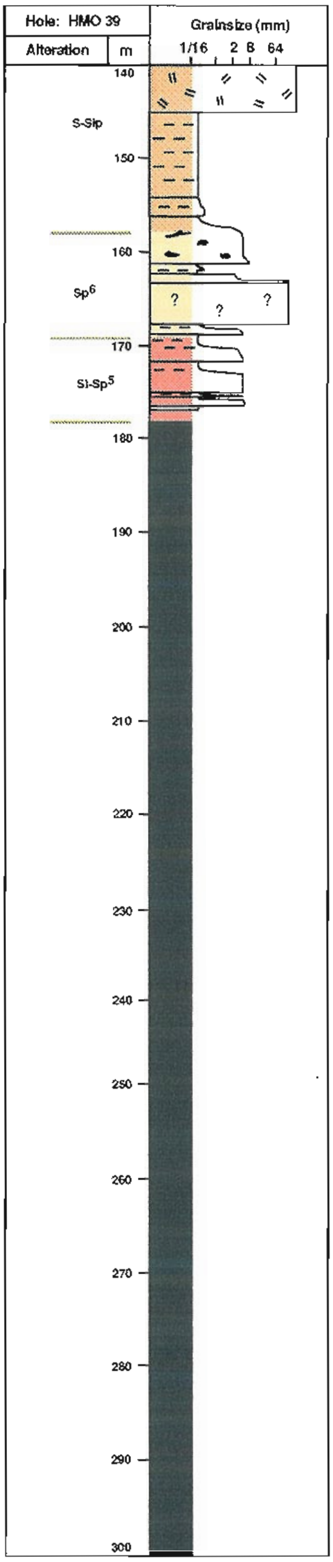

Hole: HMO 39
Grainsize (mm)
Alteration
m
1/16
2 8 64
S-Sip
Sp6
Sl-Sp5
140
150
160
170
180
190
200
210
220
230
240
250
260
270
280
290
300

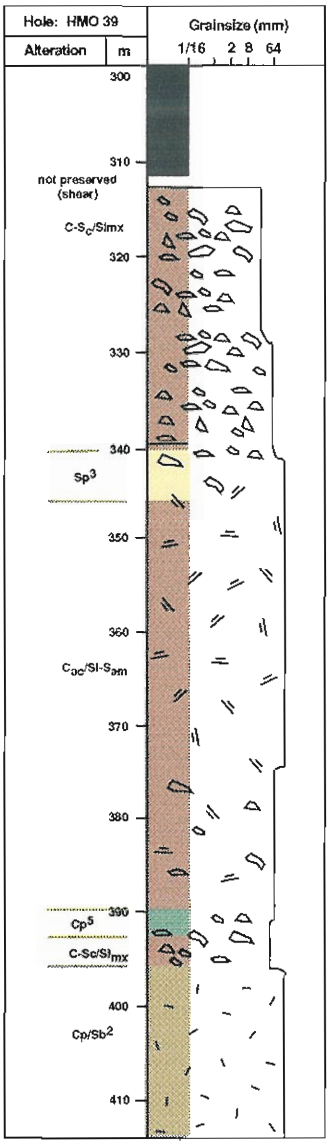

Hole: HMO 39
Grainsize (mm)
Alteration
m
1/16
2 8 64
not preserved
(shear)
C-Sc/Slmx
Sp3
Cpc/Sl-Sam
Cp5
C-Sc/Slmx
Cp/Sb2
300
310
320
330
340
350
360
370
380
390
400
410

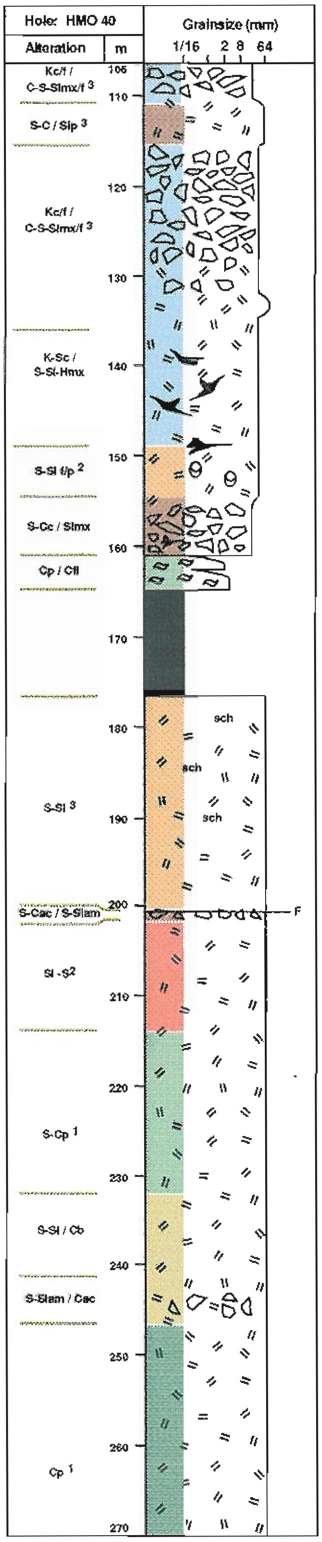
Hole: HMO 40
Grainsize (mm)
Alteration
m
1/16 2 8 64
Kc/f / C-S-Slmx/f 3
S-C / Slp 3
Kc/f / C-S-Slmx/f 3
K-Sc / S-Sl-Hmx
S-Sl f/p 2
S-Cc / Slmx
Cp / Cfl
S-Sl 3
S-Cac / S-Slam
Sl - S2
S-Cp 1
S-Sl / Cb
S-Slam / Cac
Cp 1
sch
F

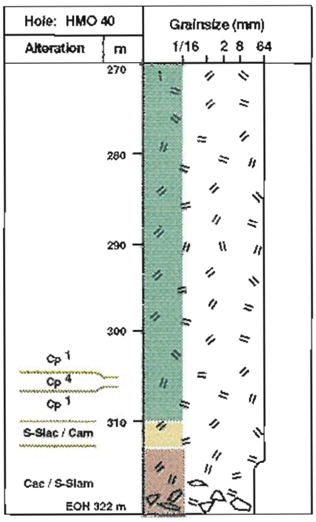
Hole: HMO 40
Grainsize (mm)
Alteration
m
1/16 2 8 64
Cp 1
Cp 4
Cp 1
S-Slac / Cam
Cac / S-Slam
EOH 322 m

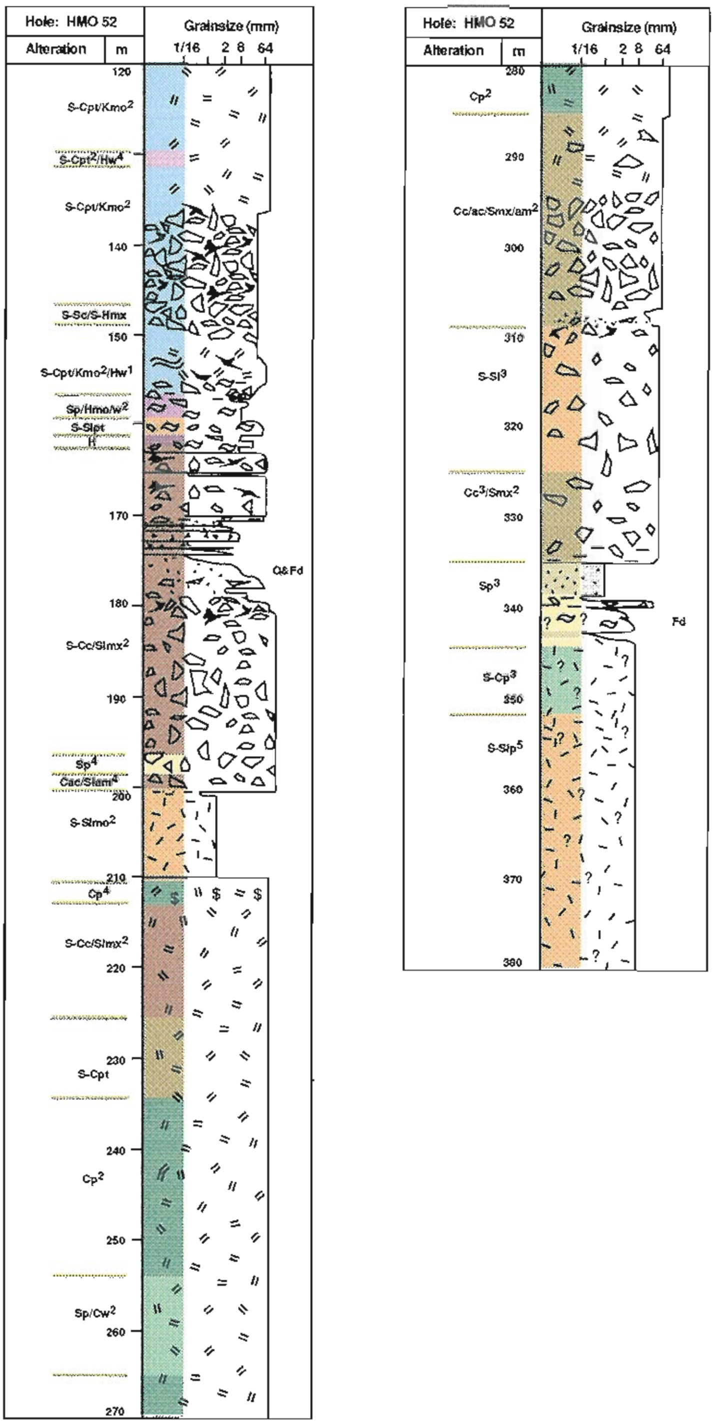

Hole: HMO 52
Alteration
m
Grainsize (mm)
1/16 2 8 64
S-Cpt/Kmo2
S-Cpt2/Hw4
S-Cpt/Kmo2
S-Sc/S-Hmx
S-Cpt/Kmo2/Hw1
Sp/Hmo/w2
S-Slpt
H
Q&Fd
S-Cc/Slmx2
Sp4
Cac/Slam4
S-Slmo2
Cp4
S-Cc/Slmx2
S-Cpt
Cp2
Sp/Cw2
Hole: HMO 52
Alteration
m
Grainsize (mm)
1/16 2 8 64
Cp2
Cc/ac/Smx/am2
S-Sl3
Cc3/Smx2
Sp3
Fd
S-Cp3
S-Slp5

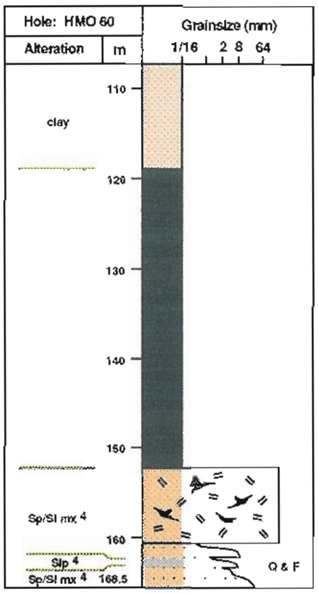
Hole: HMO 60
Grainsize (mm)
Alteration
m
1/16 2 8 64
110
clay
120
130
140
150
Sp/Sl mx 4
160
Slp 4
Sp/Sl mx 4
168.5
Q & F

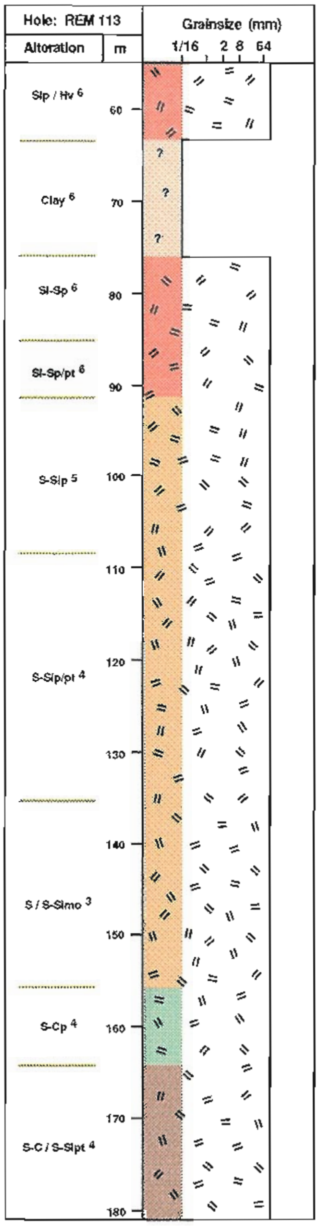
Hole: REM 113
Grainsize (mm)
Alteration
m
1/16 2 8 64
Slp / Hv 6
60
Clay 6
70
Sl-Sp 6
80
Sl-Sp/pt 6
90
S-Slp 5
100
110
S-Slp/pt 4
120
130
140
S / S-Slmo 3
150
S-Cp 4
160
170
S-C / S-Slpt 4
180

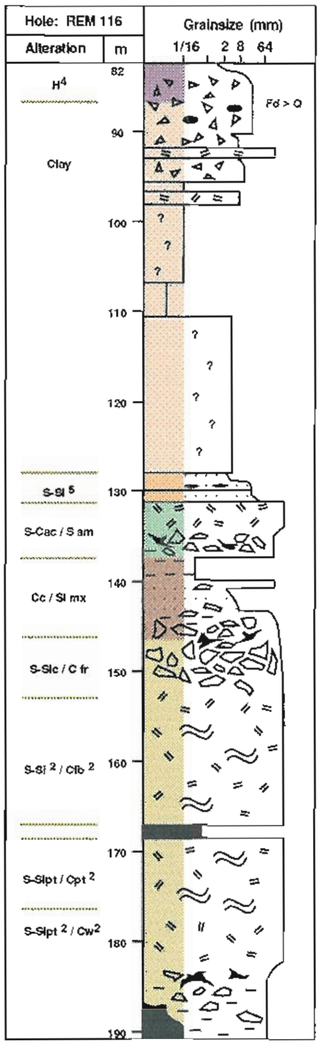
Hole: REM 116
Grainsize (mm)
Alteration
m
1/16 2 8 64
82
H4
Fd > Q
90
Clay
100
110
120
S-Sl 5
130
S-Cac / S am
140
Cc / Sl mx
S-Slc / C fr
150
S-Sl 2 / Cfb 2
160
170
S-Slpt / Cpt 2
S-Slpt 2 / Cw2
180
190

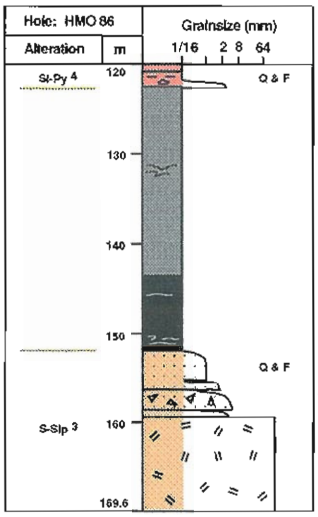
Hole: HMO 86
Grainsize (mm)
Alteration
m
1/16 2 8 64
Sl-Py 4
120
Q & F
130
140
150
Q & F
S-Slp 3
160
169.6

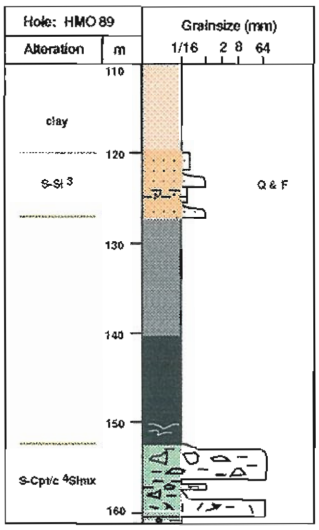
Hole: HMO 89
Grainsize (mm)
Alteration
m
1/16 2 8 64
110
clay
120
S-Sl 3
Q & F
130
140
150
S-Cpt/c 4Slmx
160

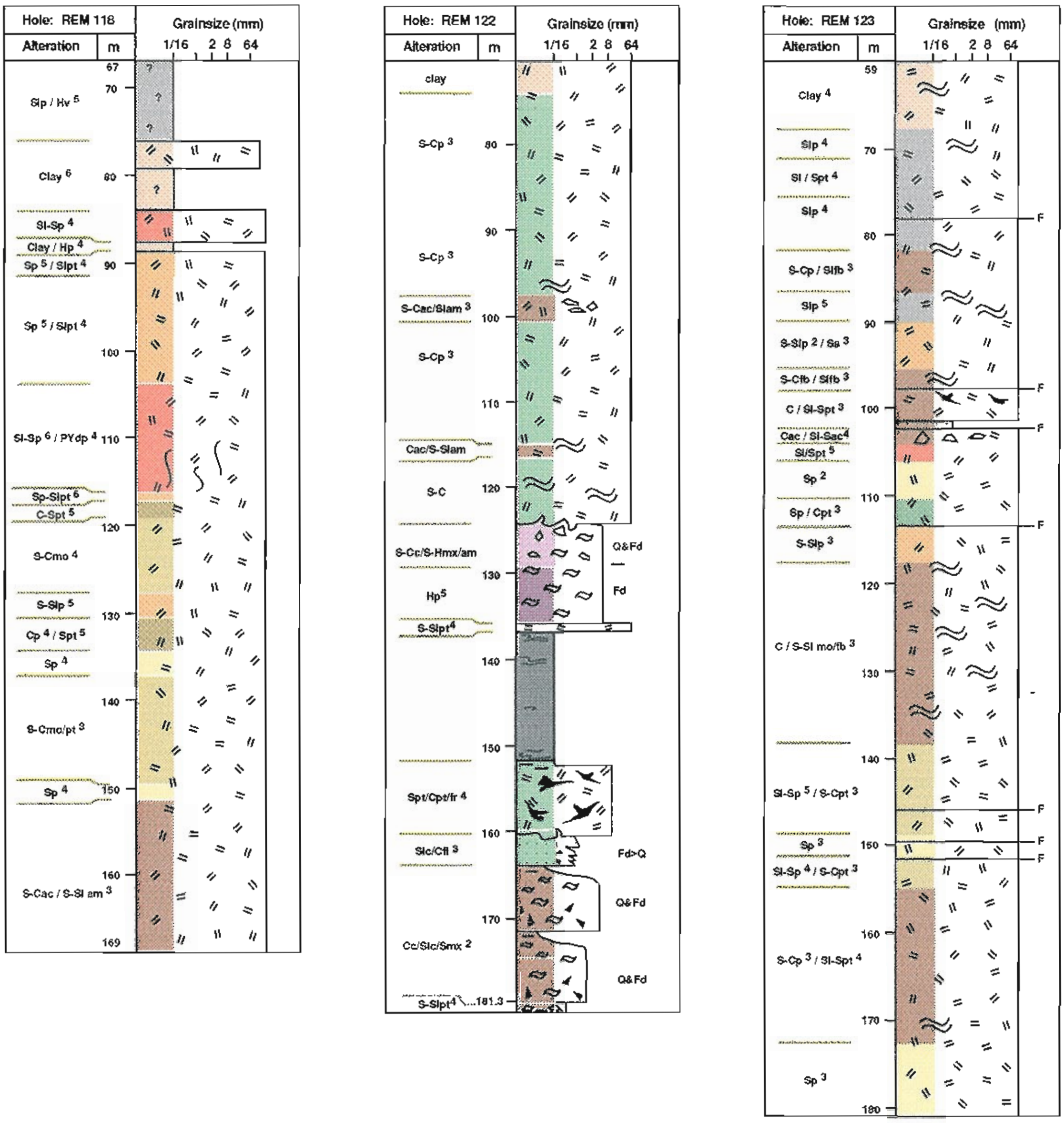

Hole: REM 118
Alteration
m
Grainsize (mm)
1/16 2 8 64
Slp / Hv 5
Clay 6
Sl-Sp 4
Clay / Hp 4
Sp 5 / Slpt 4
Sp 5 / Slpt 4
Sl-Sp 6 / PYdp 4
Sp-Slpt 6
C-Spt 5
S-Cmo 4
S-Slp 5
Cp 4 / Spt 5
Sp 4
S-Cmo/pt 3
Sp 4
S-Cac / S-Sl am 3
Hole: REM 122
Alteration
m
Grainsize (mm)
1/16 2 8 64
clay
S-Cp 3
S-Cp 3
S-Cac/Slam 3
S-Cp 3
Cac/S-Slam
S-C
S-Cc/S-Hmx/am
Hp5
S-Slpt4
Q&Fd
Fd
Spt/Cpt/fr 4
Slc/Cfl 3
Fd>Q
Q&Fd
Cc/Slc/Smx 2
Q&Fd
S-Slpt4 ...181.3
Hole: REM 123
Alteration
m
Grainsize (mm)
1/16 2 8 64
Clay 4
Slp 4
Sl / Spt 4
Slp 4
S-Cp / Slfb 3
Slp 5
S-Slp 2 / Ss 3
S-Cfb / Slfb 3
C / Sl-Spt 3
Cac / Sl-Sac4
Sl/Spt 5
Sp 2
Sp / Cpt 3
S-Slp 3
C / S-Sl mo/fb 3
Sl-Sp 5 / S-Cpt 3
Sp 3
Sl-Sp 4 / S-Cpt 3
S-Cp 3 / Sl-Spt 4
Sp 3
F

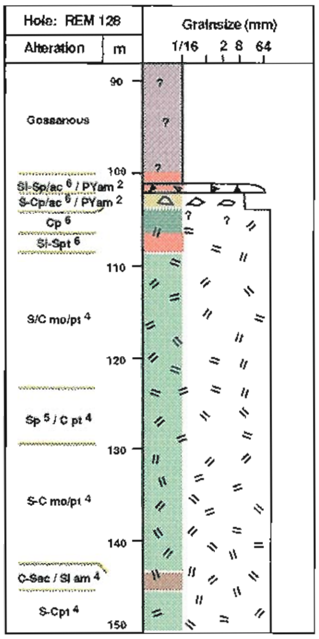
Hole: REM 128
Grainsize (mm)
Alteration
m
1/16 2 8 64
Gossanous
Sl-Sp/ac 6 / PYam 2
S-Cp/ac 6 / PYam 2
Cp 5
Sl-Spt 6
S/C mo/pt 4
Sp 5 / C pt 4
S-C mo/pt 4
C-Sac / Sl am 4
S-Cpt 4
90
100
110
120
130
140
150

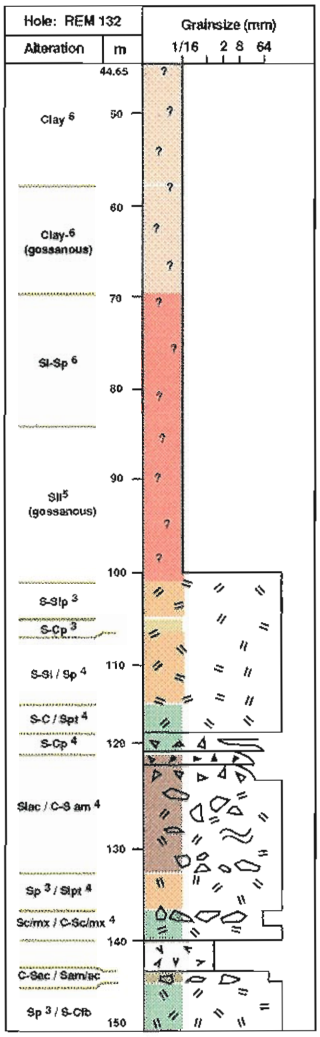
Hole: REM 132
Grainsize (mm)
Alteration
m
1/16 2 8 64
44.65
Clay 6
Clay-6 (gossanous)
Sl-Sp 6
Sll 5 (gossanous)
S-Slp 3
S-Cp 3
S-Sl / Sp 4
S-C / Spt 4
S-Cp 4
Slac / C-S am 4
Sp 3 / Slpt 4
Sc/mx / C-Sc/mx 4
C-Sac / Sam/ac
Sp 3 / S-Cfb
50
60
70
80
90
100
110
120
130
140
150

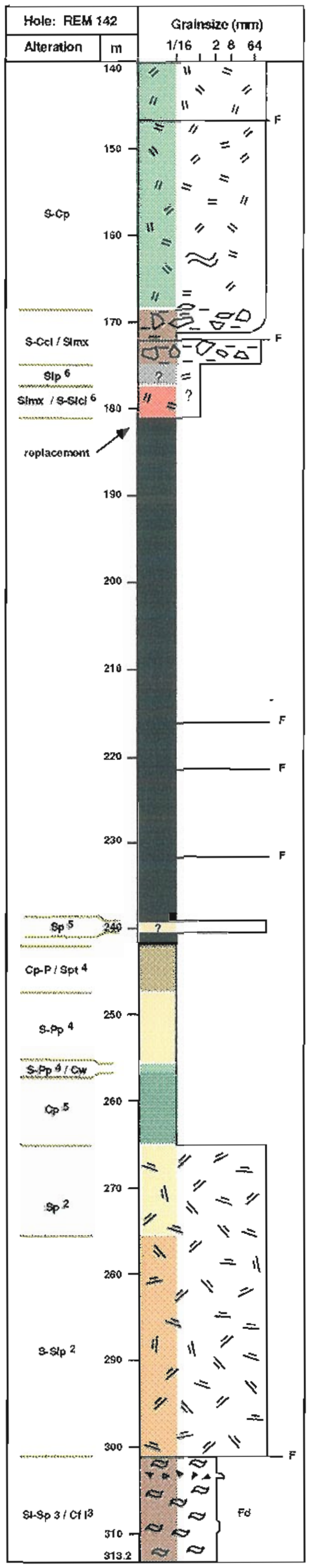
Hole: REM 142
Grainsize (mm)
Alteration
m
1/16 2 8 64
S-Cp
S-Ccl / Slmx
Slp 6
Slmx / S-Slcl 6
replacement
Sp 5
Cp-P / Spt 4
S-Pp 4
S-Pp 4 / Cw
Cp 5
Sp 2
S-Slp 2
Sl-Sp 3 / Cf l3
F
Fd
140
150
160
170
180
190
200
210
220
230
240
250
260
270
280
290
300
310
313.2

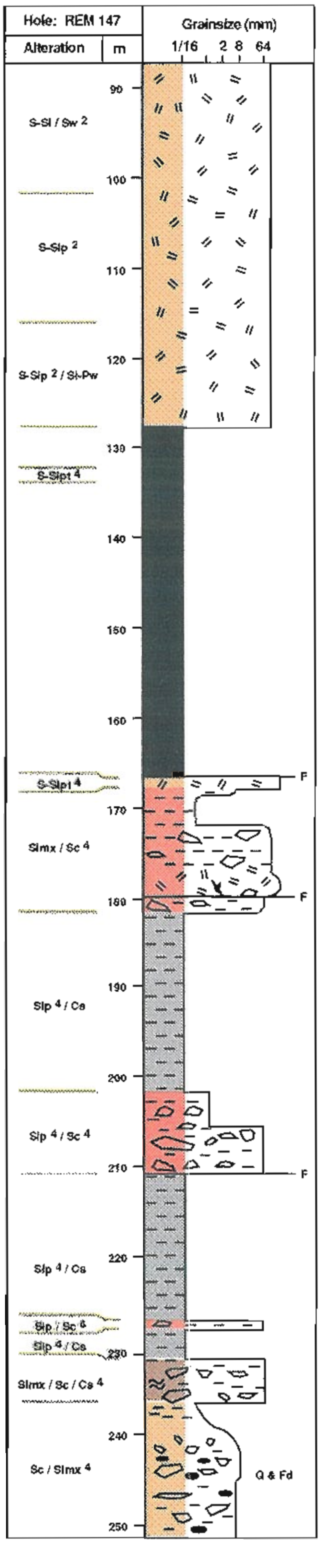

Hole: REM 147
Grainsize (mm)
Alteration
m
1/16 2 8 64
S-Sl / Sw 2
S-Slp 2
S-Slp 2 / Si-Pw
S-Slpt 4
S-Slpt 4
Slmx / Sc 4
Slp 4 / Cs
Slp 4 / Sc 4
Slp 4 / Cs
Slp / Sc 6
Slp 4 / Cs
Slmx / Sc / Cs 4
Sc / Slmx 4
F
Q & Fd

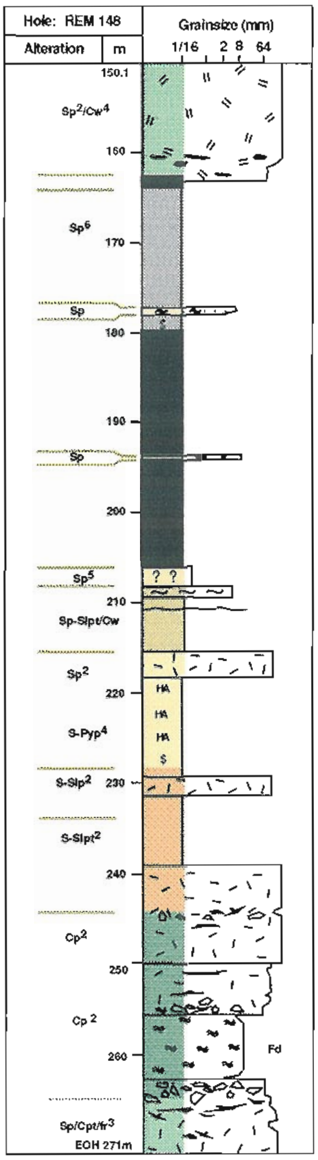

Hole: REM 148
Grainsize (mm)
Alteration
m
1/16 2 8 64
150.1
Sp2/Cw4
Sp6
Sp
Sp
Sp5
Sp-Slpt/Cw
Sp2
S-Pyp4
S-Slp2
S-Slpt2
Cp2
Cp 2
Sp/Cpt/fr3
EOH 271m
HA
Fd

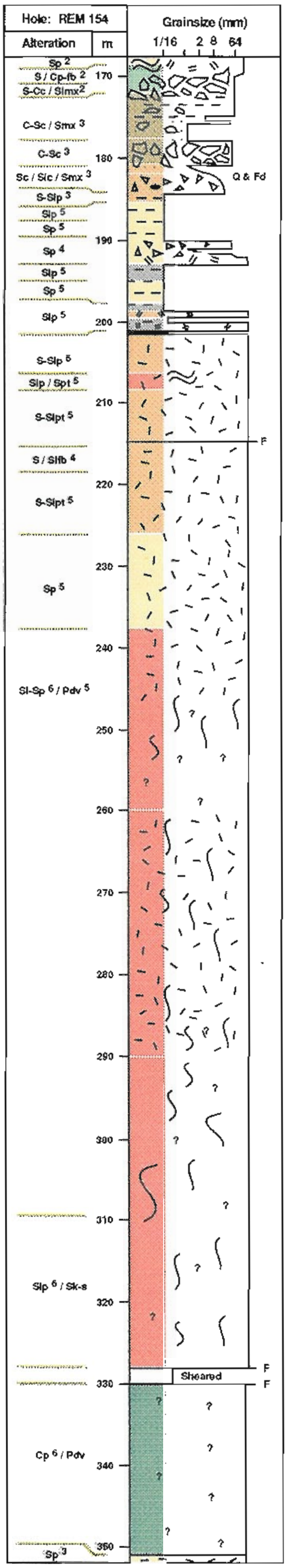
Hole: REM 154
Grainsize (mm)
Alteration
m
1/16 2 8 64
Sp 2
S / Cp-fb 2
S-Cc / Slmx 2
C-Sc / Smx 3
C-Sc 3
Sc / Slc / Smx 3
S-Slp 3
Slp 5
Sp 5
Sp 4
Slp 5
Sp 5
Slp 5
S-Slp 5
Slp / Spt 5
S-Slpt 5
S / Slfb 4
S-Slpt 5
Sp 5
Sl-Sp 6 / Pdv 5
Slp 6 / Sk-s
Cp 6 / Pdv
Sp 3
Q & Fd
Sheared
F

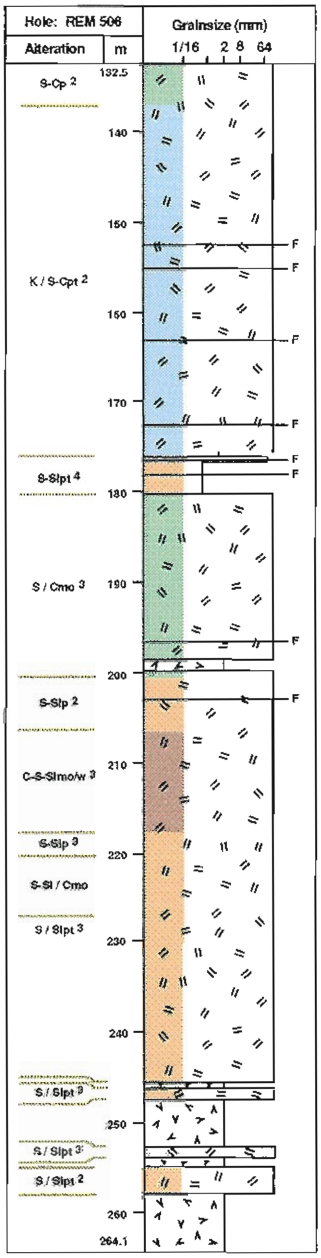
Hole: REM 506
Grainsize (mm)
Alteration
m
1/16 2 8 64
132.5
S-Cp 2
K / S-Cpt 2
S-Slpt 4
S / Cmo 3
S-Slp 2
C-S-Slmo/w 3
S-Slp 3
S-Sl / Cmo
S / Slpt 3
S / Slpt 3
S / Slpt 3
S / Slpt 2
264.1
F

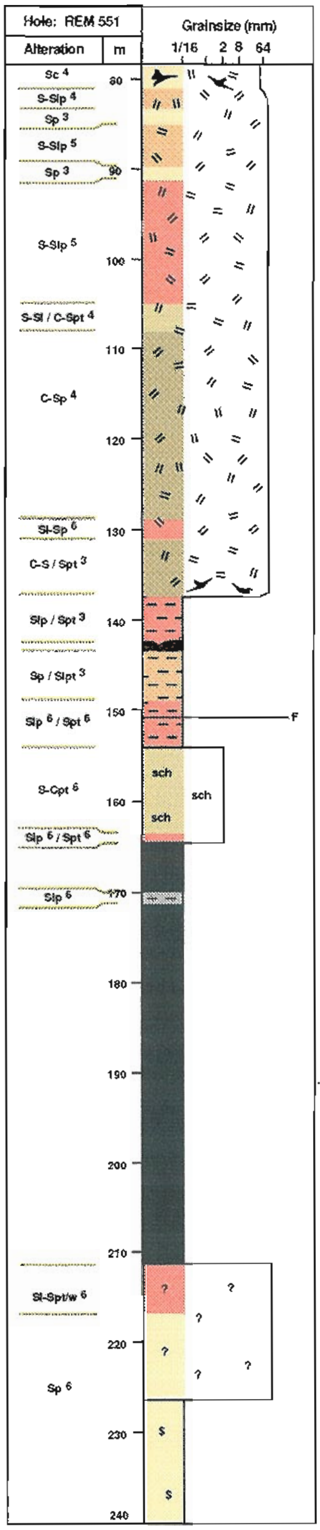
Hole: REM 551
Grainsize (mm)
Alteration
m
1/16 2 8 64
Sc 4
S-Slp 4
Sp 3
S-Slp 5
Sp 3
S-Slp 5
S-Sl / C-Spt 4
C-Sp 4
Sl-Sp 6
C-S / Spt 3
Slp / Spt 3
Sp / Slpt 3
Slp 6 / Spt 6
S-Cpt 6
Slp 6 / Spt 6
Slp 6
Sl-Spt/w 6
Sp 6
80
90
100
110
120
130
140
150
160
170
180
190
200
210
220
230
240
sch
F

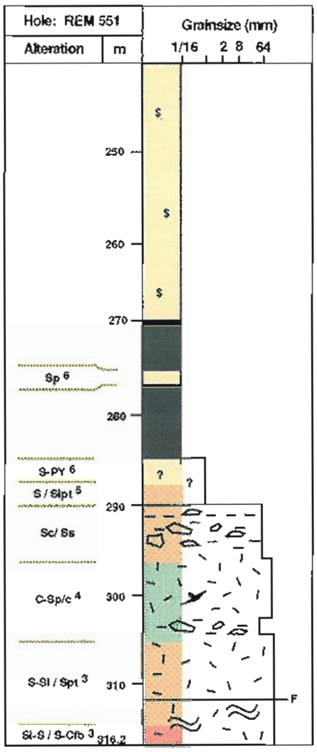
Hole: REM 551
Grainsize (mm)
Alteration
m
1/16 2 8 64
Sp 6
S-PY 6
S / Slpt 5
Sc/ Ss
C-Sp/c 4
S-Sl / Spt 3
Sl-S / S-Cfb 3
250
260
270
280
290
300
310
316.2
F

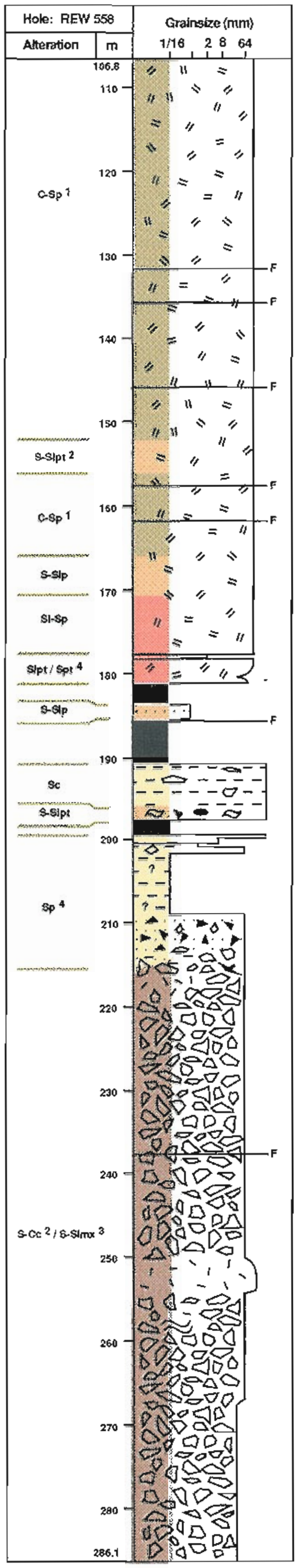
Hole: REW 558
Grainsize (mm)
Alteration
m
1/16 2 8 64
106.8
C-Sp 1
S-Slpt 2
C-Sp 1
S-Slp
Sl-Sp
Slpt / Spt 4
S-Slp
Sc
S-Slpt
Sp 4
S-Cc 2 / S-Slmx 3
110
120
130
140
150
160
170
180
190
200
210
220
230
240
250
260
270
280
286.1
F

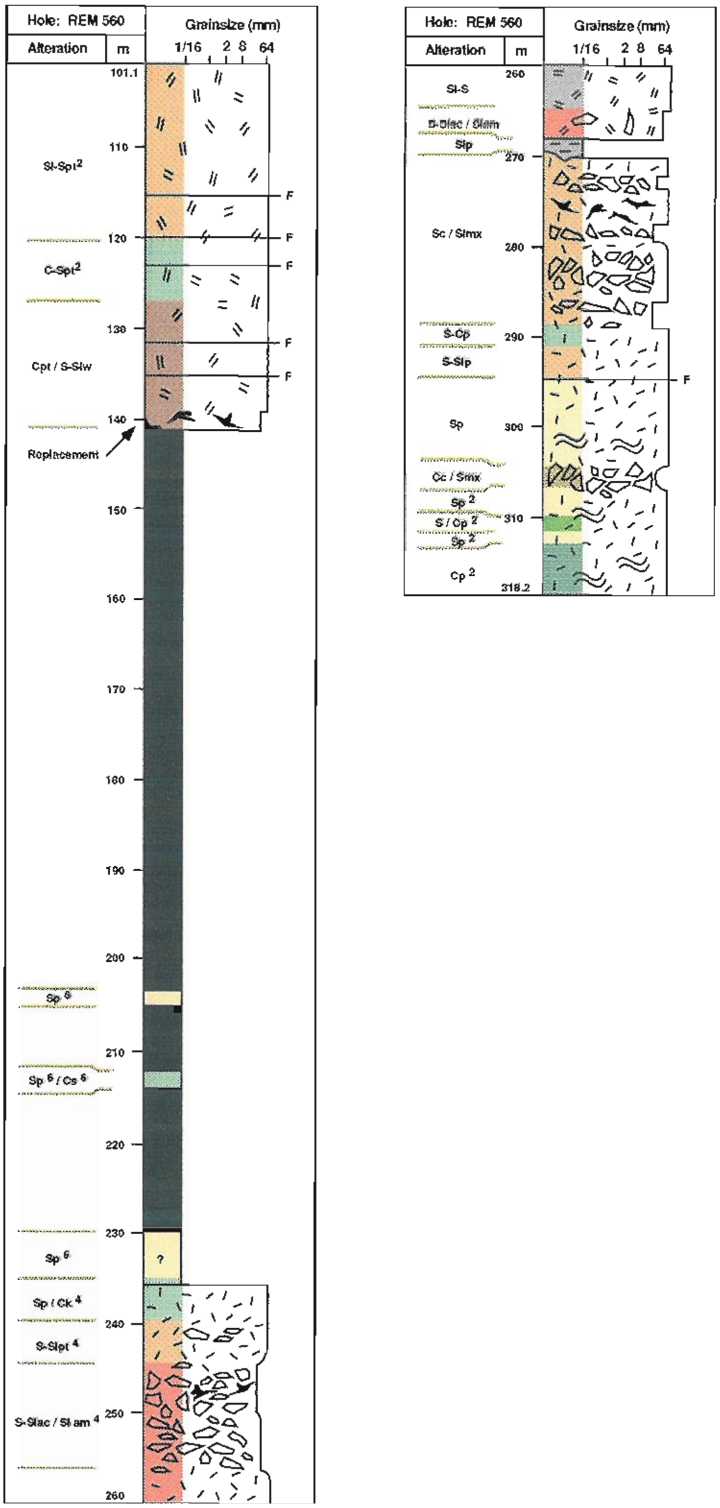
Hole: REM 560
Grainsize (mm)
Alteration
m
1/16 2 8 64
Sl-Spt2
C-Spt2
Cpt / S-Slw
Replacement
Sp 6
Sp 6 / Cs 6
Sp 6
Sp / Ck 4
S-Slpt 4
S-Slac / Sl am 4
Sl-S
S-Slac / Slam
Slp
Sc / Slmx
S-Cp
S-Slp
Sp
Cc / Smx
Sp 2
S / Cp 2
Sp 2
Cp 2
F

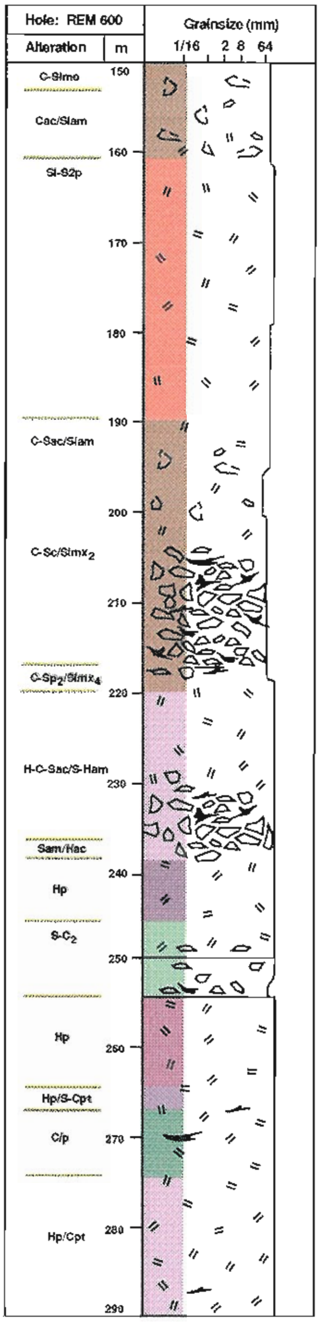

Hole: REM 600
Grainsize (mm)
Alteration
m
1/16 2 8 64
C-Slmo
Cac/Slam
Sl-S2p
C-Sac/Slam
C-Sc/Slmx2
C-Sp2/Slmx4
H-C-Sac/S-Ham
Sam/Hac
Hp
S-C2
Hp
Hp/S-Cpt
C/p
Hp/Cpt
150
160
170
180
190
200
210
220
230
240
250
260
270
280
290

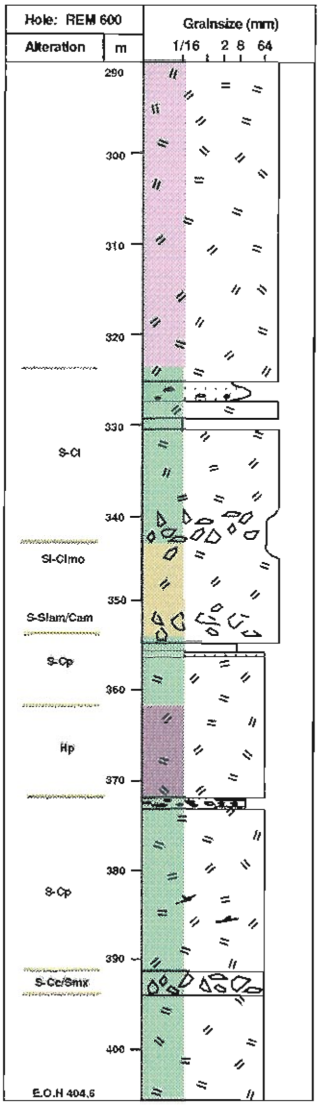

Hole: REM 600
Grainsize (mm)
Alteration
m
1/16 2 8 64
S-Cl
Sl-Clmo
S-Slam/Cam
S-Cp
Hp
S-Cp
S-Cc/Smx
E.O.H 404.6
290
300
310
320
330
340
350
360
370
380
390
400

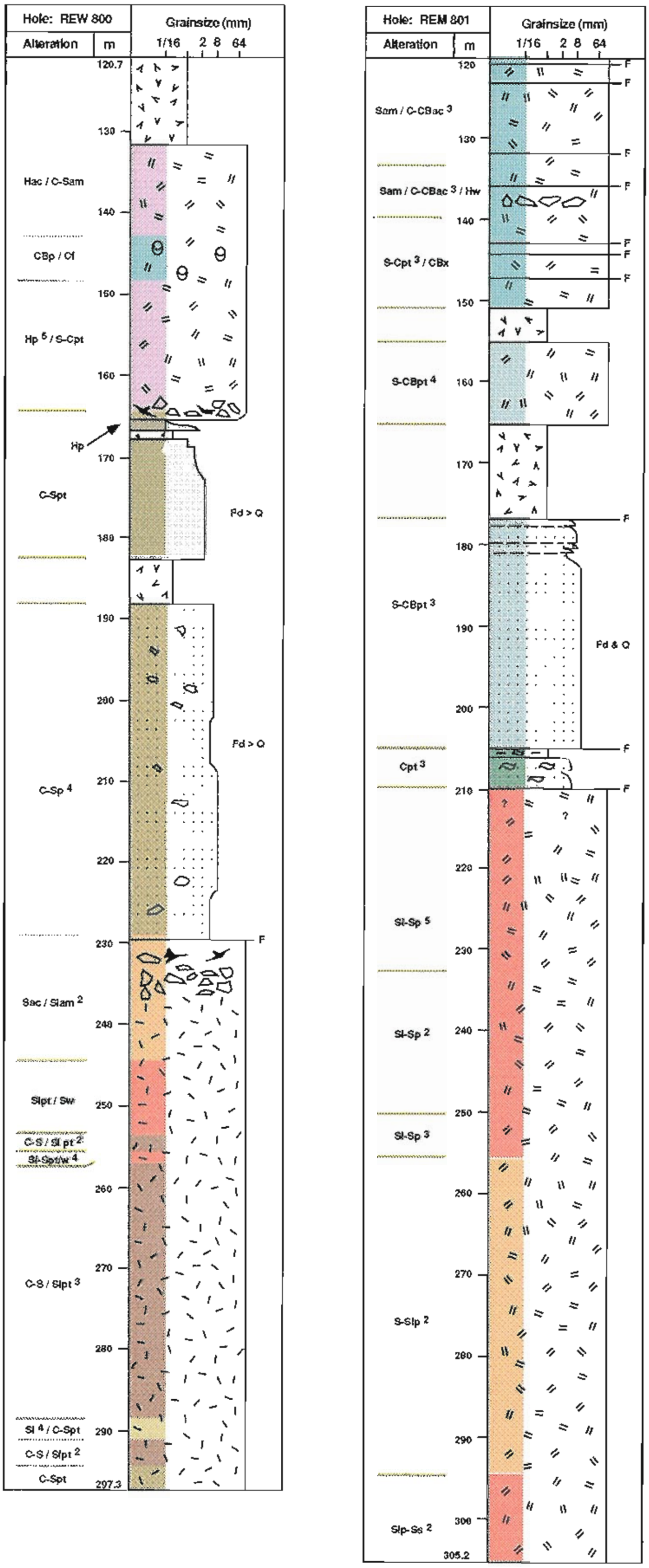

Hole: REW 800
Grainsize (mm)
Alteration
m
1/16 2 8 64
Hac / C-Sam
CBp / Cf
Hp 5 / S-Cpt
Hp
C-Spt
Fd > Q
C-Sp 4
Fd > Q
F
Sac / Siam 2
Sipt / Sw
C-S / Si pt 2
Si-Spt/w 4
C-S / Sipt 3
Si 4 / C-Spt
C-S / Sipt 2
C-Spt
120.7
297.3
Hole: REM 801
Grainsize (mm)
Alteration
m
1/16 2 8 64
Sam / C-CBac 3
Sam / C-CBac 3 / Hw
S-Cpt 3 / CBx
S-CBpt 4
S-CBpt 3
Fd & Q
Cpt 3
Si-Sp 5
Si-Sp 2
Si-Sp 3
S-Sip 2
Sip-Ss 2
F
305.2

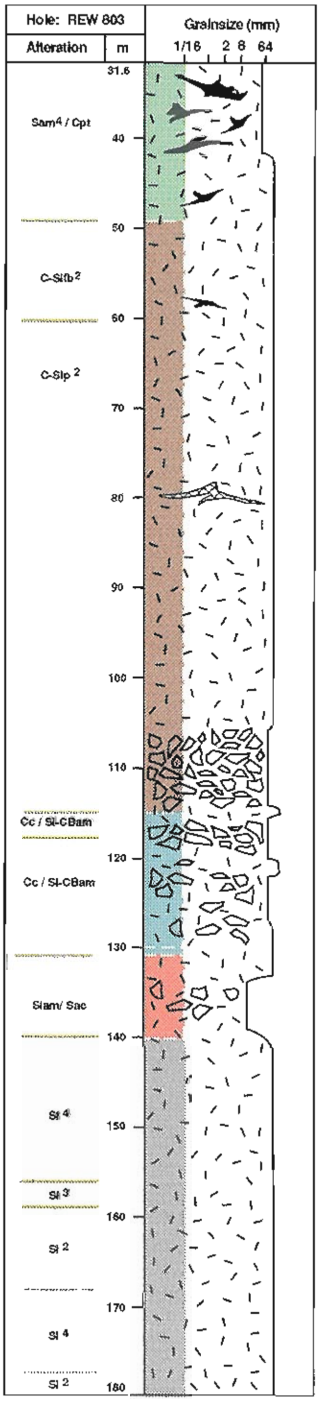
Hole: REW 803
Grainsize (mm)
Alteration
m
1/16 2 8 64
31.6
Sam4 / Cpt
40
50
C-Sifb2
60
C-Sip 2
70
80
90
100
110
Cc / Si-CBam
120
Cc / Si-CBam
130
Siam/ Sac
140
Si 4
150
Si 3
160
Si 2
170
Si 4
Si 2
180

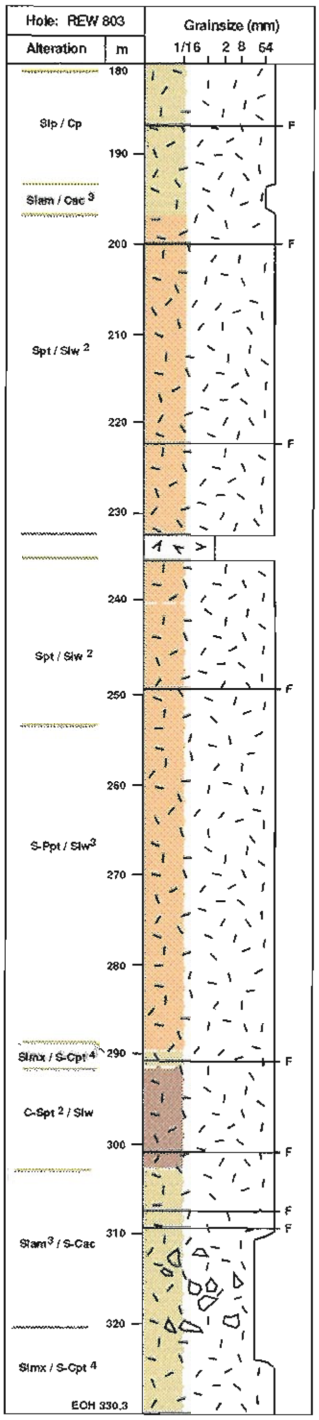
Hole: REW 803
Grainsize (mm)
Alteration
m
1/16 2 8 64
180
Sip / Cp
190
Siam / Cac 3
200
210
Spt / Siw 2
220
230
240
Spt / Siw 2
250
260
S-Ppt / Siw3
270
280
Simx / S-Cpt 4
290
C-Spt 2 / Siw
300
Siam3 / S-Cac
310
320
Simx / S-Cpt 4
EOH 330.3
F

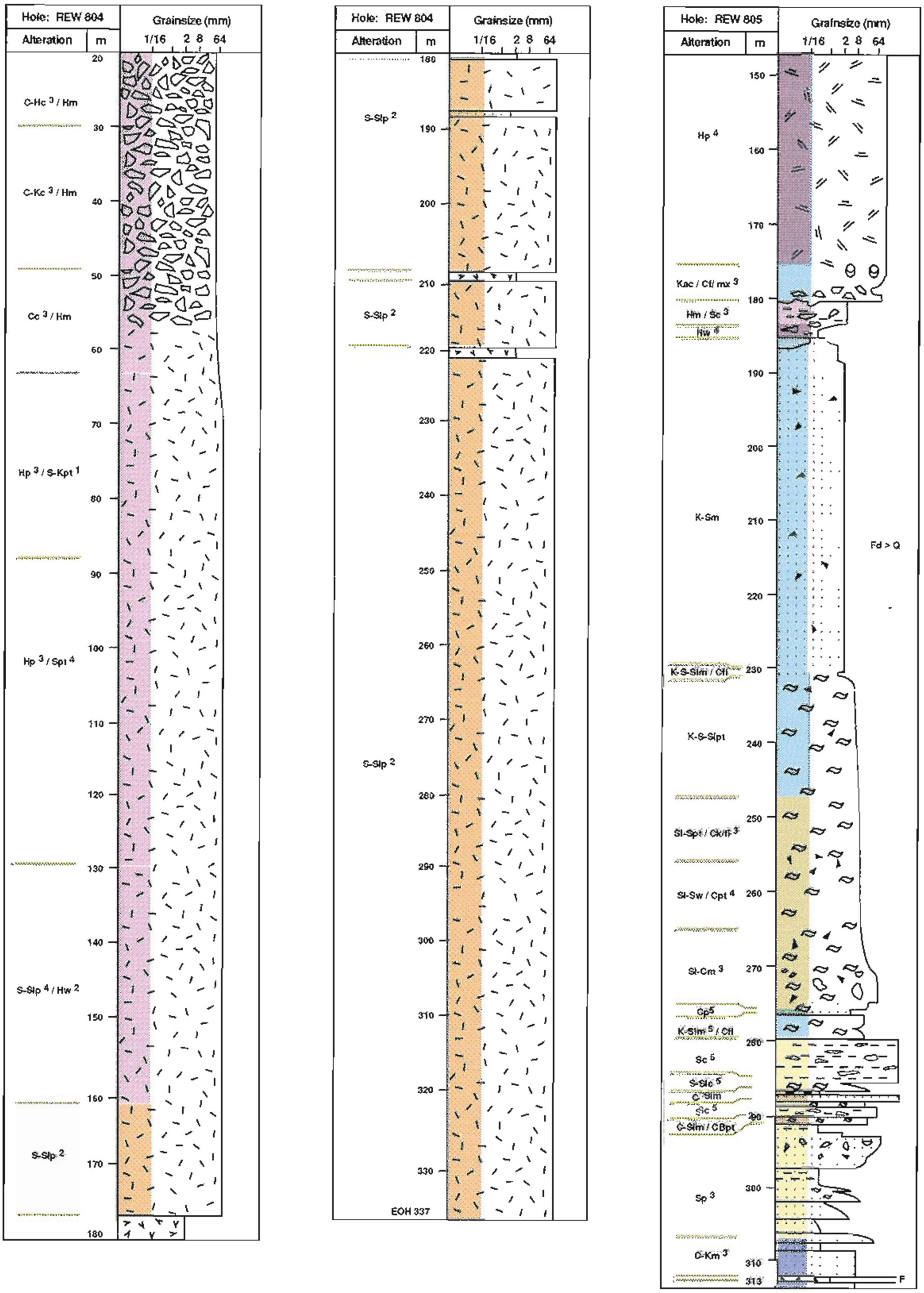
Hole: REW 804
Grainsize (mm)
Alteration
m
1/16 2 8 64
C-Hc 3 / Hm
C-Kc 3 / Hm
Cc 3 / Hm
Hp 3 / S-Kpt 1
Hp 3 / Spt 4
S-Slp 4 / Hw 2
S-Slp 2
Hole: REW 804
Grainsize (mm)
Alteration
m
1/16 2 8 64
S-Slp 2
S-Slp 2
S-Slp 2
EOH 337
Hole: REW 805
Grainsize (mm)
Alteration
m
1/16 2 8 64
Hp 4
Kac / Cf/ mx 3
Hm / Sc 3
Hw 4
K-Sm
Fd > Q
K-S-Slm / Cfl
K-S-Slpt
Sl-Spt / Ck/fi 3
Sl-Sw / Cpt 4
Sl-Cm 3
Cp5
K-Slm 5 / Cfl
Sc 5
S-Slc 5
C-Slm
Sc 5
C-Slm / CBpt
Sp 3
C-Km 3
F

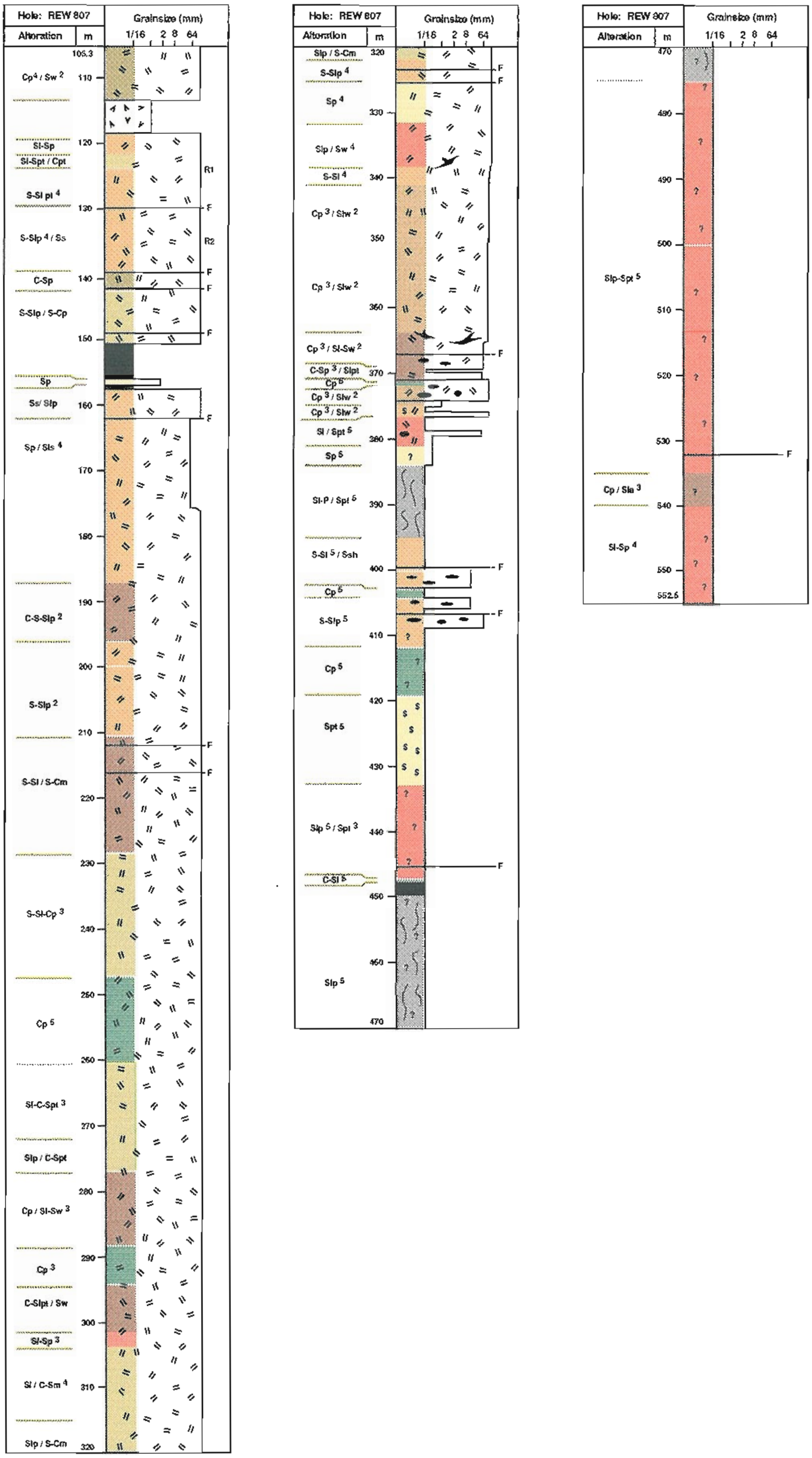

Hole: REW 807
Grainsize (mm)
Alteration
m
1/16
2
8
64
Cp 4 / Sw 2
Sl-Sp
Sl-Spt / Cpt
S-Sl pt 4
S-Slp 4 / Ss
C-Sp
S-Slp / S-Cp
Sp
Ss/ Slp
Sp / Sls 4
C-S-Slp 2
S-Slp 2
S-Sl / S-Cm
S-Sl-Cp 3
Cp 5
Sl-C-Spt 3
Slp / C-Spt
Cp / Sl-Sw 3
Cp 3
C-Slpt / Sw
Sl-Sp 3
Sl / C-Sm 4
Slp / S-Cm
R1
R2
F
Hole: REW 807
Grainsize (mm)
Alteration
m
1/16
2
8
64
Slp / S-Cm
S-Slp 4
Sp 4
Slp / Sw 4
S-Sl 4
Cp 3 / Slw 2
Cp 3 / Slw 2
Cp 3 / Sl-Sw 2
C-Sp 3 / Slpt
Cp 5
Cp 3 / Slw 2
Cp 3 / Slw 2
Sl / Spt 5
Sp 5
Sl-P / Spt 5
S-Sl 5 / Ssh
Cp 5
S-Slp 5
Cp 5
Spt 5
Slp 5 / Spt 3
C-Sl 5
Slp 5
F
Hole: REW 807
Grainsize (mm)
Alteration
m
1/16
2
8
64
Slp-Spt 5
Cp / Sla 3
Sl-Sp 4
F

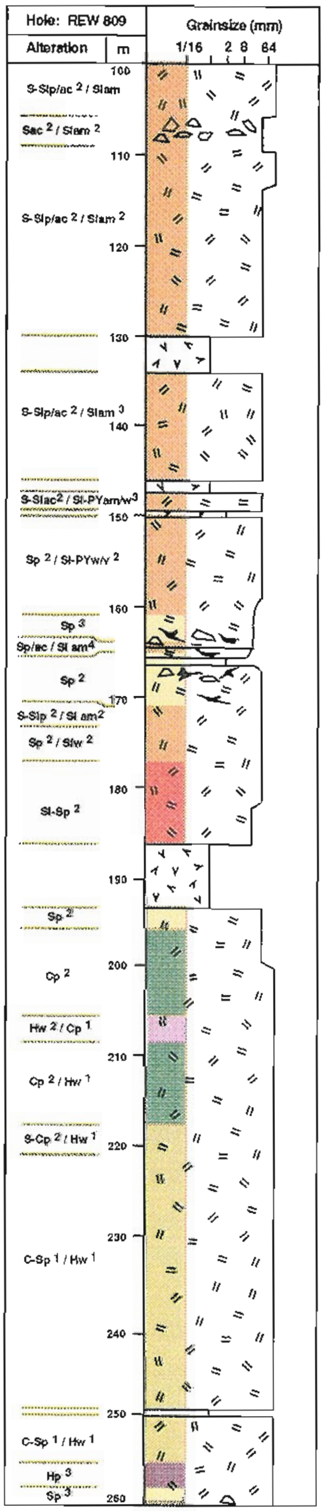
Hole: REW 809
Alteration
m
Grainsize (mm)
1/16 2 8 64
S-Sip/ac 2 / Siam
Sac 2 / Siam 2
S-Sip/ac 2 / Siam 2
S-Sip/ac 2 / Siam 3
Sp 2 / Si-PYw/v 2
Sp 3
Sp/ac / Si am4
Sp 2
S-Sip 2 / Si am2
Sp 2 / Siw 2
Si-Sp 2
Sp 2
Cp 2
Hw 2 / Cp 1
Cp 2 / Hw 1
S-Cp 2 / Hw 1
C-Sp 1 / Hw 1
C-Sp 1 / Hw 1
Hp 3
Sp 3
100
110
120
130
140
150
160
170
180
190
200
210
220
230
240
250
260

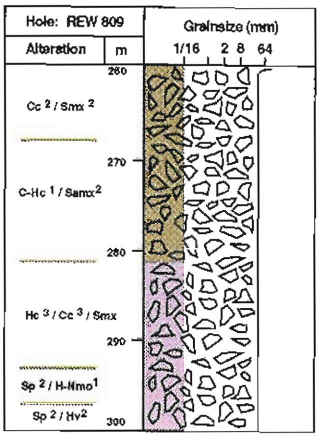
Hole: REW 809
Alteration
m
Grainsize (mm)
1/16 2 8 64
Cc 2 / Smx 2
C-Hc 1 / Samx2
Hc 3 / Cc 3 / Smx
Sp 2 / H-Nmo1
Sp 2 / Hv2
260
270
280
290
300

Appendix D

Geochemical analyses of lavas and intrusions

Appendix D1 Mount Windsor Formation
Appendix D2 Trooper Creek Formation
Appendix D3 Trooper Creek Formation

Appendix D1: Major (wt%) and trace element (ppm) analyses of volcanics from the Mount Windsor Formation and Ti-rich dykes

Sample no.	94-185A	94-286	95-56	95-65	95-70	95-114	95-165	95-168	95-169	95-185	95-186	95-187	95-191
Locality	HS416	KRH 605	KRH780	TR802	KRH810	KRH884	TC974	TC994	TC995	KR/TC1014	KR/TC1014	KR/TC1016	KR/TC1024
Lithology	rhyolite	rhyolite	rhyolite	rhyolite	rhyolite	rhyolite	dacite	dacite	dacite	rhyolite	mafic dyke	rhyodacite	dacite
Formation	MWF	MWF	MWF	MWF	MWF	MWF	MWF	MWF	MWF	MWF	Ti-rich	MWF	MWF
SiO2	79.89	81.75	78.71	76.82	74.94	78.02	77.44	78.63	79.29	78.43	51.66	80.91	73.34
TiO2	0.22	0.06	0.07	0.07	0.08	0.06	0.07	0.08	0.07	0.08	2.01	0.14	0.24
Al2O3	10.88	11.01	11.98	12.00	13.65	12.34	11.48	11.42	10.79	11.42	14.77	10.06	12.95
Fe2O3	1.67	0.71	0.76	1.21	0.97	0.64	0.91	1.25	1.09	0.82	14.33	0.71	3.71
MnO	0.06	0.01	0.01	0.04	0.01	0.03	0.01	0.02	0.02	0.02	0.22	0.01	0.05
MgO	0.33	0.19	0.30	0.54	0.16	0.17	0.40	0.46	0.33	0.42	5.11	0.35	1.65
CaO	0.41	0.13	0.29	0.05	0.11	0.16	0.09	0.13	0.11	0.26	6.79	0.35	0.73
Na2O	3.79	6.01	3.80	1.32	2.38	3.85	0.19	2.27	1.53	1.85	4.34	1.24	3.30
K2O	2.69	0.12	4.07	7.94	7.69	4.72	9.38	5.74	6.76	6.68	0.49	6.21	3.99
P2O5	0.06	0.01	0.01	0.02	0.01	0.01	0.02	0.01	0.02	0.02	0.29	0.03	0.04
TOTAL	100	100	100	100	100	100	100	100	100	100	100	100	100
L.O.I	0.73	0.6	0.66	0.51	0.48	0.47	0.41	0.51	0.41	0.4	2.37	0.45	1.17
Ti	1324	363	392	391	481	332	448	454	392	452	12063	812	1443
Nb	8	11	13	12	14	14	12	12	12	7	11	7	20
Zr	156	84	103	83	124	87	110	113	100	81	162	78	350
Sr	133	84	90	48	48	45	45	54	44	52	329	66	101
Ba	743	53	881	894	931	666	1211	653	877	1273	267	1286	1095
Sc	11	4	6	4	12	4	7	6	7	5	39	4	8
Y	25	38	30	25	66	35	28	32	66	31	43	23	48
Rb	50	4	82	151	190	94	198	156	175	175	21	166	105
Th	7	16	17	16	20	17	21	20	18	17	3	16	22
P	263	44	44	88	44	44	87	44	88	88	1264	109	179
S	<0.01	<0.01	<0.01	<0.01	<0.01	<0.01	<0.01	<0.01	<0.01	<0.01	<0.01	<0.01	<0.01
P/Zr	1.7	0.5	0.43	1.05	0.35	0.51	0.79	0.39	0.87	1.08	7.79	1.41	0.51
Ti/Zr	8.5	4.3	3.80	4.71	3.88	3.82	4.06	4.03	3.91	5.58	74.32	10.46	4.12
Nb/Y	0.7	0.8	0.44	0.48	0.22	0.39	0.43	0.38	0.18	0.24	0.27	0.31	0.41
La	14.1	30.3	22.6	23	18.5	14.4	20	18.1	76.8	32.7	15.2	22.6	40.8
Ce	31.1	65.6	54.4	47.6	49	39.6	51.3	49	112.1	74.3	33.8	51.3	96.3
Nd	17.1	30.3	25.8	20	28.2	21.1	24.8	24.3	73.5	31.5	21.9	19.8	42

MWF - Mount Windsor Formation

[1] Total Fe as Fe_2O_3

[2] Analyses recalculated to 100% anhydrous

Appendix D2: Major (wt%) and trace element (ppm) analyses of volcanics from the Trooper Creek Formation

Sample no.	94-12	94-13	94-44	94-49	94-60	94-84	94-94	94-169	94-187	94-214	94-225	94-260	94-268	94-273
Locality	HC21	HC27	TU117	TU126	TU149	HE196	HE229	HS392	HS427	TC466	TC480	HE572	HE582	HE587
Lithology	rhyolite	rhyolite	andesite	diorite	rhyolite	rhyodacite	rhyolite	site/dacite (si)	andesite	dacite	dacite	dacite	dacite	dacite
Formation	TCF	TCF	TCF	TCF	TCF	TCF	TCF	TCF	TCF	TCF	TCF	TCF	TCF	TCF
SiO2	74.95	70.24	60.4	55	74.18	73.46	76.39	73.1	71.1	67.12	74.23	72.57	78.54	74.7
TiO2	0.31	0.46	0.48	0.68	0.29	0.34	0.24	0.53	0.78	0.53	0.39	0.37	0.27	0.41
Al2O3	13.2	14.24	14.17	16.08	13.45	13.38	12.43	12.94	12.55	14.38	12.64	13.55	10.97	14.12
Fe2O3	3.02	4.33	8.23	9.08	2.99	2.64	2.39	5.16	6.07	5.04	3.88	3.59	2.82	2.41
MnO	0.02	0.11	0.13	0.17	0.04	0.07	0.06	0.13	0.15	0.11	0.06	0.09	0.03	0.03
MgO	1.04	1.28	5.61	6.8	1.11	0.55	0.6	1.22	2.65	2.42	1.12	0.93	0.51	0.39
CaO	0.41	1.84	4.39	8.31	0.77	1.82	0.4	0.23	0.68	2.66	0.27	2.54	0.82	0.25
Na2O	6.93	5.46	5.3	3.24	5.94	3.9	4.44	5.64	4.35	4.84	5.09	4.32	5.73	6.98
K2O	0.06	1.92	1.19	0.44	1.17	3.75	3	0.94	1.45	2.81	2.22	1.96	0.25	1.07
P2O5	0.05	0.12	0.1	0.19	0.06	0.08	0.05	0.11	0.21	0.09	0.09	0.08	0.05	0.11
TOTAL	100	100	100	100	100	100	100	100	100	100	100	100	100	100
L.O.I	1.05	1.73	2.04	2.47	1.1	2.1	0.76	1.29	1.81	1.74	1	2.23	0.96	0.69
Ti	1875.7	2739.6	2857	4098.1	1757.8	2016.8	1451.5	3158.1	4681.1	3167	2361.6	2195.2	1634.5	2482.5
Nb	7.3	7.7	3.9	3.6	7.2	6.5	7.5	11	9.3	7.6	9.2	7.1	6.1	6.5
Zr	140.3	132	69	56.1	130.4	124.4	152.3	168.2	144	130	149.5	128.2	91.9	123.2
Sr	122.1	120.8	227.1	616.3	234.6	96.8	62.6	86.1	89.2	184.9	61.6	125.1	165.6	87.9
Ba	190.8	591	412.7	213.2	782.6	966.5	885.8	308	536.5	723.4	548.5	381.4	109.1	504
Sc	9.1	14.2	34.5	34.7	11.1	14.3	10.1	20.3	18.3	19.3	13.1	13.2	9.1	16.2
Y	20.2	24.4	15.2	23.5	18.2	19.4	24.2	35.5	30.4	25.4	29.3	24.4	14.1	20.2
Rb	2	26.4	15.2	10.2	20.2	64.2	40.4	13.2	24.3	55.9	31.3	40.7	7.1	20.2
Th	8.6	6.4	3.5	3.5	7.5	6.6	7.5	7.6	6.7	8.6	7.1	6.7	5.4	6.3
P	220.2	531.8	442.5	845.9	264.7	355.9	220.1	486.3	929.3	399	396.7	355.1	220.3	484.8
S	<0.01	<0.01	<0.01	0.01	<0.01	0.01	0.05	<0.01	<0.01	0.03	<0.01	0.09	<0.01	<0.01
P/Zr	1.6	4	6.4	15.1	2	2.9	1.4	2.9	6.5	3.1	2.7	2.8	2.4	3.9
Ti/Zr	13.4	20.8	41.4	73	13.5	16.2	9.5	18.8	32.5	24.4	15.8	17.1	17.8	20.1
Nb/Y	0.9	0.7	0.7	0.7	0.8	0.8	0.8	0.9	0.7	0.7	0.8	0.7	1	0.7
La	17.2	15.2	10.1	12.2	13.1	15.3	17.2	36.5	17.2	20.3	23.2	13.2	16.2	9.1
Ce	37.3	34.5	19.3	29.6	34.4	34.7	41.4	69.9	41.6	39.6	47.5	36.6	32.3	22.2
Nd	17.2	17.3	10.1	16.3	15.2	15.3	19.2	32.4	22.3	18.3	23.2	17.3	14.1	13.1

TCF - Trooper Creek Formation

[1] Total Fe as Fe_2O_3

[2] Analyses recalculated to 100% anhydrous

Appendix D2 continued

Sample no.	94-275	94-279	94-280	94-338	94-347	94-352	95-50	95-232	95-236	95-264	95-265	95-297	95-299
Locality	HE591	HE598	HE599	TC540	HE550	HE557	HE764	W6 (Coronat)	W17 (Corona)	W151 (Vice)	W158 (Vice)	W229 (Trun)	W231 (HE)
Lithology	rhyodacite	rhyodacite	dacite	dolerite	rhyolite	dacite	rhyolite clast	rhyodacite	dacite	dacite	rhyolite	andesite	andesite
Formation	TCF	TCF	TCF	TCF	TCF	TCF	KRHM (TCF)	HM (TCF)	HM (TCF)	TCF/RRF	HM (TCF)	HM (TCF)	HM (TCF)
SiO2	72.96	73.35	73.53	53.29	73.31	71.89	80.21	78.21	75.14	64.87	76.89	67.48	51.06
TiO2	0.36	0.34	0.37	1.11	0.36	0.38	0.22	0.26	0.46	0.63	0.27	0.61	0.41
Al2O3	14.15	13.75	13.45	16.94	13.58	14.09	10.69	11.81	12.79	15.09	12.56	15.00	18.59
Fe2O3	3.35	2.83	3.47	9.68	3.03	3.89	2.18	1.85	3.09	7.47	2.22	5.82	8.31
MnO	0.09	0.13	0.18	0.14	0.06	0.08	0.05	0.07	0.08	0.14	0.04	0.17	0.25
MgO	1.35	0.34	1.22	5.19	0.62	0.89	1.29	1.68	1.31	2.61	0.31	2.88	7.19
CaO	0.4	1.61	0.79	8.89	1.27	1.38	0.35	0.35	1.27	3.75	1.14	1.81	8.02
Na2O	5.02	5.45	4.74	4.3	6.03	5.82	4.79	5.61	5.57	4.07	4.89	5.72	5.39
K2O	2.24	2.14	2.17	0.26	1.66	1.49	0.19	0.13	0.19	1.18	1.62	0.32	0.72
P2O5	0.08	0.07	0.09	0.2	0.08	0.09	0.03	0.03	0.10	0.18	0.05	0.20	0.05
TOTAL	100	100	100	100	100	100	100	100	100	100	100	100	100
L.O.I	1.61	1.92	1.87	0.56	1.05	0.99	1.17	1.49	1.12	5.12	1.72	3.63	9.04
Ti	2129.7	2013.5	2206	6652	2180.4	2248.4	1304.8	1552.4	2762.7	3791.3	1631.4	3653.4	2463.8
Nb	6	6.3	7.6	8	7.3	7.7	7.6	6.1	6.4	6.7	7	7.6	1.5
Zr	120.8	118.1	123.7	111	142.5	135.8	154.7	131.9	124	102.7	145.2	105.9	26.6
Sr	101.5	83.5	111.4	306.2	146.5	152.1	130.2	83.5	158.1	204.2	63.5	119.8	240.8
Ba	643.5	428.5	669.5	298	469.8	390.3	195.7	199.5	152.8	430.3	407	143.2	290.2
Sc	13.2	13.2	13.3	27.7	13.1	13.2	9.6	6	15	26.5	8	20.4	38.5
Y	21.3	20.4	22.5	24.7	24.2	25.3	21.3	13.1	22.9	20.5	16.9	26.5	8.6
Rb	53.8	39.7	35.8	6.2	31.3	30.4	6.5	3.2	5.3	23.3	38.3	9	24.4
Th	6	5.7	7	4.1	7.2	6.7	9.7	6.5	6.5	5.7	8.8	6.1	<1.5
P	354.3	310.9	401.5	851.9	352.7	398.1	132.5	132.9	442.0	782.0	224.1	863.8	239.1
S	<0.01	<0.01	0.35	<0.01	0.03	<0.01	0.03	<0.01	0.01	<0.01	<0.01	<0.01	<0.01
P/Zr	2.9	2.6	3.2	7.7	2.5	2.9	0.9	1.0	3.6	7.6	1.5	8.2	9.0
Ti/Zr	17.6	17.1	17.8	59.9	15.3	16.6	8.4	11.8	22.3	36.9	11.2	34.5	92.6
Nb/Y	0.7	0.7	0.6	0.6	0.8	0.8	0.4	0.5	0.3	0.3	0.4	0.3	0.2
La	12.2	10.2	7.2	12.3	18.2	17.2	30.8	19.7	14.6	18	17.1	15.5	3.9
Ce	29.4	27.5	20.4	29.8	38.4	40.5	59.3	38.8	35.6	36.4	34.7	34.5	8.7
Nd	15.2	13.2	13.3	15.4	19.2	19.3	27.3	14	19.3	18.2	14	19.7	2.5

TCF - Trooper Creek Formation

[1] Total Fe as Fe_2O_3

[2] Analyses recalculated to 100% anhydrous

typographic error!

Appendix D3: Major (wt%) and trace element (ppm) analyses of volcanics from the Trooper Creek Formation at Highway-Reward

Ident	39/403.8	116/182.2	140/157.08	144/157.08	148/268.8	151/350.5	515/218.5	551/313.5	560/124.4	560/316.3	600/184.3	800/127.6	800/140.2A	800/140.2B
Locality	HR	HR	~~HR~~	HR	HR	HR	HR	HR	HR	HR	HR	HR	HR	HR
Unit	rhyodacite 2	rhyolite 4	rhyolite 3	rhyolite 4	rhyodacite 1	Dacite 1	rhyodacite 3	dacite 1	rhyolite 4	dacite 1	rhyolite 9	andesite	rhyolite 6	rhyolite 6
Formation	TCF	TCF	TCF	TCF	TCF	TCF	TCF	TCF	TCF	TCF	TCF	TCF	TCF	TCF
SiO2	77.29	68.7	68.49	77.32	75.86	70.88	63.45	75.2	75.49	68.49	74.95	59.49	68.63	68.45
TiO2	0.41	0.43	0.6	0.28	0.34	0.51	0.51	0.46	0.31	0.56	0.3	0.38	0.4	0.4
Al2O3	11.62	17.41	17.69	12.41	13.57	15.87	21.35	13.97	13.27	17.07	11.55	18.51	16.37	16.22
Fe2O3	5.83	3.87	4.32	2.9	3.08	6.12	6.43	3.29	4.27	4.41	3.43	7.16	3.08	3.1
MnO	0.03	0.13	0.2	0.14	0.05	0.11	0.01	0.11	0.12	0.18	0.15	0.21	0.05	0.06
MgO	1.06	5	3.19	4.1	2.51	1.87	0.82	1.65	3.23	2.55	6.78	2.47	2.81	2.87
CaO	0.09	0.14	0.24	0.07	0.16	0.12	0.14	0.27	0.11	0.19	0.22	6.86	1.37	1.54
Na2O	0.1	0.21	1.35	0.09	1.93	0.13	0.33	2.52	0.08	4.52	1.98	3.69	5.27	5.35
K2O	3.36	3.54	3.67	2.55	2.36	4.04	6.59	2.37	2.94	1.86	0.56	0.86	1.9	1.89
P2O5	0.08	0.07	0.1	0.05	0.06	0.08	0.12	0.08	0.05	0.1	0.06	0.33	0.07	0.07
Total*	100	100	100	100	100	100	100	100	100	100	100	100	100	100
LOI	3.62	4.19	3.8	3.37	2.88	3.36	5.91	2.6	3.25	2.42	3.12	3.09	3.12	3.12
Ti	2446	2564	3581	1699	2035	3038	3043	2741	1867	3384	1803	2294	2403	2393
Nb	8	11	6	9	9	7	9	7	9	9	6	5	10	11
Zr	158	211	118	159	149	133	189	128	167	161	123	86	203	208
Sr	35	23	11	15	41	22	31	53	15	68	35	550	110	110
Ba	1547	5181	406	927	635	2523	2110	787	1241	515	260	208	414	423
Sc	17	13	6	9	11	14	20	14	8	17	10	7	11	12
Y	27	25	16	21	19	12	19	19	21	25	19	16	28	29
Rb	79	69	29	58	48	93	113	59	66	44	12	33	62	63
Th	8	8	6	7	8	7	11	7	8	8	7	12	10	10
P	365	319	457	229	269	361	508	363	227	448	272	1444	314	321
S (in loss)	3	<0.01	1	<0.01	1	1	5	<0.01	<0.01	<0.01	<0.01	<0.01	<0.01	<0.01
P/Zr	2.3	1.5	3.9	1.4	1.8	2.7	2.7	2.8	1.4	2.8	2.2	16.8	1.6	1.5
Ti/Zr	15.5	12.2	30.2	10.7	13.6	22.8	16.1	21.4	11.2	21	14.6	26.7	11.9	11.5
Nb/Y	0.3	0.5	0.4	0.4	0.4	0.5	0.5	0.4	0.4	0.4	0.3	0.3	0.4	0.4
La	16.4	19.7	11	19.9	14.9	8.1	26.1	17.4	20.6	19.1	16.7	26.4	23.5	23.6
Ce	38.5	52.6	24.2	40.3	32.1	23.5	57.7	35.9	41.6	39.3	30.2	50.3	46.2	47.7
Nd	17.2	24.3	10	17.9	14.5	10.1	23	16.6	17	18.7	12.4	24.7	18.7	19.1

TCF - Trooper Creek Formation

[1] Total Fe as Fe_2O_3

[2] Analyses recalculated to 100% anhydrous

Appendix D3 continued

Ident	800/242	801/291.2	803/62	804/177.5	805/160.05	807/319
Locality	HR	HR	HR	HR	HR	HR
Unit	rhyodacite 3	rhyodacite 3	dacite 1	andesite	rhyodacite 3	rhyolite 2
Formation	TCF	TCF	TCF	TCF	TCF	TCF
SiO2	67.39	67.22	74.94	62.09	76.63	73.71
TiO2	0.4	0.38	0.43	0.29	0.3	0.43
Al2O3	18.62	16.72	13.04	18.12	12.68	13.94
Fe2O3	4.8	7.48	3.4	5.45	2.41	6.51
MnO	0.13	0.08	0.14	0.21	0.03	0.01
MgO	3.41	3.78	1.75	1.84	0.41	0.58
CaO	0.12	0.1	0.79	5.23	0.16	0.07
Na2O	0.17	0.18	2.54	2.4	6.7	0.15
K2O	4.68	3.85	2.79	3.94	0.58	4.25
P2O5	0.09	0.08	0.08	0.23	0.05	0.07
Total*	100	100	100	100	100	100
LOI	4.14	5.25	2.8	5.68	0.46	4.86
Ti	2384	2285	2599	1712	1813	2592
Nb	8	7	7	5	8	6
Zr	176	152	121	96	143	111
Sr	23	23	57	275	77	23
Ba	1843	1046	950	1941	252	2234
Sc	16	15	12	6	8	11
Y	18	16	23	15	17	18
Rb	99	72	57	101	5	76
Th	11	9	6	12	7	6
P	411	370	360	1016	220	322
S(in loss)	1	3	<0.01	<0.01	<0.01	5
P/Zr	2.3	2.4	3	10.5	1.5	2.9
Ti/Zr	13.6	15	21.5	17.8	12.7	23.4
Nb/Y	0.5	0.4	0.3	0.3	0.5	0.3
La	12.4	25	22.4	24	12.9	21
Ce	28.7	50.8	45.1	55.3	26.8	48
Nd	14.5	21.9	21.5	25.8	13.6	23

TCF - Trooper Creek Formation

[1] Total Fe as Fe_2O_3

[2] Analyses recalculated to 100% anhydrous

Appendix E

Geochemical analyses of ironstones

Appendix E1 XRD analyses for massive ironstone
Appendix E2 Major, trace and REE analyses
Appendix E3 Calculations for isocon plots

Appendix E1: XRD analyses for massive ironstone

Sample	Quartz	Hematite
95-130	95	5
95-150	85	15
95-316B	85	15

Appendix E2: Major (wt%), trace element (ppm) and rare earth element (ppm) analyses of iron oxide±silica rocks from the study area

Sample number	94-18	94-25	94-246	94-327	94-334	94-401	95-130	95-150	95-200	95-206	95-210	95-212	95-214	95-217	95-272
Lithology	cherty irn	cherty irn	massive irn	tuff irn	hem pumice	cherty irn	massive irn	massive irn	strom irn	massive irn	massive irn	tuff irn	tuff irn	strom irn	andesite bx
SiO2	96.58	90.97	97.19	66.99	72.86	93.16	94.91	88.63	88.31	79.4	81.01	73.12	65.54	79.43	56.4
TiO2	0.01	0.06	<0.01	0.3	0.26	0.01	<0.01	<0.01	0.08	0.04	0.03	0.08	0.12	0.17	1.42
Al2O3	0.22	0.85	0.04	4.61	8.75	0.07	0.06	0.26	2.45	1.84	0.74	1.92	3.47	3.26	14.62
Fe2O3	2.14	6.9	2.14	24.5	10.98	2.43	5.01	8.11	6.82	16.79	16.36	23.16	28.5	11.08	10.33
MnO	0.01	0.02	<0.01	0.03	0.06	<0.01	0.01	0.02	0.05	0.02	0.07	0.01	0.01	0.09	0.12
MgO	0.01	0.09	0.01	0.42	1.31	0.01	<0.01	0.06	0.17	0.29	0.41	0.05	0.02	0.36	4.47
CaO	0.01	0.02	0.02	0.05	0.11	0.01	<0.01	0.2	0.3	0.16	0.21	0.01	0.01	3.26	2.5
Na2O	<0.05	<0.05	<0.05	0.05	0.42	<0.05	<0.05	<0.05	0.63	<0.05	<0.05	<0.05	<0.05	0.45	1.18
K2O	0.05	0.13	0.02	1.38	2.72	<0.01	<0.01	0.01	0.34	0.61	0.05	0.08	0.02	0.12	3.95
P2O5	0.01	0.03	0.02	0.03	0.02	0.05	0.01	0.03	0.04	0.02	0.02	0.02	0.05	1.11	0.19
BaO(disc)	0.02	0.13	<0.01	0.03	0.04	1.85	0.01	<0.01	0.02	0.01	0.01	0.04	0.07	0.04	0.02
S	0.73	0.45	0.05	0.01	0.01	0.86	0.01	0.01	0.01	0.01	0.01	0.02	0.03	0.01	0.01
Loss	0.91	0.96	0.42	1.49	2.21	1.21	0.26	0.32	0.61	0.75	0.79	1.21	2.14	0.74	5
Total	100.7	100.61	99.91	99.89	99.75	99.66	100.28	97.65	99.83	99.94	99.71	99.72	99.98	100.12	100.21
SiO2/Fe2O3	45.13	13.18	45.42	2.73	6.64	38.34	18.94	10.93	12.95	4.73	4.95	3.16	2.30	7.17	5.46
Ti/Zr	12.49	29.48	0.00	34.59	14.55	21.41	0.00	0.00	11.84	21.60	20.44	18.81	16.24	23.21	58.07
Ti	0.01	0.04	0.00	0.18	0.16	0.01	0.00	0.00	0.05	0.02	0.02	0.05	0.07	0.10	0.85
Sc	<2	<2	<2	8	9	<2	<2	<2	3	<2	<2	2	6	7	30
V	5	18	5	170	1337	58	10	17	22	20	27	14	49	66	238
Cr	3	4	2	11	26	24	3	4	7	5	5	7	7	7	3
Ni	<2	<2	<2	11	18	2	3	8	6	12	11	<2	<2	15	<2
Cu	38	20	8	35	68	191	4	5	19	10	14	17	23	79	7
Zn	16	73	<2	20	196	108	<2	4	9	12	16	6	10	18	98
Pb	11	24	9	16	39	942	2	8	21	7	8	9	6	51	6
Rb	<1	4	<1	68	103	<1	<1	1	13	31	3	4	<1	5	171
Sr	16	42	4	22	26	337	1	11	55	4	6	10	14	421	35
Y	3	14	1	25	10	<1	<1	5	12	4	2	8	7	36	36
Zr	5	12	1	52	107	3	<1	4	41	11	9	26	44	44	147
Nb	1	2	<1	6	4	1	<1	<1	4	1	1	2	3	4	12
Ba	219	1523	36	419	522	18500	106	79	138	72	149	459	909	429	290
Ag	0.6	0.5	<0.1	<0.1	<0.1	2.3	<0.1	<0.1	<0.1	-	<0.1	<0.1	0.1	0.1	0.1
As	76	8	14	7	<4	31	8	13	11	7	12	10	13	50	<4
Bi	<2	<2	<2	<2	<2	<2	<2	<2	<2	<2	<2	<2	<2	<2	<2
Mo	1.2	6.1	2.5	0.6	1	13.7	3.4	1.1	1.8	0.8	1.7	2.1	1.7	1.6	0.7
Sb	<2	<2	<2	4	<2	3	<2	<2	<2	2	<2	4	3	4	<2
La	1.57	14.3	0.35	17.2	7.27	1.8	0.74	4.1	13.8	-	2.1	13.1	10.6	40.7	22.5
Ce	2.53	9.51	0.4	35.2	15.2	3.29	1.43	4.78	28	-	4.58	13.9	18.8	64.1	41.4
Pr	0.29	2.46	0.05	3.69	1.66	0.46	0.17	0.73	3.31	-	0.5	2.98	2.21	8.27	5.71
Nd	1.1	8.4	0.2	14.3	6.4	1.9	0.06	2.7	12.5	-	2	11.2	7.6	31.9	23.2
Sm	0.2	2.1	<0.1	3.4	1.5	0.5	0.2	0.7	2.9	-	0.5	2.6	1.6	7.1	6
Eu	0.11	0.59	<0.05	0.78	0.47	0.95	<0.05	0.13	0.6	-	0.1	0.57	0.42	1.62	1.79
Gd	0.2	2.1	<0.1	3.5	1.3	0.3	0.1	0.6	2.4	-	0.4	1.9	1.3	6.8	5.7
Dy	0.3	2.2	<0.1	3.2	1.3	0.1	<0.1	0.7	2.2	-	0.5	1.5	1.2	5.5	5.4
Er	0.3	1.2	<0.1	1.7	0.7	<0.1	<0.1	0.5	1.3	-	0.3	0.7	0.6	2.8	3.2
Yb	0.3	1.1	<0.1	1.4	0.5	<0.1	<0.1	0.5	1.4	-	0.3	0.7	0.7	2.2	2.7

Abbreviations: irn=ironstone; tuff=tuffaceous ironstone; bx=breccia; strom=stromatolitic ironstone.

Appendix E2 continued

Sample no.	95-273	95-274	95-275	95-276	95-308	95-316B	95-317B	95-318
Lithology	massive irn	hem pumice	tuff irn	massive irn	pumice bx	massive irn	andesite bx	andesite bx
SiO2	61.94	57.34	62.7	82.2	70.65	90.9	63.73	56.57
TiO2	0.08	0.71	0.18	0.04	0.49	0.01	0.8	1.22
Al2O3	1.7	13.54	4.86	0.58	13.84	0.09	15.17	13.78
Fe2O3	33.08	17.05	25.85	15.32	4.19	7.47	8.35	9.1
MnO	0.1	0.04	0.1	0.06	0.12	0.03	0.06	0.17
MgO	0.7	2.28	2.37	0.3	1.38	0.02	1.69	2.99
CaO	0.06	0.18	0.11	0.25	1.15	0.04	2.3	4.87
Na2O	<0.05	0.44	0.88	<0.05	2.92	<0.05	5.8	4.55
K2O	0.23	4.76	0.12	0.03	3.73	<0.01	0.07	1.38
P2O5	0.03	0.04	0.04	0.04	0.11	0.02	0.02	0.6
BaO(disc)	0.04	0.03	0.03	<0.01	0.1	<0.01	<0.01	0.05
S	0.01	0.01	0.01	0.01	<0.01	0.01	<0.01	<0.01
Loss	0.88	3.53	2.68	1.03	2.14	0.26	1.71	4.72
Total	98.85	99.95	99.93	99.86	100.82	98.85	99.7	100
SiO2/Fe2O3	1.87	3.36	2.43	5.37	16.86	12.17	7.63	6.22
Ti/Zr	18.30	23.44	19.84	19.18	18.13	39.97	146.22	47.80
Ti	0.05	0.43	0.11	0.02	0.29	0.01	0.48	0.73
Sc	4	19	6	2	14	<2	31	28
V	35	71	50	23	31	19	196	177
Cr	8	6	10	6	7	13	23	4
Ni	24	65	12	13	2	2	13	3
Cu	11	6	57	68	22	4	4	13
Zn	41	144	73	13	74	<2	63	109
Pb	11	49	18	9	15	2	4	4
Rb	14	210	8	2	99	<1	2	24
Sr	6	28	27	5		3	281	77
Y	9	34	8	5	32	1	11	44
Zr	26	182	54	13	162	2	33	153
Nb	2	14	4	2	11	<1	4	13
Ba	508	414	475	60	851	21	78	700
Ag	<0.1	<0.1	<0.1	0.2	-	<0.1	<0.1	<0.1
As	9	9	6	19	<3	7	<4	<4
Bi	<2	<2	<2	<2	2	<2	<2	<2
Mo	1.9	0.8	1.3	1.3	0.3	2.4	0.7	1.4
Sb	5	3	<2	<2	<2	<2	<2	<2
La	10.7	44.2	7.51	4.36	-	0.89	5.34	27
Ce	17.2	68.4	17.1	8.13	-	0.87	11.4	55.3
Pr	2.14	9.47	1.75	1.01	-	0.19	1.41	7.18
Nd	8.3	36.1	6.6	3.8	-	0.7	5.4	29
Sm	1.9	7.8	1.5	0.9	-	0.2	1.5	7.3
Eu	0.52	1.77	0.43	0.16	-	0	0.59	2.14
Gd	1.8	6.5	1.4	0.7	-	0.2	1.4	6.8
Dy	1.5	5.7	1.3	0.6	-	0.1	1.6	6.9
Er	0.7	3	0.8	0.4	-	0.1	1.1	4.2
Yb	0.5	2.7	0.6	0.4	-	0.1	1	4.1

Abbreviations: irn=ironstone; tuff=tuffaceous ironstone; bx=breccia; strom=stromatolitic ironstone.

Appendix E3: Calculations for isocon plots

Trooper Creek prospect - massive ironstone

Element (wt%)	least altered **Co(i) 308**	altered **C(i) 210+276**	ratio rank **alt./l.a**	**n(i)**	**F(i)**	**Cs(i)**	**m**	**m(ave)**	**CA(i)**
Si	70.65	81.605	1.155	1	0.01	1.16			1221.62
Fe	4.19	15.84	3.780	2	0.48	7.56		0.09	4225.55
Cr	0.0007	0.000565	0.807	3	4285.71	2.42			823.53
Cu	0.0022	0.004095	1.861	4	1818.18	7.45			2029.77
Nb	0.0011	0.000145	0.132	5	4545.45	0.66	0.13		50.83
Zn	0.0074	0.001445	0.195	6	810.81	1.17		Ma(%)	123.43
Pb	0.0015	0.00084	0.560	7	4666.67	3.92		1044.2	540.75
Y	0.0032	0.000385	0.120	8	2500.00	0.96	0.12		37.66
Sr	0.0162	0.00057	0.035	9	555.56	0.32			-59.74
Rb	0.0099	0.000215	0.022	10	1010.10	0.22			-75.15
Mn	0.12	0.065	0.542	11	91.67	5.96			519.77
Zr	0.0162	0.001065	0.066	12	740.74	0.79	0.07		-24.78
Na	2.92	0	0.000	13	4.45	0.00			-100.00
Mg	1.38	0.355	0.257	14	10.14	3.60			194.34
Ca	1.15	0.23	0.200	15	13.04	3.00			128.84
Al	13.84	0.66	0.048	16	1.16	0.76	0.05		-45.44
P	0.11	0.03	0.273	17	154.55	4.64			212.05
K	3.73	0.04	0.011	18	4.83	0.19			-87.73
Ti	0.49	0.035	0.071	19	38.78	1.36	0.07		-18.27
Ba	0.0851	0.01047	0.123	20	235.02	2.46			40.77

Trooper Creek prospect - tuffaceous ironstone

Element (wt%)	least altered **Co(i) 308**	altered **C(i) 275**	ratio rank **alt./l.a**	**n(i)**	**F(i)**	**Cs(i)**	**m**	**m(ave)**	**CA(i)**
Si	70.65	62.7	0.887	1	0.01	0.89			165.5
Fe	4.19	25.85	6.169	2	0.48	12.34		0.3343	1745.6
Cr	0.0007	0.00096	1.371	3	4285.71	4.11			310.28
Cu	0.0022	0.00571	2.595	4	1818.18	10.38			676.45
Nb	0.0011	0.00039	0.355	5	4545.45	1.77	0.35		6.0655
Zn	0.0074	0.0073	0.986	6	810.81	5.92		Ma(%)	195.12
Pb	0.0015	0.00182	1.213	7	4666.67	8.49		199.16	262.98
Y	0.0032	0.00084	0.263	8	2500.00	2.10	0.26		-21.47
Sr	0.0162	0.00268	0.165	9	555.56	1.49			-50.51
Rb	0.0099	0.00075	0.076	10	1010.10	0.76			-77.34
Mn	0.12	0.1	0.833	11	91.67	9.17			149.3
Zr	0.0162	0.00544	0.336	12	740.74	4.03	0.34		0.4584
Na	2.92	0.88	0.301	13	4.45	3.92			-9.842
Mg	1.38	2.37	1.717	14	10.14	24.04			413.77
Ca	1.15	0.11	0.096	15	13.04	1.43			-71.38
Al	13.84	4.86	0.351	16	1.16	5.62	0.35		5.0516
P	0.11	0.04	0.364	17	154.55	6.18			8.7852
K	3.73	0.12	0.032	18	4.83	0.58			-90.38
Ti	0.49	0.18	0.367	19	38.78	6.98	0.37		9.8952
Ba	0.0851	0.0475	0.558	20	235.02	11.16			66.981

Appendix E3: Calculations for isocon plots

Trooper Creek prospect - stromatolitic ironstone

Element	least altered	altered	ratio rank						
(wt%)	Co(i) 308	C(i) 200	alt./l.a	n(i)	F(i)	Cs(i)	m	m(ave)	CA(i)
Si	70.65	88.31	1.250	1	0.01	1.25			362.97
Fe	4.19	6.82	1.628	2	0.48	3.26		0.27	502.87
Cr	0.0007	0.00071	1.014	3	4285.71	3.04			275.68
Cu	0.0022	0.00185	0.841	4	1818.18	3.36			211.46
Nb	0.0011	0.00043	0.391	5	4545.45	1.95	0.39		44.79
Zn	0.0074	0.00092	0.124	6	810.81	0.75		Ma(%)	-53.95
Pb	0.0015	0.00211	1.407	7	4666.67	9.85		270.38	421.01
Y	0.0032	0.00118	0.369	8	2500.00	2.95	0.37		36.58
Sr	0.0162	0.00551	0.340	9	555.56	3.06			25.98
Rb	0.0099	0.00128	0.129	10	1010.10	1.29			-52.11
Mn	0.12	0.05	0.417	11	91.67	4.58			54.33
Zr	0.0162	0.00405	0.250	12	740.74	3.00	0.25		-7.40
Na	2.92	0.63	0.216	13	4.45	2.80			-20.09
Mg	1.38	0.17	0.123	14	10.14	1.72			-54.37
Ca	1.15	0.3	0.261	15	13.04	3.91			-3.38
Al	13.84	2.45	0.177	16	1.16	2.83	0.18		-34.43
P	0.11	0.04	0.364	17	154.55	6.18			34.69
K	3.73	0.34	0.091	18	4.83	1.64			-66.24
Ti	0.49	0.08	0.163	19	38.78	3.10	0.16		-39.53
Ba	0.0851	0.0138	0.162	20	235.02	3.24			-39.94

Trooper Creek prospect - hematite-altered pumice breccia

Element	least altered	altered	ratio rank						
(wt%)	Co(i) 308	C(i) 274	alt./l.a	n(i)	F(i)	Cs(i)	m	m(ave)	CA(i)
Si	70.65	57.34	0.812	1	0.01	0.81			-31.13
Fe	4.19	17.05	4.069	2	0.48	8.14		1.1785	245.28
Cr	0.0007	0.00055	0.786	3	4285.71	2.36			-33.33
Cu	0.0022	0.00062	0.282	4	1818.18	1.13			-76.09
Nb	0.0011	0.00141	1.282	5	4545.45	6.41	1.28		8.7649
Zn	0.0074	0.01441	1.947	6	810.81	11.68		Ma(%)	65.232
Pb	0.0015	0.00485	3.233	7	4666.67	22.63		-15.15	174.35
Y	0.0032	0.0034	1.063	8	2500.00	8.50	1.06		-9.845
Sr	0.0162	0.00284	0.175	9	555.56	1.58			-85.12
Rb	0.0099	0.02096	2.117	10	1010.10	21.17			79.646
Mn	0.12	0.04	0.333	11	91.67	3.67			-71.72
Zr	0.0162	0.01816	1.121	12	740.74	13.45	1.12		-4.882
Na	2.92	0.44	0.151	13	4.45	1.96			-87.21
Mg	1.38	2.28	1.652	14	10.14	23.13			40.19
Ca	1.15	0.18	0.157	15	13.04	2.35			-86.72
Al	13.84	13.54	0.978	16	1.16	15.65	0.98		-16.99
P	0.11	0.04	0.364	17	154.55	6.18			-69.14
K	3.73	4.76	1.276	18	4.83	22.97			8.2831
Ti	0.49	0.71	1.449	19	38.78	27.53	1.45		22.949
Ba	0.0851	0.0414	0.486	20	235.02	9.73			-58.72

Appendix E3: Calculations for isocon plots

Trooper Creek prospect - massive ironstone

Element	least altered	altered	ratio rank						
(wt%)	Co(i) 308	C(i) 206+273	alt./l.a	n(i)	F(i)	Cs(i)	m	m(ave)	CA(i)
Si	70.65	70.67	1.000	1	0.01	1.00			588.7901
Fe	4.19	24.935	5.951	2	0.48	11.90		0.14522	3997.881
Cr	0.0007	0.000625	0.893	3	4285.71	2.68			514.8171
Cu	0.0022	0.001035	0.470	4	1818.18	1.88			223.9527
Nb	0.0011	0.000175	0.159	5	4545.45	0.80	0.16		9.549235
Zn	0.0074	0.00263	0.355	6	810.81	2.13		Ma(%)	144.7305
Pb	0.0015	0.0009	0.600	7	4666.67	4.20		588.60	313.1571
Y	0.0032	0.000645	0.202	8	2500.00	1.61	0.20		38.79497
Sr	0.0162	0.000465	0.029	9	555.56	0.26			-80.2348
Rb	0.0099	0.00221	0.223	10	1010.10	2.23			53.7167
Mn	0.12	0.06	0.500	11	91.67	5.50			244.2976
Zr	0.0162	0.001865	0.115	12	740.74	1.38	0.12		-20.7265
Na	2.92	0	0.000	13	4.45	0.00			-100
Mg	1.38	0.495	0.359	14	10.14	5.02			146.9961
Ca	1.15	0.11	0.096	15	13.04	1.43			-34.1344
Al	13.84	1.77	0.128	16	1.16	2.05	0.13		-11.9354
P	0.11	0.025	0.227	17	154.55	3.86			56.49891
K	3.73	0.42	0.113	18	4.83	2.03			-22.4638
Ti	0.49	0.06	0.122	19	38.78	2.33	0.12		-15.6822
Ba	0.0851	0.029005	0.341	20	235.02	6.82			134.6969

Trooper Creek prospect - horizon 4

Element	least altered	altered	ratio rank						
(wt%)	Co(i) 308	C(i) 316B	alt./l.a	n(i)	F(i)	Cs(i)	m	m(ave)	CA(i)
Si	70.65	90.9	1.287	1	0.01	1.29		0.0176	7195.31
Fe	4.19	7.47	1.783	2	0.48	3.57			10008.77
Cr	0.0007	0.00131	1.871	3	4285.71	5.61			10511.21
Cu	0.0022	0.00036	0.164	4	1818.18	0.65			827.84
Nb	0.0011	0	0.000	5	4545.45	0.00	0.00		-100.00
Zn	0.0074	0	0.000	6	810.81	0.00		Ma(%)	-100.00
Pb	0.0015	0.00018	0.120	7	4666.67	0.84		5570.11	580.41
Y	0.0032	0.00011	0.034	8	2500.00	0.28	0.03		94.91
Sr	0.0162	0.00026	0.016	9	555.56	0.14			-9.00
Rb	0.0099	0	0.000	10	1010.10	0.00			-100.00
Mn	0.12	0.03	0.250	11	91.67	2.75			1317.53
Zr	0.0162	0.00015	0.009	12	740.74	0.11	0.01		-47.50
Na	2.92	0	0.000	13	4.45	0.00			-100.00
Mg	1.38	0.02	0.014	14	10.14	0.20			-17.82
Ca	1.15	0.04	0.035	15	13.04	0.52			97.22
Al	13.84	0.09	0.007	16	1.16	0.10	0.01		-63.13
P	0.11	0.02	0.182	17	154.55	3.09			930.93
K	3.73	0	0.000	18	4.83	0.00			-100.00
Ti	0.49	0.01	0.020	19	38.78	0.39	0.02		15.72
Ba	0.0851	0.00206	0.024	20	235.02	0.48			37.26

Appendix E3: Calculations for isocon plots

Trooper Creek prospect - western lenses (95-212, 214, 275)

Element	least altered	altered	ratio rank						
(wt%)	**Co(i) 308**	**C(i)**	**alt./l.a**	**n(i)**	**F(i)**	**Cs(i)**	**m**	**m(ave)**	**CA(i)**
Si	70.65	68.55	0.970	1	0.01	0.97			210.55
Fe	4.19	22.843916	5.452	2	0.48	10.90		0.3124	1644.99
Cr	0.0007	0.00082667	1.181	3	4285.71	3.54			277.98
Cu	0.0022	0.00247333	1.124	4	1818.18	4.50			259.83
Nb	0.0011	0.00035333	0.321	5	4545.45	1.61	0.32		2.81
Zn	0.0074	0.00119333	0.161	6	810.81	0.97		Ma(%)	-48.39
Pb	0.0015	0.001	0.667	7	4666.67	4.67		220.06	113.38
Y	0.0032	0.00131	0.409	8	2500.00	3.28	0.41		31.03
Sr	0.0162	0.00150333	0.093	9	555.56	0.84			-70.30
Rb	0.0099	0.00240667	0.243	10	1010.10	2.43			-22.19
Mn	0.12	0.01666667	0.139	11	91.67	1.53			-55.55
Zr	0.0162	0.00406	0.251	12	740.74	3.01	0.25		-19.79
Na	2.92	0.012364	0.004	13	4.45	0.06			-98.64
Mg	1.38	0.16333333	0.118	14	10.14	1.66			-62.12
Ca	1.15	0.02333333	0.020	15	13.04	0.30			-93.51
Al	13.84	3.33333333	0.241	16	1.16	3.85	0.24		-22.91
P	0.11	0.03333333	0.303	17	154.55	5.15			-3.01
K	3.73	0.49333333	0.132	18	4.83	2.38			-57.67
Ti	0.49	0.16666667	0.340	19	38.78	6.46	0.34		8.87
Ba	0.0851	0.05955	0.700	20	235.02	14.00			123.97

Appendix F

Publications

Doyle MG, Allen RL, and McPhie J, 1993. Textural effects of devitrification and hydrothermal alteration in silicic lavas and shallow intrusions, Mount Read Volcanics (MRV), Cambrian, Tasmania. IAVCEI General Assembly, Canberra, Australia. Abstracts: 28.

Doyle MG, 1994. Facies architecture of a submarine felsic volcanic centre: Highway-Reward, Mount Windsor Volcanics, Cambro-Ordovician, north Queensland. In Henderson RA and Davis BK, New developments in geology and metallogeny: Northern Tasman Orogenic Zone: Economic Geology Research Unit, Contribution 50: 149-150.

Doyle MG and McPhie J, 1994. A silicic submarine syn-sedimentary intrusive-dome-hyaloclastite host sequence to massive sulfide mineralisation: Mount Windsor Volcanics, Cambro-Ordovician, Australia. IAVCEI International Volcanological Congress, Ankara, Turkey. Abstracts, Theme 10.

Large RR, Doyle M, Cooke D and Raymond O, 1994. Evaluation of the role of Cambrian Granites in the genesis of world class volcanogenic-hosted massive sulphide deposits in Tasmania. Geological Society of Australia, Abstracts 37: 236-237.

Large RR, Doyle M, Raymond O, Cooke D, Jones A and Heasman L, 1996. Evaluation of the role of Cambrian Granites in the genesis of world class VHMS deposits in Tasmania. Ore Geology Reviews, 10: 215-230.

Doyle MG, Allen RL, and McPhie J, 1993. Textural effects of devitrification and hydrothermal alteration in silicic lavas and shallow intrusions, Mount Read Volcanics (MRV), Cambrian, Tasmania. IAVCEI General Assembly, Canberra, Australia. Abstracts: 28.

TEXTURAL EFFECTS OF DEVITRIFICATION AND HYDROTHERMAL ALTERATION IN SILICIC LAVAS AND SHALLOW INTRUSIONS, MOUNT READ VOLCANICS (MRV), CAMBRIAN, TASMANIA

DOYLE, M.G., C.O.D.E.S., University of Tasmania, Hobart, Tasmania 7001, Australia, Allen R.L., Volcanic Resources, Bous de Jongpark 41, 2283 TJ Rijswijk ZH, The Netherlands, and McPhie J., C.O.D.E.S., University of Tasmania, Hobart, Tasmania 7001, Australia

Submarine silicic lava flows, domes and shallow intrusions in the MRV comprise coherent , massive and flow banded lava, hyaloclastite and autobreccia. Margins of lavas and intrusions were formerly glassy whereas interiors varied from glassy to crystalline. Perlitic fracturing, devitrification, and hydrothermal and diagenetic alteration acted on primary volcanic textures to generate diverse alteration textures, including false volcaniclastic textures, in the originally glassy parts of the silicic lavas and intrusions.

Perlitic fracturing of glass commenced during cooling of the silicic lavas and intrusions, generating pathways for migrating fluids. Devitrification refers to the nucleation and growth of crystalline minerals in glasses at subsolidus temperatures. “High” temperature devitrification of glass accompanied emplacement, and generated spherulites, lithophysae, and micropoikilitic texture. “Low” temperature devitrification of silicic glass to an assemblage of sericite, chlorite, quartz and feldspar is attributed to interaction with syn-volcanic hydrothermal fluids and early to late diagenetic fluids, and can be referred to as hydrothermal and diagenetic alteration. The textural effects of these alteration processes were strongly influenced by the pre-existing texture which was created by eruption and primary fragmentation, “high” temperature devitrification, and hydration. Textures were either enhanced, modified or destroyed during “low” temperature devitrification.

During lower greenschist facies metamorphism earlier mineral assemblages were recrystallised or replaced by coarse metamorphic minerals, overprinting or mimicking primary and alteration textures.

The outcome of this textural progression is that both coherent and autoclastic facies of silicic lavas and shallow intrusions in the MWV resemble matrix supported, monomict and polymict, welded and non-welded volcaniclastic deposits.

Doyle MG, 1994. Facies architecture of a submarine felsic volcanic centre: Highway-Reward, Mount Windsor Volcanics, Cambro-Ordovician, north Queensland. In Henderson RA and Davis BK, New developments in geology and metallogeny: Northern Tasman Orogenic Zone: Economic Geology Research Unit, Contribution 50: 149-150.

Facies architecture of a submarine felsic volcanic centre: Highway-Reward, Mount Windsor Volcanics, Cambro-Ordovician, Northern Queensland

by

M.G. Doyle

Centre for Ore Deposit and Exploration Studies
University of Tasmania

Evaluating the prospectivity of ancient volcanic sequences for volcanic-hosted massive sulfide (VHMS) deposits can be greatly enhanced by identifying original lithologies and emplacement processes (McPhie et al., 1993). In particular, distinguishing between syn-volcanic intrusions, lava flows, domes and cryptodomes and between autoclastic, resedimented volcaniclastic and epiclastic facies is critical in recognising palaeo-sea floor positions which are important sites for exhalative and shallow sub-surface base metal sulfide accumulation in many VHMS systems. Detailed core logging and petrography of host rocks to the Cu-Au-Pb-Zn Highway and Reward deposits have revealed the nature of volcanic processes in a near vent, subaqueous (submarine), below-wave-base depositional environment.

The volcanic facies architecture at Highway and Reward includes the products of both intrabasinal and basin margin or subaerial eruptions. Rhyolitic, rhyodacitic and dacitic lava domes, partly extrusive cryptodomes, syn-sedimentary intrusions and associated in situ and resedimented autoclastic deposits are from an intrabasinal source. Contact relationships and phenocryst mineralogy, size and percentages indicate the presence of up to nine distinct porphyritic units within an area of approximately 1 x 1 x 0.5 km at Highway-Reward. Massive coherent and flow banded lava, hyaloclastite, autobreccia and peperite are the main component facies of the porphyritic units. Peperites vary from sediment-matrix-supported breccias in which porphyry clasts are sparse (dispersed peperite), through sediment-poor jigsaw-fit aggregates of porphyry clasts (compact peperite), to relatively coherent porphyry enclosing isolated stringers and/or globules of sediment. Porphyry clasts vary from blocky with curviplanar margins (blocky peperite) to lenticular with ragged margins (ragged peperite), which may reflect, respectively, the relative importance of cooling contraction granulation and dynamic stressing of chilled lava surfaces during emplacement. The peperitic upper margins to many porphyry sheets demonstrate their intrusion into wet unconsolidated sediments. The high relative density of magma to wet sediment favoured emplacement as syn-sedimentary intrusions rather than extrusions (cf. McBirney, 1963; Walker, 1989). Dewatering and induration of the sediment pile by early syn-sedimentary intrusions may have favoured the subsequent eruption of lava domes and partly emergent cryptodomes at Highway-Reward. The shape and distribution of lava domes and cryptodomes was further influenced by the positions of previously or concurrently emplaced porphyritic units, and possibly by syn-volcanic faults which may have acted as conduits for magma. Because they are constructional, lava domes and cryptodomes influenced subsequent volcaniclastic sedimentation. Lava domes, cryptodomes and deposits of resedimented hyaloclastite sourced from over-steepened dome margins are an important indicator of palaeo-sea floor positions.

Porphyries intruded or were overlain by a volcaniclastic and sedimentary facies association comprising suspension-settled siltstone, graded turbiditic sandstone and thick mass-flow-emplaced pumiceous- and crystal-rich sandstone-breccia. Pumiceous mass-flow deposits are emplaced rapidly in large volumes, erupted infrequently and are widely distributed (McPhie & Allen, 1992), and so provide an important framework for correlation within the Trooper Creek Formation at Highway-Reward. Quartz-feldspar and feldspar only, pumiceous and crystal-rich sandstone-breccia units are non-welded, up to 65 m thick, and normally graded with fine grained tops, and in some instances, polymict lithic-rich bases. Deposition from high-concentration turbidity currents sourced from explosive eruptions at a subaerial or shallow subaqueous basin margin centre is suggested.

Perlitic fracturing, devitrification, hydrothermal and diagenetic alteration have acted on originally glassy parts of lavas and intrusions, and pumiceous breccias to generate diverse alteration textures, including false volcaniclastic and welding textures. Alteration of lavas commenced during cooling from magmatic temperatures (high temperature devitrification) generating spherulites, micropoikilitic texture and lithophysae. Hydration of residual glass to form perlitic fractures supplemented fracture and matrix permeability generated by autoclastic processes, both of which were important for migration of fluids during hydrothermal and diagenetic alteration. Hydrothermal and diagenetic alteration were also influenced by textural and compositional domains generated during high temperature devitrification. Apparent polymict and monomict volcaniclastic textures formed during this textural progression further evolved during greenschist facies metamorphism and tectonic deformation. Pumiceous breccias show the textural effects of early polyphase diagenetic and syn-volcanic hydrothermal alteration. Initial heterogeneous quartz-feldspar alteration replaced glassy vesicle walls of individual pumice shreds and domains within breccias, thereby largely preserving non-welded tube-vesicle textures. Remaining pumice clasts were phyllosilicate-altered and flattened by diagenetic compaction, resulting in false welding textures. Intensely silicified pumice shreds isolated in chloritic domains resemble felsic volcanic lithic fragments.

The density and complexity of non-explosive, coherent, intrusive-extrusive units at Highway-Reward is similar to that described by Horikoshi (1969) for Kuroko host sequences in the Miocene Kosaka Formation of NE-Japan. Analogues of the initial, explosive, tuff cone forming eruptions at the "Kosaka volcano" are not recorded in the stratigraphy at Highway-Reward, possibly reflecting differences in the volatile content of erupted magma, and/or the external confining pressure (lithostatic and hydrostatic pressure).

References:

Horikoshi E., 1969. Volcanic activity related to the formation of the Kuroko-type deposits in the Kosaka district, Japan. Mineralium Deposita (Berlin) 4, 321-345.

McBirney A.R., 1963. Factors governing the nature of submarine volcanism. Bulletin Volcanologique 26, 455-469.

McPhie J., & Allen R.L., 1992. Facies architecture of mineralised submarine volcanic sequences: Cambrian Mount Read Volcanics, Tasmania. Economic Geology 87, 587-596.

McPhie J., Doyle M.G., & Allen R.L., 1993. Volcanic Textures. CODES Key Centre, University of Tasmania, Hobart: 208 pp.

Walker G.P.L., 1989. Gravitational (density) controls on volcanism, magma chambers and intrusions. Australian Journal of Earth Sciences 36, 149-165.

Doyle MG and McPhie J, 1994. A silicic submarine syn-sedimentary intrusive-dome-hyaloclastite host sequence to massive sulfide mineralisation: Mount Windsor Volcanics, Cambro-Ordovician, Australia. IAVCEI International Volcanological Congress, Ankara, Turkey. Abstracts, Theme 10.

A SILICIC SUBMARINE SYN-SEDIMENTARY INTRUSIVE - DOME - HYALOCLASTITE HOST SEQUENCE TO MASSIVE SULFIDE MINERALISATION: MOUNT WINDSOR VOLCANICS, CAMBRO-ORDOVICIAN, AUSTRALIA

DOYLE, M.G., and McPHIE, J., C.O.D.E.S., University of Tasmania, Hobart, Tasmania 7001, Australia.

The Cu-Au-Pb-Zn Highway and Reward massive sulfide deposits are hosted by a silicic intrusive and volcanic sequence intercalated with sedimentary facies that indicate a submarine, below-storm-wave-base environment of deposition. Contact relationships and phenocryst mineralogy, size and percentages indicate the presence of up to nine distinct porphyritic units in an area of 1 x 1 x 0.5 km. The peperitic upper margins to many porphyries demonstrate their intrusion into wet unconsolidated-sediment. Syn-sedimentary intrusions, partly emergent cryptodomes, lava domes, and associated in situ and resedimented autoclastic deposits have been recognised. These are the principal facies in the environment of mineralisation and represent a proximal facies association from intrabasinal, intrusive/extrusive, non-explosive magmatism. The shape, distribution and emplacement mechanisms of porphyritic units were influenced by: (a) the relative density of magma to wet sediment; (b) the positions of previously or concurrently emplaced porphyries; and (c) possibly by syn-volcanic faults which may have acted as conduits for magma. Lava domes, partly emergent cryptodomes, and deposits of resedimented hyaloclastite and peperite are important indicators of palaeo-sea-floor positions at Highway-Reward. Sills and cryptodomes may have influenced sea- floor topography and therefore sedimentation, but do not mark sea-floor positions. Massive sulfide ores are primarily sub-sea-floor syn-volcanic replacements of the host sedimentary rocks, syn-sedimentary intrusions, lava domes, and autoclastic breccia.

Porphyries intruded or were overlain by a volcaniclastic and sedimentary facies association comprising suspension-settled siltstone, graded turbiditic sandstone and thick, non-welded pumice- and crystal-rich sandstone-breccia. Pumiceous and crystal-rich deposits record episodes of explosive silicic volcanism in an extrabasinal or marginal basin environment, and were emplaced by cold, water-supported, high-concentration turbidity currents.

Large RR, Doyle M, Cooke D and Raymond O, 1994. Evaluation of the role of Cambrian Granites in the genesis of world class volcanogenic-hosted massive sulphide deposits in Tasmania. Geological Society of Australia, Abstracts 37: 236-237.

EVALUATION OF THE ROLE OF CAMBRIAN GRANITES IN THE GENESIS OF WORLD CLASS VOLCANOGENIC-HOSTED MASSIVE SULPHIDE DEPOSITS IN TASMANIA

Ross R. Large[1], Mark Doyle[1], David Cooke[1] and Ollie Raymond[2]
[1]CODES Key Centre, Geology Dept., University of Tasmania, HOBART TAS 7005
[2]AGSO, GPO Box 378, CANBERRA ACT 2601

Summary - New data on the distribution, composition and alteration zonation of Cambrian granites in the Mt. Read Volcanics provide evidence that there may have been a direct input of magmatic fluids during the genesis of the copper-gold volcanogenic-hosted massive sulphide (VHMS) mineralisation in the Mt. Lyell district.

INTRODUCTION

There has been considerable debate on the role of granitic magmas during the generation of volcanic hosted massive sulphide deposits; are they simply heat engines driving seawater (e.g. Ohmoto & Rye 1974, and Solomon 1976) or do they directly supply magmatic components to ore-forming solutions (e.g. Henley & Thornley 1979, Stanton 1985)? Pioneering research by Solomon and his students in the Mount Read Volcanics (e.g. Solomon 1976, Solomon 1981, Polya et al 1986 and Eastoe et. al. 1987) clearly demonstrated a relationship between hydrothermal alteration and sulphur isotope zonation around the granites, indicating that the granites acted as heaters for the ore-forming convective fluid. In this paper we provide evidence to suggest that the Cambrian granites may have also provided important metal contributions to the ore-forming fluid, especially Fe, Cu, Au, P, F ± Ti and Zr

FACTORS LINKING THE CAMBRIAN GRANITES TO MINERALISATION

Distribution; Two narrow bodies of Cambrian granite (Murchison Granite and Darwin Granite) intrude the eastern margin of the Central Volcanic Complex (CVC) in the Mt. Read Volcanics. Interpretations based on magnetic and gravity data indicate that the two granite bodies form a semi-continuous narrow vertical sheet of granite 65 km long and about 2 km wide. A series of copper-gold and basemetal prospects occur along the margins of the granite sheet (e.g. Prince Darwin, Jukes Pty., Lake Selina). The Mt. Lyell Cu-Au VHMS deposits are located immediately west of the projected continuation of the subsurface granite.

Timing: Previous mapping by Corbett (1989) suggested that the Murchison granite intruded the Tyndal Group volcanics (which unconformably overlie the CVC) and is therefore younger than the VHMS deposits. However, later work (e.g. Corbett, 1992) has revised this interpretation, and recent dating by Perkins and Walshe (1993) has confirmed that the Murchison granite has an age of 501 ± 5.7 Ma (Ar/Ar), the same age as the host rocks to the massive sulphide deposits.

Composition: Both the Murchison and Darwin granites are high-K, magnetite series granites which show anomalous enrichment in barium and potassium. The Murchison granite varies in composition from granodiorite to granite (58 to 78% SiO_2; Abbott, 1992), while the Darwin granite is composed of two highly fractionated granite phases (74-78% SiO_2; Jones, 1993). K_2O varies up to 8.5% and Ba up to 3000 ppm; however, some of this enrichment is related to alteration.

Alteration: Well developed zones of hydrothermal alteration have been mapped around the margins of the granites (e.g. Polya et. al 1986, Eastoe et. al. 1987, Hunns 1987, Doyle 1990). An extensive zone (Z_1) of pink K-feldspar alteration extends from the outer part of the granites into the surrounding volcanics. An overlapping shell (Z_2) of chlorite ± pyrite ± magnetite alteration overprints and extends outwards from the K-feldspar zone. Sericite-chlorite ± pyrite forms a distal alteration zone (Z_3). At both Jukes Pty. and Lake Selina, Cu ± Au mineralisation occurs in the chlorite ± pyrite ± magnetite zone (Z_2).

Magnetite - apatite association: The strongest link between the granites and VHMS Cu-Au mineralisation is provided by the common occurrence of magnetite - apatite - Cu ± Au vein style and disseminated mineralisation both within the Z2 alteration halo of the granites and within the centre of the Prince Lyell ore deposit in the Mt. Lyell VHMS district. A good linear correlation exists between Cu and P_2O_5, and Fe and P_2O_5 both within the mineralised alteration halo of the granites and in the Prince Lyell ores. Oxygen isotopes indicate that the magnetite veins within the granite halo and the Prince Lyell deposit have $d^{18}O$ values that are consistent with a magmatic source (Doyle 1990, Raymond 1993). Apatite, which is commonly intergrown with magnetite, pyrite and chalcopyrite, has consistently high F/Cl ratios, with a mean of about 6 wt% F

RELATIONSHIP OF COPPER-GOLD TO LEAD-ZINC-COPPER VHMS DEPOSITS

The Mt. Lyell field contains both stringer-style copper-gold deposits such as Prince Lyell and separate stratiform lead-zinc-copper deposits such as Comstock and Tasman & Crown Lyell Extended. Most previous workers (e.g. Solomon 1976, and Walshe & Solomon 1981) consider that the Cu-Au and Pb-Zn-Cu deposits formed as part of the same hydrothermal system; the Cu-Au stringer-style forming by subsurface replacement and the Pb-Zn-Cu massive sulphides by contemporaneous seafloor exhalation. Although our work suggests a source for Cu and Au from the Cambrian granites, the source for Pb, Zn, Ag and S remains unresolved and may be either magmatic or related to seawater leaching.

CONCLUSIONS

Cambrian granites in the Mt. Read Volcanics form a thin linear discontinuous sheet 65 km long which is spatially related to Cu-Au mineralisation, including the VHMS deposits at Mt. Lyell. The highly fractionated, oxidised, magnetite series granites have overlapping alteration shells of K-feldspar, chlorite-magnetite and sericite. Preliminary evidence suggests that the VHMS copper-gold mineralisation at Mt. Lyell may be associated with fluids enriched in Fe-Cu-Au-P_2O_5-F-Zr-Ti released directly from the granite magma.

REFERENCES

Abbott, P.D.B., 1992. Geology of a barite-galena occurrence exposed in the Anthony Power Development Tunnel, western Tasmania. Unpublished Honours Thesis. University of Tasmania: 62 p.

Corbett, K.D., 1989. Stratigraphy, palaeogeography and geochemistry of the Mt. Read Volcanics. In Burrett, C.T., and Martin, E.L. (eds.), Geology and mineral resources of Tasmania: Special Publication: Geological Society of Australia 15, 86-119.

Corbett, K.D., 1992 Stratigraphic-volcanic setting of massive sulfide deposits in the Cambrian Mount Read Volcanics, Tasmania. Economic Geology 87, 564-586.

Doyle, M.G., 1990. The geology of the Jukes Proprietary prospect Mt. Read Volcanics, Unpublished Honours Thesis, University of Tasmania 114 p.

Eastoe, C.J., Solomon. M., and Walshe, J.L., 1987. District-scale alteration associated with massive sulfide deposits in the Mount Read Volcanics, western Tasmania. Economic Geology 82, 1239-1258.

Henley, R.W., and Thornley, P., 1979. Some geochemical aspects of polymetallic massive sulfide formation. Economic Geology 74. 1600-1612.

Hunns, S.R.. 1987. Geology and geochemistry of the Lake Selina prospect western Tasmania: Unpublished Masters Qualifying Thesis, University of Tasmania:

Jones, A.T., 1993. The geology, geochemistry and structure of the Mount Darwin - South Darwin Peak Area western Tasmania. Unpublished Honours Thesis, University of Tasmania 120 p.

Ohmoto, H., and Rye, R.P., 1974. Hydrogen and oxygen isotopic compositions of fluid inclusions in the kuroko deposits, Japan. Economic Geology 69, 947-953.

Perkins, C., and Walshe, J.L., 1993. Geochronology of the Mount Read Volcanics. Tasmania: Australia Economic Geology 88, 1176-1197

Polya, D.A., Solomon. M., Eastoe, C.J., and Walshe, J.L., 1986. The Murchison Gorge, Tasmania - a possible cross-section through a Cambrian massive sulfide system. Economic Geology 76. 1341-1355.

Raymond, 0.L., 1993. Geology and mineralisation of the Southern Prince Lyell Deeps. Queenstown, Tasmania. Unpubl. MSc Thesis. University of Tasmania 160p.

Solomon, M., 1976. "Volcanic" massive sulphide deposits and their host rocks - a review and an explanation. In Wolf, K.A., ed., Handbook of strata-bound and stratiform ore deposits, II, Regional studies and specific deposits: Amsterdam, Elsevier, 21-50.

Solomon, M., 1981. An introduction to the geology and metallic mineral resources of Tasmania. Economic Geology 76, 194-208

Stanton, R.L., 1985. Stratiform ores and geological processes: Royal Society of New South Wales 118, 77-100.

Walshe, J.K. and Solomon, M., 1981. An investigation into the environment of formation of the volcanic-hosted Mount Lyell copper deposits using geology, mineralogy, stable isotopes, and a six-component chlorite solid solution model. Economic Geology 76, 246-284.

Acknowledements: Permission to use geochemical data for Cambrian granites from the Mineral Resources Tasmania data-base, and from Steve Hunns for unpublished analyses on the Lake Selina prospect is gratefully acknowledged.

Large RR, Doyle M, Raymond O, Cooke D, Jones A and Heasman L, 1996. Evaluation of the role of Cambrian Granites in the genesis of world class VHMS deposits in Tasmania. Ore Geology Reviews, 10: 215-230.

ELSEVIER

Ore Geology Reviews 10 (1996) 215–230

ORE GEOLOGY REVIEWS

Evaluation of the role of Cambrian granites in the genesis of world class VHMS deposits in Tasmania

Ross Large [a], Mark Doyle [a], Ollie Raymond [b], David Cooke [a], Andrew Jones [a], Lachlan Heasman [a]

[a] *Centre for Ore Deposit & Exploration Studies, University of Tasmania, G.P.O. Box 252C, Hobart, Tasmania, 7001, Australia*
[b] *AGSO, P.O. Box 378, Canberra, ACT 2601, Australia*

Received 24 March 1995; accepted 26 July 1995

Abstract

An analysis of the distribution, composition and alteration zonation of Cambrian granites which intrude the Mt Read Volcanics of western Tasmania provides evidence that there may have been a direct input of magmatic fluids containing Fe, Cu, Au and P to form the copper–gold volcanic-hosted massive sulphide (VHMS) mineralisation in the Mt Lyell district.

Interpretation of regional gravity and magnetic data indicates that a narrow discontinuous body of Cambrian granite (2–4 km wide) extends along the eastern margin of the Mt Read Volcanic belt for over 60 km. The Cambrian granites are altered magnetite series types which show enrichment in barium and potassium, and contrast markedly with the fractionated ilmenite series Devonian granites related to tin mineralisation elsewhere in the Dundas Trough.

Copper mineralisation occurs in a linear zone above the apex of the buried Cambrian granite body at the southern end of the belt, from Mt Darwin to the Mt Lyell district over a strike length of 25 km. Gold and zinc mineralisation are concentrated higher in the volcanic stratigraphy more distant from the granite. Overlapping zones of alteration extend from the granite into the surrounding volcanic rocks. An inner zone of K-feldspar alteration is overprinted by chlorite alteration, which passes outwards into sericite alteration. Magnetite ± pyrite ± chalcopyrite ± apatite mineralisation is concentrated in the chlorite alteration zone as veins and low grade disseminations. The Mt Lyell copper–gold stringer and disseminated mineralisation is hosted in felsic volcanic rocks 1 to 2 km west of the interpreted buried granite position. Magnetite–apatite ± pyrite veins in the Prince Lyell deposit at Mt Lyell are very similar to the veins in the halo of the granite, further south, and provide evidence for magmatic fluid input during the formation of the copper–gold VHMS deposits.

A model involving deeply penetrating convective seawater, mixing with a magmatic fluid released from the Cambrian granites, best explains the features of VHMS mineralisation in the Mt Lyell district.

1. Introduction

There has been considerable debate over the past 25 years on the role of granitic magmas during the generation of volcanic-hosted massive sulphide (VHMS) deposits. Some workers (e.g. Urabe and Sato, 1978; Henley and Thornley, 1979; Sawkins and Kowalik, 1981; and Stanton, 1985, Stanton, 1990) have argued for a direct input of volatiles and metals from the magma to form the ore solutions, while others (e.g. Kajiwara, 1973; Spooner and Fyfe, 1973; Ohmoto and Rye, 1974; Solomon, 1976; Large,

SSDI 0169-1368(95)00024-0